

Electronic Thesis and Dissertation Repository

8-12-2016 12:00 AM

Glycosylation on Stromal Interaction Molecule-1 Ca²⁺ sensing region enhances Store Operated Ca²⁺ Entry

Yoo Jung Choi, *The University of Western Ontario*

Supervisor: Dr. Peter B. Stathopoulos, *The University of Western Ontario*

A thesis submitted in partial fulfillment of the requirements for the Master of Science degree in Physiology and Pharmacology

© Yoo Jung Choi 2016

Follow this and additional works at: <https://ir.lib.uwo.ca/etd>



Part of the [Cellular and Molecular Physiology Commons](#)

Recommended Citation

Choi, Yoo Jung, "Glycosylation on Stromal Interaction Molecule-1 Ca²⁺ sensing region enhances Store Operated Ca²⁺ Entry" (2016). *Electronic Thesis and Dissertation Repository*. 4005.
<https://ir.lib.uwo.ca/etd/4005>

This Dissertation/Thesis is brought to you for free and open access by Scholarship@Western. It has been accepted for inclusion in Electronic Thesis and Dissertation Repository by an authorized administrator of Scholarship@Western. For more information, please contact wlsadmin@uwo.ca.

Abstract

A major intracellular calcium (Ca^{2+}) uptake pathway in excitable and non-excitable eukaryotic cells is store-operated Ca^{2+} entry (SOCE). Stromal interaction molecule-1 (STIM1) is the key regulator of SOCE and responds to changes in endoplasmic reticulum (ER)-stored Ca^{2+} through luminal sensing machinery composed of EF-hand and SAM domains (EFSAM). EFSAM can undergo *N*-glycosylation at Asn131 and Asn171 sites; however, the exact molecular and functional effects of *N*-glycosylation are unclear. By establishing a site-specific chemical approach to covalently linking glucose to EFSAM and subsequently examining EFSAM biophysical properties, I found that this modification enhances STIM1 activation through localized structural perturbations, decreased Ca^{2+} binding affinity, reduced stability and enhanced oligomerization. Further, Ca^{2+} influx via SOCE in HEK293 cells co-expressing Orai1 and STIM1 was diminished when *N*-glycosylation was blocked. Collectively, my data suggests that *N*-glycosylation enhances EFSAM response to ER Ca^{2+} depletion thereby augmenting the role of STIM1 as the ON/OFF regulator of SOCE.

Keywords

stromal interaction molecule-1, calcium, store-operated calcium entry, *N*-glycosylation, nuclear magnetic resonance spectroscopy, fura2, EFSAM, stability, structure, oligomerization, calcium binding affinity

Co-Authorship Statement

Dr. Peter B. Stathopoulos supervised and contributed to the design of all experiments.

Acknowledgments

First and foremost, I owe my deepest gratitude to Dr. Peter B. Stathopoulos for being the best supervisor ever. His incomparable patience and dedication to his students really helped me to have the best possible graduate student experience and have nurtured my passion for research. Also, his involvement in lab allowed me to gain numerous research techniques as well as how to be a critical thinker in research as well as in life. Without his help and guidance, this project would not have been possible. Thank you so much Peter, you are the best!

Secondly, I would like to thank my advisory committee members, Drs. Lina Dagnino, Qingping Feng, and Timothy Regnault for their undivided attention and support regarding my project. Their insights were very beneficial to my project.

From the Stathopoulos lab, I would like to thank Sam Lee for all his help from day one. As the original members of the lab, without you it would have been very lonely. Also a huge thank you to Yue Zhao for growing all those bacterial cells, your help allowed me to complete my experiments efficiently and effectively.

I would also like to thank all my friends of PhysPharm, especially Catherine Nevin, Michelle Kim, and Nicole Edwards for giving me so many great memories and making my time as a graduate student so much better. I also want to give a shout-out to Melissa Fenech for all the coffee breaks we took together and for suffering through my endless tales of failed experiments. My friends, you have made the last two years mean so much more in my life.

I would also like to acknowledge Ontario Graduate Scholarship for their funding. I am very honored to have received this scholarship.

Lastly, I would like to thank my family for always being there to guide and support me in good times and bad. Their unconditional love and continuous belief in me has always been my fundamental energy to overcome any obstacles I face in life. I love you all.

Table of Contents

Abstract	i
Co-Authorship Statement	ii
Acknowledgments	iii
Table of Contents	iv
List of Tables	vii
List of Figures	viii
List of Abbreviations	x
Chapter 1: Introduction	1
1.1 Calcium.....	2
1.2 Store operated Ca ²⁺ entry (SOCE).....	4
1.2.1 Discovery of the SOCE pathway	4
1.2.2 Molecular players mediating SOCE	5
1.3 Stromal interaction molecule (STIM) and Orai	8
1.3.1 STIM and Orai domain architectures.....	8
1.3.2 STIM1 and Orai1 in the activation of SOCE.....	12
1.4 STIM1 luminal domain.....	14
1.4.1 STIM1 luminal domain structure.....	14
1.4.2 Biophysical properties of STIM1 luminal domain	17
1.5 <i>N</i> -glycosylation of STIM1	18
1.5.1 <i>N</i> -linked glycosylation	18
1.5.2 <i>N</i> -glycosylation of EFSAM	19
1.6 Rationale, hypothesis, and objectives	20
1.6.1 Rationale and hypothesis	20
1.6.2 Objectives	21

Chapter 2: Methods	23
2.1 Constructs and Mutations	24
2.2 Protein expression and purification	27
2.2.1 Protein expression.....	27
2.2.2 Protein purification	28
2.2.3 Anion Exchange chromatography.....	31
2.2.4 Preparation of Ca ²⁺ -free apo protein samples.....	31
2.3 Neo-glycosylation of EFSAM	33
2.4 Far-UV circular dichorism (CD) spectroscopy.....	36
2.4.1 Thermal stability using far-UV CD spectroscopy	36
2.4.2 Ca ²⁺ binding affinity using far-UV CD spectroscopy.....	36
2.5 Solution NMR spectroscopy	37
2.6 Static Light Scattering (SLS).....	38
2.7 Live cell experiments.....	39
2.7.1 Cell culture.....	39
2.7.2 Transfection	39
2.7.3 Fura2- ratiometric Ca ²⁺ imaging.....	40
Chapter 3: Results	42
3.1 Double neo-glycosylated EFSAM constitutively loses α -helicity.....	43
3.2 Neo-glycosylated EFSAM proteins are destabilized.....	46
3.3 Neo-glycosylation of EFSAM proteins cause local structural perturbations.....	49
3.4 Neo-glycosylation lowers EFSAM Ca ²⁺ binding affinity.....	63
3.5 Neo-glycosylation alters Ca ²⁺ -dependent oligomerization propensity of EFSAM.	67
3.6 Blocking EFSAM glycosylation within full-length STIM1 suppresses SOCE.....	70
Chapter 4: Discussion	72
4.1 Summary of key findings.....	73

4.2 Neo-glycosylation alters the fundamental Ca ²⁺ sensing properties EFSAM proteins.....	74
4.2.1 Glycosylation structurally perturbs STIM1 EFSAM.....	74
4.2.2 Glycosylation lowers the Ca ²⁺ affinity of STIM1 EFSAM	76
4.2.3 Glycosylation enhances oligomerization of STIM1 EFSAM.....	76
4.3 SOCE is suppressed after blocking of STIM1 glycosylation in mammalian cells. .	77
4.4 Future studies	79
4.5 Overall Conclusion	81
References	85
Curriculum Vitae	94

List of Tables

Table 2.1. Primers used for mutagenesis and sequencing.	25
Table 2.2. PCR amplification template on LifeECO (Bioer).....	26
Table 2.3. Components of the experimental buffers used in the thesis research.	30
Table 3.1. Summary of thermal stability changes for mutated and/or glucose modified EFSAM proteins.	48
Table 3.2. Summary of the equilibrium dissociation constants (K_d) extracted from the far-UV CD-derived Ca^{2+} binding curves.....	66
Table 4.1. Summary of the changes in EFSAM Ca^{2+} sensing function and SOCE activation due to <i>N</i> -glycosylation.	83

List of Figures

Figure 1.1. Schematic diagram of the Ca ²⁺ signaling pathway and homeostasis.	3
Figure 1.2. STIM1 domain architecture and sequence alignment.	10
Figure 1.3. Schematic diagram of the SOCE molecular activation mechanism.	13
Figure 1.4. Depiction of the backbone structure of the Ca ²⁺ -loaded EFSAM domain.	16
Figure 2.1. SDS-PAGE gel analyses of STIM1 EFSAM purification.	29
Figure 2.2. Anion exchange chromatographic separation of the wild-type EFSAM protein.	32
Figure 2.3. Positive ionization electrospray mass spectrum of glucose conjugated Asn171Cys EFSAM protein.	35
Figure 3.1. Far-UV CD spectra of wild-type, Asn131Cys, Asn171Cys, Asn131Cys/Asn171Cys, gl-Asn131Cys, gl-Asn171Cys, and gl-Asn131Cys/gl-Asn171Cys EFSAM proteins.	44
Figure 3.2. Thermal stability of wild-type, Asn131Cys, Asn171Cys, Asn131Cys/Asn171Cys, gl-Asn131Cys, gl-Asn171Cys, and gl-Asn131Cys/gl-Asn171Cys EFSAM proteins.	47
Figure 3.3. ¹ H- ¹⁵ N HSQC spectrum of gl-Asn131Cys (magenta crosspeaks) overlaid with the wild-type (black crosspeaks) spectrum.	50
Figure 3.4. Normalized CSPs derived from the ¹ H- ¹⁵ N HSQC spectra.	51
Figure 3.5. The largest magnitude CSPs of gl-Asn131Cys relative to wild-type EFSAM mapped on the 3D structure of wild-type EFSAM.	53
Figure 3.6. ¹ H- ¹⁵ N HSQC spectrum of gl-Asn171Cys (cyan crosspeaks) overlaid with the wild-type (black crosspeaks) spectrum.	55
Figure 3.7. Normalized CSPs derived from the ¹ H- ¹⁵ N HSQC spectra.	56
Figure 3.8. The largest magnitude CSPs of gl-Asn171Cys relative to wild-type EFSAM mapped on the 3D structure of wild-type EFSAM.	58
Figure 3.9. ¹ H- ¹⁵ N HSQC spectrum of gl-Asn131Cys/gl-Asn171Cys (orange crosspeaks) overlaid with the wild-type (black crosspeaks) spectrum.	59
Figure 3.10. Normalized CSPs derived from the ¹ H- ¹⁵ N HSQC spectra.	60
Figure 3.11. The largest magnitude CSPs of gl-Asn131Cys/gl-Asn171Cys relative to wild-type EFSAM mapped on the 3D structure of wild-type EFSAM.	62

Figure 3.12. Ca ²⁺ binding curves derived from changes in far-UV CD ellipticity as a function of Ca ²⁺ concentration.	64
Figure 3.13. Oligomerization propensity of EFSAM proteins assessed by SLS intensity.	69
Figure 3.14. Assessment of SOCE mediated by wild-type and glycosylation-incompetent full length STIM1 proteins in HEK293 live cells.	71
Figure 4.1. Proposed model of non-glycosylated and <i>N</i> -glycosylated STIM1-mediated SOCE activation.	84

List of Abbreviations

Asn	asparagine
Ca ²⁺	calcium
CaM	calmodulin
CC	coiled-coil
CD	circular dichroism
cEF	canonical EF-hand
CRAC	Ca ²⁺ release activated Ca ²⁺
CSP	chemical shift perturbation
Cys	cysteine
DTT	dithiothreitol
EDTA	ethylenediamine tetraacetic acid
eGFP	enhanced green fluorescent protein
EndoH	endoglycosidase H
ER	endoplasmic reticulum
Gln	glutamine
GPCR	G-protein coupled receptor
HSQC	heteronuclear single quantum coherence
IP ₃	inositol 1,4,5-triphosphate
IPTG	isopropyl β-D-1-thiogalactopyranoside
K ⁺	potassium
K _d	equilibrium dissociation constant
LB	luria broth
mCh	monomeric Cherry
MTS-5-glucose	N-(β-D-glucopyranosyl)-N'-[2-methanethiosulfonyl]ethyl]urea
NCX	Na ⁺ /Ca ²⁺ exchanger
nEF	non-canonical EF-hand
NMR	nuclear magnetic resonance
PM	plasma membrane
PMCA	plasma membrane Ca ²⁺ -ATPase

RNAi	RNA interference
RTK	receptor tyrosine kinase
SAM	sterile alpha motif
SCID	severe combined immunodeficiency
SERCA	sarco/endoplasmic reticulum Ca ²⁺ -ATPase
siRNA	small inhibitory RNA
SLS	static light scattering
SOCE	store-operated Ca ²⁺ entry
STIM	stromal interaction molecule
TCEP	tris(2-carboxyethyl)phosphine
TCR	T-cell receptor
TG	thapsigargin
TIRF	total internal reflection fluorescence
T _m	apparent midpoint of temperature denaturation
TM	transmembrane

Chapter 1
Introduction

1.1 Calcium

Calcium ions (Ca^{2+}) are essential for numerous intracellular signals that regulate a plethora of cellular processes and are necessary to maintain cellular homeostasis. For example, at the synaptic junction, Ca^{2+} triggers exocytosis within microseconds, whereas Ca^{2+} has to signal over minutes to hours to drive events such as transcription and cell proliferation (Berridge *et al.*, 2003). Therefore, precise control of Ca^{2+} levels in the cytoplasm is crucial for mediating these important processes. Furthermore, recognizing how these different Ca^{2+} signaling systems work and studying the delicate balance between the production and removal of Ca^{2+} signals in the cytoplasm is important for understanding the basis for myriad processes in both health and disease (Berridge *et al.*, 2003).

While each cell type possesses unique Ca^{2+} signaling properties, most systems function by transient Ca^{2+} pulses generated from a combination of addition and removal of cytosolic Ca^{2+} (Figure 1.1). The release of Ca^{2+} into the cytoplasm can be derived either from internal cellular stores or the external medium. The endoplasmic reticulum (ER) is considered to be a major internal Ca^{2+} store (Berridge, 1993; Clapham, 1995) with Ca^{2+} levels maintained in the $\sim 100\text{-}800\ \mu\text{M}$ range. Release of Ca^{2+} from the ER lumen is mediated by Ca^{2+} itself or by other messengers, such as inositol 1,4,5-trisphosphate (IP_3). For example, the activation of G-protein coupled receptors (GPCR) on the plasma membrane (PM) leads to the activation of phospholipases, in turn resulting in the metabolism of phosphatidylinositol 4,5-bisphosphate generating diacylglycerol and IP_3 . IP_3 is a small diffusible molecule that binds to the IP_3 receptor on the cytosolic side of ER membrane. IP_3 receptor which is also a channel, opens upon stimulation causing the release of Ca^{2+} from the lumen and into the cytoplasm (i.e., $\sim 0.1\text{-}1\ \mu\text{M}$) (Bootman *et al.*, 2001; Berridge *et al.*, 2003).

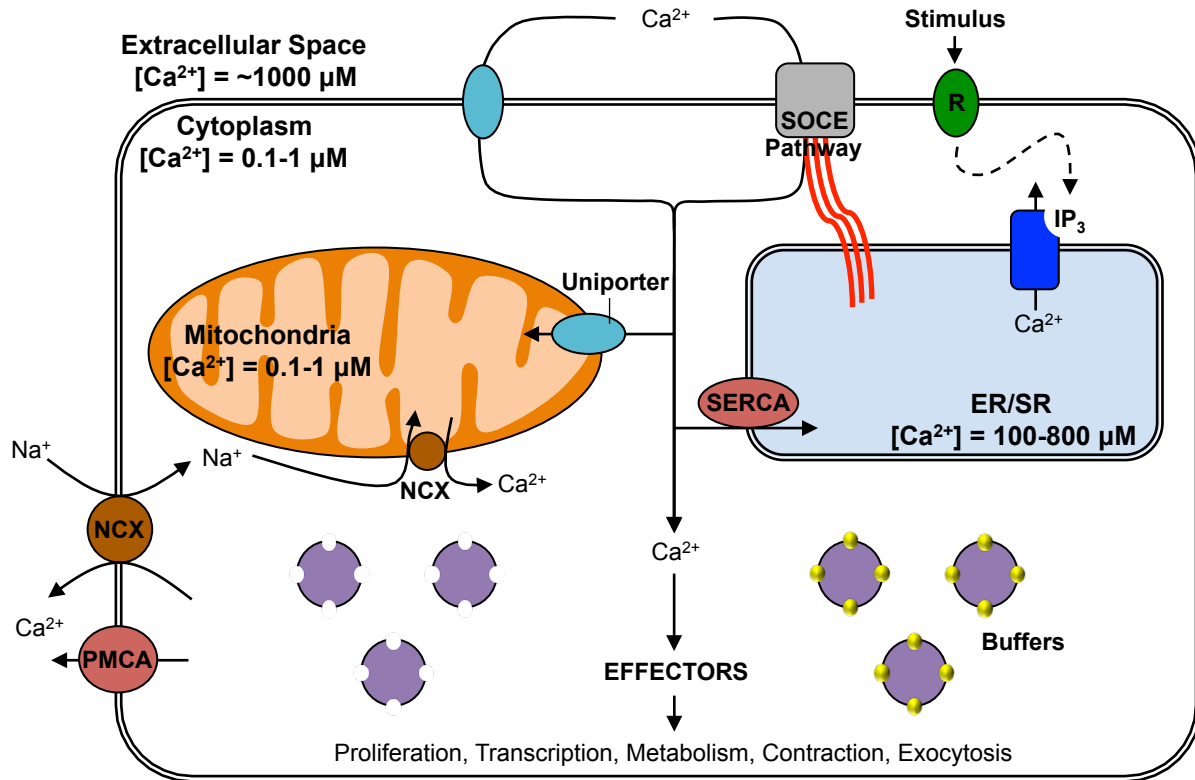


Figure 1.1. Schematic diagram of the Ca^{2+} signaling pathway and homeostasis. This diagram was modified from Berridge *et al.*, 2003. Plasma membrane GPCRs, TCRs and RTKs are shown in green, labeled as R. Downstream of PM receptor activation, the second messenger IP_3 binds to its receptor on the S/ER membrane depicted in blue. Binding of IP_3 to the IP_3 receptor causes efflux of Ca^{2+} from the S/ER lumen and depletion of this major intracellular Ca^{2+} store. The S/ER Ca^{2+} depletion activates PM Ca^{2+} channels (grey square) and Ca^{2+} influx from the extracellular space ensues in the process of SOCE. The process is fully reversible once the Ca^{2+} store in S/ER lumen is replenished by the SERCA pump. Mitochondria also sequesters cytosolic Ca^{2+} quickly through a uniporter, and then released slowly for SERCA and Ca^{2+} -ATPase (PMCA) uptake. Most cytosolic Ca^{2+} are bound to buffers, whereas a small proportion binds to the effectors to mediate various cellular processes. When these signals are no longer needed nor present, Ca^{2+} is removed from the cells by various exchangers and pumps such as Na^+/Ca^{2+} exchanger (NCX), PMCA, SERCA.

Although the ER lumen is a major intracellular Ca^{2+} store, it is only a limited and exhaustible source of Ca^{2+} . Whereas local and acute increases in cytosolic Ca^{2+} may trigger many processes, many of them rely on prolonged cytosolic Ca^{2+} signals to elicit responses such as gene transcription and cell proliferation (Hogan *et al.*, 2003). Therefore, for maintained increases in cytosolic Ca^{2+} levels, an influx of Ca^{2+} is required beyond what is capable of being sourced from the ER. The extracellular space represents an essentially inexhaustible source of Ca^{2+} (i.e., $>1000 \mu\text{M}$), which can facilitate maintained increases in cytosolic Ca^{2+} . Thus, opening of Ca^{2+} channels on the plasma membrane can result in an influx of Ca^{2+} down a steep concentration gradient (Feske, 2007). Importantly, the uptake of Ca^{2+} from the extracellular space is needed not only to sustain elevated cytosolic Ca^{2+} levels, but also to prevent depletion of ER Ca^{2+} levels and to replenish the ER Ca^{2+} stores. One of the major pathways that regulates ER Ca^{2+} levels and facilitates extracellular space Ca^{2+} influx is the store operated Ca^{2+} entry (SOCE) pathway (Putney, 1986).

1.2 Store operated Ca^{2+} entry (SOCE)

1.2.1 Discovery of the SOCE pathway

SOCE is a major Ca^{2+} entry pathway in excitable and non-excitable cells (Varga-Szabo *et al.*, 2011; Shaw & Feske, 2013). Starting from the discovery and appreciation for the role of Ca^{2+} as an intracellular signal over a century ago (Ringer, 1883), there was considerable interest on the sources of such cellular Ca^{2+} (Rasmussen, 1970; Janis & Triggler, 1983), eventually leading to the conception of the SOCE model (Putney, 1986). The origin of the SOCE theory is associated with an investigation of the kinetics of the potassium (K^+) permeability response in the parotid gland using a unidirectional isotope flux technique

(Putney, 1976). This experiment revealed increased K^+ permeability in two phases: a transient phase followed by a sustained phase. Interestingly, Putney and his colleagues also found that in the absence of extracellular Ca^{2+} , only the sustained phase was no longer present (Putney, 1976). Moreover, it was demonstrated that the initial transient response was dependent on Ca^{2+} from inside the cell, and it could only be restored by external Ca^{2+} via plasma membrane Ca^{2+} channels, and upon depletion of the internal Ca^{2+} store (Parod & Putney, 1978). It was only realized 8 years later that the influx of Ca^{2+} to restore the internal Ca^{2+} levels was not a direct consequence of the activation of the plasma membrane GPCRs, but rather it was a result of the depletion of the Ca^{2+} levels in the intracellular stores (Putney, 1986).

1.2.2 Molecular players mediating SOCE

SOCE, also known as capacitative Ca^{2+} entry, occurs subsequently to the release of intracellular Ca^{2+} stores, thereby causing an influx of Ca^{2+} from the extracellular space into the cytoplasm. Specifically, decreases in ER luminal Ca^{2+} levels result in the interaction between ER- and PM-resident proteins, which open PM Ca^{2+} channels that facilitate influx of Ca^{2+} from the extracellular space, thus elevating cytosolic Ca^{2+} levels and replenishing/maintaining high levels of Ca^{2+} in the ER lumen (Putney, 1986). In addition to the previously mentioned GPCRs in section 1.1, there is large range of other PM receptors that lead to IP_3 production and subsequently to the depletion of ER Ca^{2+} stores, such as T-cell receptors (TCR) (van Leeuwen & Samelson, 1999; Lucas *et al.*, 2003) and receptor tyrosine kinases (RTK) (Clapham, 1995; Schlessinger, 2000) (Figure 1.1). Following the efflux, the decrease in Ca^{2+} levels within ER lumen is detected and signals are sent to the PM of the cell to open Ca^{2+} channels and allow external Ca^{2+} to move down the concentration gradient into the cytosol.

These Ca^{2+} ions not only elevate the cytosolic levels of Ca^{2+} but are also an important source for sarco/endoplasmic reticulum Ca^{2+} ATPase (SERCA) pumps located on ER membrane to recycle Ca^{2+} back into the ER lumen. It is important to note that the ER is not only a source of Ca^{2+} , but this organelle also carries out critical processes that are Ca^{2+} dependent such as protein folding, vesicle trafficking, initiation of apoptosis, and many others (Berridge, 2002).

Although the concept of SOCE was first proposed in 1986, it was not until two decades later that the principal molecular players in this process were identified. Liou and colleagues generated small interfering RNAs (siRNAs) against 2,304 proteins with known human signaling domains identified in the National Center for Biotechnology Information database and used them to test their role in receptor triggered Ca^{2+} signals in HeLa cells (Liou *et al.*, 2005). HeLa cells were stimulated with histamine, a GPCR ligand (Hill, 1990; Leurs *et al.*, 1995), and thapsigargin (TG), a non-competitive SERCA pump inhibitor (Jackson *et al.*, 1988; Lytton *et al.*, 1991; Treiman *et al.*, 1998), fura2., a small molecule fluorescent cytosolic Ca^{2+} indicator, was used to assess the peak of the cytosolic Ca^{2+} increase followed by the plateau (Liou *et al.*, 2005). The observed plateau phase was due to maintenance of high cytosolic Ca^{2+} levels from the activated SOCE pathway. Knockdown of stromal interaction molecule (STIM) proteins that are involved in the SOCE pathway resulted in a near complete loss of the cytosolic Ca^{2+} plateau due to downregulation of the a vital molecular component of the SOCE pathway (Liou *et al.*, 2005). STIM1 and STIM2 siRNA transfected cells showed a significantly reduced plateau of cytosolic Ca^{2+} levels and the reduction of this level was detected following the same magnitude of initial Ca^{2+} peak (i.e., same level of transient Ca^{2+} release from the ER store). Interestingly, these two proteins had already been biochemically characterized to some extent even prior to the discovery of their link to SOCE. Specifically, STIM1 and STIM2 were known to contain a transmembrane

(TM) domain, an EF-hand Ca^{2+} binding domain, and were found to form homo- and hetero-oligomers (Williams *et al.*, 2001, 2002). Consequently, Liou *et al.* (2005) concluded that the two homologues, STIM1 and STIM2, must be the critical players of SOCE.

An independent study by Roos and colleagues (Roos *et al.*, 2005) investigated the essential players of the SOCE pathway in *Drosophila* S2 cells. They suppressed several targeted genes using RNA interference (RNAi), and by using TG and fura2, they discovered the *Drosophila* STIM orthologue protein was vital for mediating SOCE in this cell type. Furthermore, to distinguish which of the two mammalian homologues, STIM1 or STIM2, is responsible for SOCE, Roos and colleagues performed RNAi-mediated knockdown of human STIM1 in HEK293 and SH-SY5Y neuroblastoma cells over expressing STIM1 (Roos *et al.*, 2005). In both cases, cells displayed reduced Ca^{2+} influx upon TG treatment. However, knockdown of STIM2 in these cells showed unaltered levels of Ca^{2+} influx. Therefore, Roos *et al.* (2005) concluded STIM1, a protein that is ubiquitously expressed and conserved from *Drosophila* to mammalian cells, is an essential molecular player in SOCE.

In 2006, Prakriya and colleagues identified a protein called Orai1, a previously uncharacterized protein with four putative TM segments, to be involved in the SOCE pathway (Prakriya *et al.*, 2006). They performed a pedigree analysis to identify the missense mutation in Orai1 leading to defective Ca^{2+} entry via SOCE associated with severe combined immunodeficiency disease (SCID) (Feske *et al.*, 2006; Prakriya *et al.*, 2006). Furthermore, other groups that conducted a genome-wide RNAi screen in *Drosophila* cells to identify the gene responsible for SOCE Ca^{2+} influx similarly identified the orthologue of human Orai1 (Yeromin *et al.*, 2006; Zhang *et al.*, 2006a). Based on these early studies we now know that the identities of the molecules that mediate SOCE include the ER-inserted STIM proteins and the PM-resident Orai proteins. Importantly, it was found that co-overexpression of STIM1

and Orai1 results in very large increases (5-10-fold) in sustained cytosolic Ca^{2+} levels after ER lumen Ca^{2+} store depletion using TG, further reinforcing the role of STIM1 and Orai1 in the SOCE pathway (Mercer *et al.*, 2006). Additionally, when STIM1 interacted with Orai1 reconstituted in liposomes, a SOCE-like phenomenon was observed indicating that these proteins are the minimal requirements for SOCE (Gudlur *et al.*, 2014).

1.3 Stromal interaction molecule (STIM) and Orai

1.3.1 STIM and Orai domain architectures

After the discovery of STIM and Orai proteins as the principal molecular players of SOCE, determining the three-dimensional (3D) atomic resolution structure of these proteins was vital to understanding the precise mechanisms activating the SOCE pathway.

1.3.1.1 *STIM domain architectures*

STIM proteins are single-pass type I TM proteins and, in vertebrates, there are two homologues, STIM1 and STIM2. Although it was discovered that a small fraction of STIM1 is located on the PM, STIM proteins are mainly localized to the ER membrane (Manji *et al.*, 2000; Williams *et al.*, 2001; Zhang *et al.*, 2005; Cai, 2007a). The ER lumen-oriented region of STIM is composed of EF-hand and sterile α -motif (SAM) domains, and immediately following the TM domain there are three coiled-coil (CC) domains located on the cytosolic side of the protein (Figure 1.2). A long CC1 is located closest to the TM domain followed immediately by two shorter CC domains (i.e., CC2 and CC3); further, proximal to the CC region are proline- and serine-rich regions and lysine-rich region near the C-terminus (Figure 1.2) (Stathopoulos & Ikura, 2013a). The sequence comparison of the two human STIM homologues as well as STIMs from lower to higher eukaryotes (Stathopoulos & Ikura, 2013a),

reveals that the above mentioned domains are conserved, suggesting that they are vital to the function of STIM proteins across species.

There are two human STIM homologues, STIM1 and STIM2 with 76% sequence identity (Stathopoulos & Ikura, 2013a). Previously, more focus has been on studying STIM1 as the regulator of SOCE pathway activation but both homologues play a major role in regulating Ca^{2+} homeostasis in the cell. STIM1 and STIM2 differ in of the manner in which they maintain optimal Ca^{2+} levels in the cell with STIM1 being the ON/OFF switch of SOCE and STIM2 directly involved in sustaining basal Ca^{2+} levels (Stathopoulos & Ikura, 2013a). Both STIM1 and STIM2 proteins contain an ER localization sequence near the N-terminus. Whereas STIM1 contains a 22-residue ER signal peptide, STIM2 has an 87-residue insertion into this N-terminal region, resulting in a much longer ER signal peptide (Stathopoulos & Ikura, 2013a). Interestingly, the longer signal peptide of STIM2 is believed to decrease its ER localization efficiency, resulting in a small fraction of the pre-protein found in the cytoplasm instead of inserted in the membrane. Furthermore, such cytosolic STIM2 pre-protein is believed to regulate Orai1 in a Ca^{2+} store-independent manner, where it maintains basal Ca^{2+} levels and Ca^{2+} -dependent transcription (Graham *et al.*, 2011). STIM1 is expressed in most human tissues (Darbellay *et al.*, 2011; Horinouchi *et al.*, 2012).

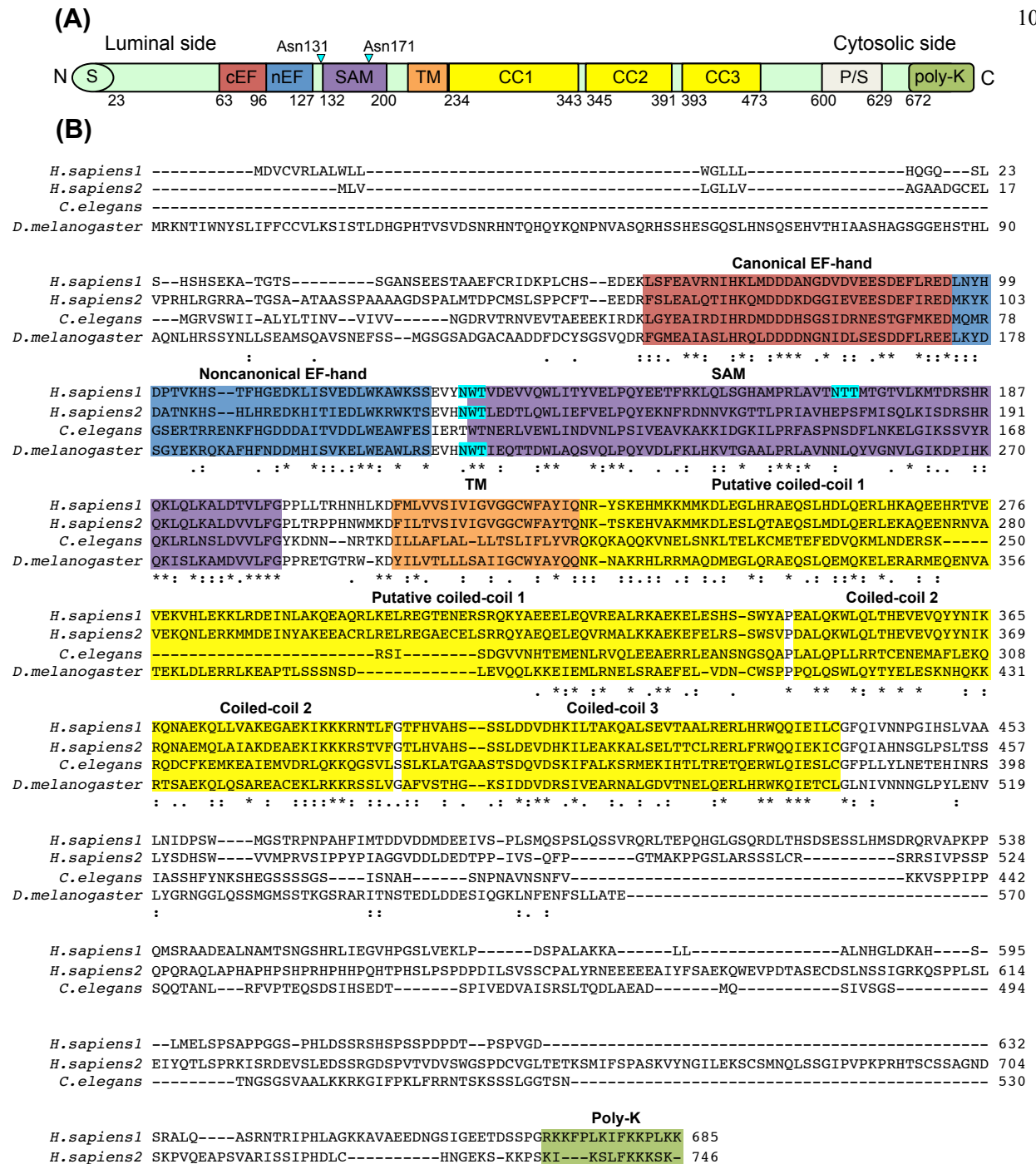


Figure 1.2. STIM1 domain architecture and sequence alignment. (A) STIM1 domain architecture. S indicates signaling peptide, cEF is the canonical EF-hand, nEF is the noncanonical EF-hand, SAM is the sterile alpha motif domain, and TM represents transmembrane domain. The relative positions of the Asn131 and Asn171 sites are shown as blue triangles above the domain positions. After the TM are three coiled coil domain (i.e., CC1-3), a proline and serine rich region (P/S) and a lysine rich region (poly-K) near the C-terminal domain. (B) Multiple sequence alignment of human and lower order STIM proteins. *H. sapiens* STIM1 (NCBI, NP_003147.2), *H. sapiens* STIM2 (NCBI, NP_065911.3), *Caenorhabditis elegans* STIM (NCBI, CCD73857.1), and *Drosophila melanogaster* STIM (NCBI, NP_523357.2) sequences were aligned using Clustal Omega (Sievers *et al.*, 2011) with the default settings. The (*) indicates fully conserved residue, (:) strongly similar residues, and (.) weakly similar residue. Conserved residue regions are shaded to correspond with the domain color scheme in A; glycosylation sites are highlighted in cyan.

1.3.1.2 *Orai domain architectures*

Orai proteins are PM-localized and are predicted to contain four TM domains; further, there are three human homologues, Orai1, Orai2, and Orai3 (Cai, 2007*b*). The three types of human Orai homologues share conserved primary sequence including specific residues responsible for dictating the channel characteristics, such as ion permeability, ion selectivity, and formation of a hydrophobic gate (Stathopoulos & Ikura, 2013*a*). Moreover, both N- and C-termini face the cytoplasm and are believed to play a role in the interaction with STIM1 that mediates channel assembly and gating (Stathopoulos & Ikura, 2013*a*). TM segment 1 (TM1) was identified to line the Ca²⁺ permeation pore within the Ca²⁺ channel, and Glu106 of TM1 and Glu190 of TM3 were found to form the Ca²⁺ binding site and provide Ca²⁺ selectivity, respectively (Prakriya *et al.*, 2006; Yeromin *et al.*, 2006). Similar to STIM proteins, different Orai proteins of lower order eukaryotes contain highly conserved TM regions and loop regions located between TMs. All Orai human homologues, when exogenously expressed have successfully formed functional Ca²⁺ released activated Ca²⁺ (CRAC) channels (Dehaven *et al.*, 2007; Gwack *et al.*, 2007; Lis *et al.*, 2007; Frischauf *et al.*, 2009; Bogeski *et al.*, 2010). However, the three homologues differ in sensitivity to Ca²⁺-dependent inactivation (Lis *et al.*, 2007) and even though Orai1, Orai2, and Orai3 are all widely expressed across human tissues (Gwack *et al.*, 2007; Schindl *et al.*, 2009), endogenous CRAC channels are only formed by the homomeric assembly of Orai1 proteins (Mignen *et al.*, 2008; Hou *et al.*, 2012; Thompson & Shuttleworth, 2013). It is still unclear how many Orai1 subunits are required to make a CRAC channel, and the two leading possibilities for the functional stoichiometry are hexamer or tetramer (Mignen *et al.*, 2008; Hou *et al.*, 2012; Thompson & Shuttleworth, 2013).

1.3.2 STIM1 and Orai1 in the activation of SOCE

The activation of SOCE involving STIM1 and Orai1 proteins is a multistep process (Figure 1.3). The pathway is initiated by the response of STIM1 to ER Ca^{2+} levels. As mentioned above, STIM1 acts as the ER luminal Ca^{2+} sensor, and the luminal domain contains a canonical Ca^{2+} binding EF-hand motif (Roos *et al.*, 2005; Liou *et al.*, 2005; Stathopoulos *et al.*, 2006). When the Ca^{2+} levels in the ER are at rest (i.e., $\sim 400\text{-}800\ \mu\text{M}$), Ca^{2+} ions are normally bound to the canonical EF-hand motif of STIM1. However, upon decreases in ER luminal Ca^{2+} levels (i.e., $\sim 100\text{-}400\ \mu\text{M}$) and a loss in the EF-hand Ca^{2+} binding, a structural change occurs in the STIM1 luminal domain that initiates oligomerization of the protein. The oligomerization of the STIM1 luminal domain induces structural changes in the cytosolic region of STIM1 that enhances the oligomerization of the molecule. The oligomerized STIM1 subsequently translocates to ER-PM junctions, forming puncta. At ER-PM junctions, oligomerized STIM1 recruits Orai proteins to the same punctate aggregates (Liou *et al.*, 2005, 2007; Zhang *et al.*, 2005). Puncta formation was shown using total internal reflective fluorescence (TIRF) microscopy in HeLa and HL1 cardiomyocyte cells co-expressing monomeric cherry tagged (mCh)-STIM1 and enhanced green fluorescence protein (eGFP)-Orai1 (Stathopoulos *et al.*, 2013). At resting ER Ca^{2+} levels, mCh and eGFP fluorescence is pervasive along the ER membrane and PM, respectively. However, when TG passively depletes the ER Ca^{2+} store, there is an accumulation of the fluorescence signal at ER-PM junctions, indicating puncta formation and the co-localization of STIM1 and Orai1 proteins within $\sim 100\ \text{nm}$ of the surface of the cell (Stathopoulos *et al.*, 2013). STIM1 assembles Orai proteins into open CRAC channels within these puncta at ER-PM junctions, thereby mediating Ca^{2+} influx from the extracellular space.

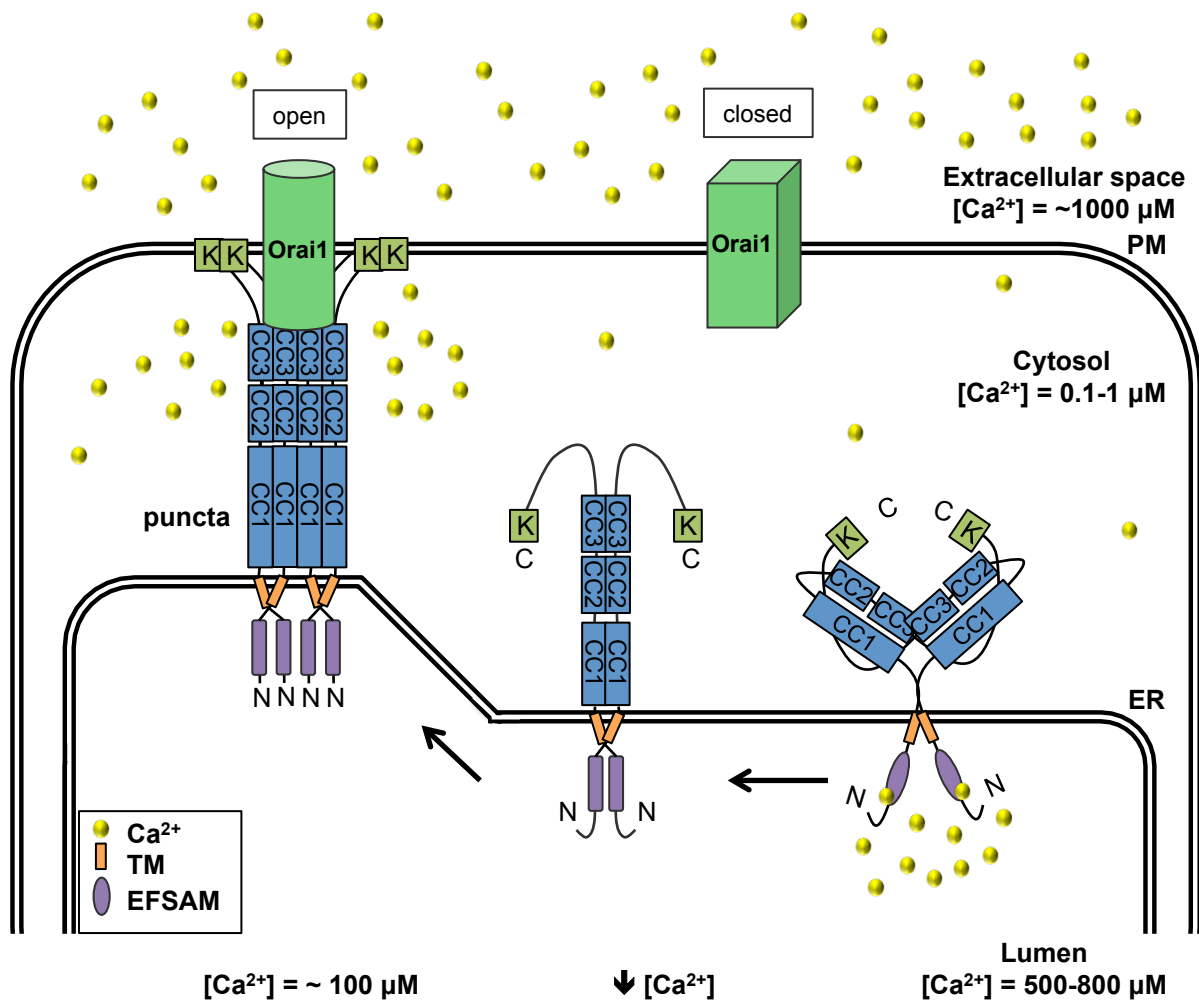


Figure 1.3. Schematic diagram of the SOCE molecular activation mechanism. Decreases of ER luminal Ca^{2+} levels initiates EFSAM oligomerization. Oligomerization promotes rearrangement of the coiled-coil domains that promotes translocation of STIM1 to ER-PM junctions. The STIM1 puncta at ER-PM junctions recruit Orai1 to the same sites, assembling and opening CRAC channels that promote cytosolic Ca^{2+} influx down a steep concentration gradient from the extracellular space that contains high Ca^{2+} into the cytosol.

1.4 STIM1 luminal domain

1.4.1 STIM1 luminal domain structure

The STIM1 luminal domain has conserved EF-hand and SAM domains close in sequence space that fold cooperatively into a single globular domain. Therefore, this region is also known as the EFSAM domain of STIM1. The EFSAM domain is highly conserved from lower to higher functioning eukaryotes. The human STIM1 EFSAM domain includes residues 63 to 201 and consists of a canonical Ca^{2+} binding EF-hand (cEF) motif, a non-canonical EF-hand (nEF) motif and a SAM domain. Stathopoulos and his colleagues discovered that an EFSAM mutant consisting of residues 58 to 201 contained a high fraction of α -helical secondary structure in the presence of Ca^{2+} and showed a well-dispersed ^1H - ^{15}N heteronuclear single quantum coherence (HSQC) spectrum, indicative of a well-folded protein (Stathopoulos *et al.*, 2006, 2008).

Based on primary sequence, the cEF motif was identified as the only EF-hand in STIM1 because of a conventional helix-loop-helix motif characteristics and the appropriate negatively charged residues in the loop (Kretsinger & Nockolds, 1973). However, the high resolution 3D structure solved by solution nuclear magnetic resonance (NMR) revealed that a second EF-hand was present in EFSAM (Stathopoulos *et al.*, 2008). This was an important discovery since the cEF was considered to be functioning as a stand-alone Ca^{2+} binding domain (Williams *et al.*, 2001; Roos *et al.*, 2005; Liou *et al.*, 2005; Zhang *et al.*, 2005; Baba *et al.*, 2006; Mercer *et al.*, 2006) prior to the elucidation of the EFSAM structure. Furthermore, it was found that one important role of the nEF motif is to stabilize cEF through backbone hydrogen (H)-bonding between the loop regions of each motif, creating a small β -sheet as observed in other conventional cEF pairs such as calmodulin (CaM) (Ikura *et al.*,

1985; Stathopoulos *et al.*, 2008). CaM is made up of two EF-hand domains linked through a flexible linker, and each of these domains is made up of two cEF motifs (Ikura *et al.*, 1985; Chin & Means, 2000). Ca²⁺-loaded CaM has interhelix EF-hand angles of 81.4° and 107.7° indicative of an “open” EF-hand motif conformation; the cEF (α 1- β 1- α 2) and nEF (α 3- β 2- α 4) of EFSAM also adopt this “open” conformation with approximately perpendicular interhelix angles of ~80° and 96.7° (Stathopoulos *et al.*, 2008). This feature of EF-hand domains results in the formation of a hydrophobic pocket that promotes interactions with target proteins. In the case of EFSAM, the SAM domain intramolecularly interacts with this extensive hydrophobic area created by the STIM1 EF-hand pair (Stathopoulos *et al.*, 2008).

There is a cooperative interaction between the STIM1 EF-hand and SAM domains of STIM1 (Figure 1.4). The EF-hand domain is linked to the SAM domain with a short helix (α 5), and the SAM domain consists of five helices (α 6- α 10) folded in a five-helix bundle (Stathopoulos *et al.*, 2008). The hydrophobic pocket created by cEF and nEF allows the α 10 helix of the SAM domain to tightly pack into this pocket forming a compact globular shape overall (Stathopoulos *et al.*, 2008). Thus, the EF-hand and SAM domains are not only linked in sequence space through α 5, but they also interact through regions that are distant in sequence space. The intramolecular interaction between EF-hand and SAM domain is an important structural feature that plays an essential role in the regulation of STIM1 activation and function in the SOCE pathway.

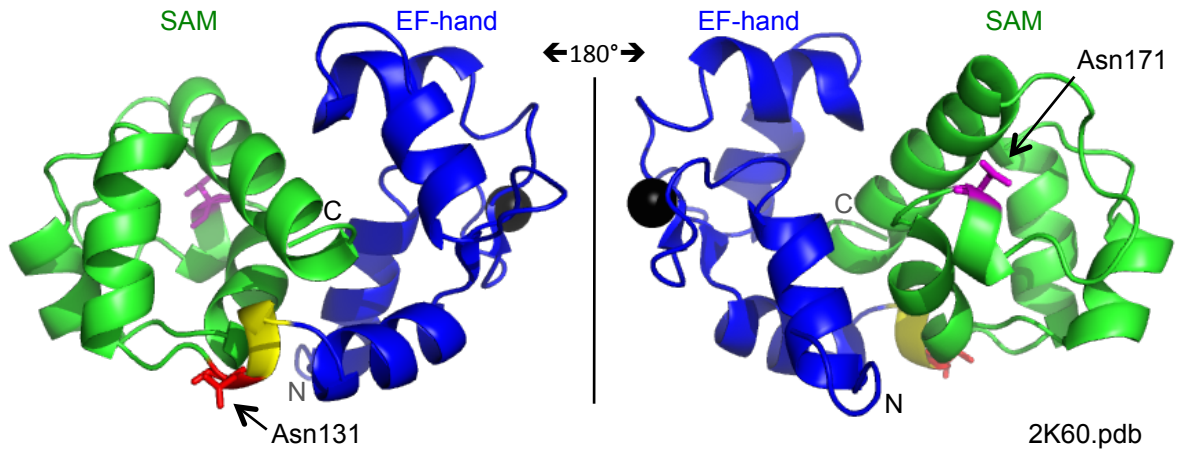


Figure 1.4. Depiction of the backbone structure of the Ca²⁺-loaded EFSAM domain. The EF-hands are coloured blue, the SAM domain is coloured green and the short linker helix is coloured yellow. Ca²⁺ is represented as a black sphere; N, amino terminus; C, carboxy terminus. The two asparagine residues, Asn131 and Asn171, are highlighted as red and magenta sticks, respectively. The Asn131 and Asn171 residues undergo *N*-linked glycosylation (see below).

1.4.2 Biophysical properties of STIM1 luminal domain

The initial step of the SOCE pathway starts with the depletion of ER Ca^{2+} levels. Under resting ER Ca^{2+} levels, the STIM1 luminal EFSAM domain is bound to Ca^{2+} (Stathopoulos *et al.*, 2006; Stathopoulos & Ikura, 2013b). With the cEF coordinating Ca^{2+} , the EF-hand and SAM domains are well folded, forming the stable and compact monomeric conformation within STIM1 described above (Stathopoulos *et al.*, 2006, 2008). However, in the absence of Ca^{2+} , this region loses a large fraction of its α -helicity and is drastically destabilized (Stathopoulos *et al.*, 2006, 2008). Dissociation of Ca^{2+} from the cEF binding site triggers an EFSAM unfolding event. This partial protein unfolding is coupled with a decreased stability and results in oligomerization of the STIM1 luminal domains. The EFSAM oligomers are polydisperse, consisting of dimers and larger order oligomers. STIM1 oligomerized through the luminal domains results in a rearrangement of the cytosolic domains, oligomerization of the CC regions and translocation to the ER-PM junctions, establishing puncta. Thus, luminal EFSAM STIM1 oligomerization is the initiation event that leads to STIM1 translocation, recruitment and gating of Orai1 channels at ER-PM junctions, resulting in open CRAC channels on the PM (Zhang *et al.*, 2005; Stathopoulos *et al.*, 2006, 2008; Liou *et al.*, 2007).

Assessment of EFSAM Ca^{2+} binding using a $^{45}\text{Ca}^{2+}$ equilibrium ultrafiltration procedure and positive electrospray ionization mass spectrometry revealed a single low affinity Ca^{2+} binding site with an equilibrium dissociation constant (K_d) of $\sim 200\text{-}600\ \mu\text{M}$ (Stathopoulos *et al.*, 2006; Huang *et al.*, 2009; Zheng *et al.*, 2011). Furthermore, this K_d range is consistent with the physiological range of Ca^{2+} concentrations found in the ER lumen, suggesting that the EFSAM Ca^{2+} binding property is optimized to the Ca^{2+} fluctuations of the lumen for the regulation of SOCE.

1.5 N-glycosylation of STIM1

In eukaryotes, most proteins undergo post-translational modifications for an added layer of protein regulation and selective participation in cellular processes (Walsh *et al.*, 2005; Boscher *et al.*, 2011). A common modification is glycosylation where there is an attachment and processing of oligosaccharide structures, also known as glycans, through various biosynthetic steps in the ER and Golgi (Dennis *et al.*, 2009; Nilsson *et al.*, 2009; Stanley, 2011). The process of glycosylation can distinctly be separated into two types: *N*-linked and *O*-linked glycosylation based on specific amino acid and linkage it forms.

1.5.1 *N*-linked glycosylation

In *N*-linked glycosylation, glycans are attached to the side chain amide of asparagine (Asn), and in most cases, the initiation step occurs in the ER as the polypeptide chain moves into the lumen and is still being translated outside the membrane; therefore, it is sometimes considered a co-translational modification (Gerlach *et al.*, 2012). On the other hand, *O*-linked glycosylation refers to the addition of glycans on the side chain hydroxyl group of serine or threonine residues, and this modification occurs entirely after translation in the Golgi complex (Gerlach *et al.*, 2012). The consensus amino acid sequence needed in the nascent polypeptide chain for *N*-linked modification is Asn-X-Ser/Thr/Cys, where X can be any amino acid except proline. When this sequence is recognized, the first step is the transfer of a fourteen-sugar structure made up of glucose (Glc), mannose (Man), and N-acetylglucosamine (GlcNAc) (i.e., Glc₃Man₉GlcNAc₂) from an ER membrane lipid by oligosaccharyltransferase (Pearse & Hebert, 2010; Stanley *et al.*, 2014). Further steps, such as cleavage or transfer of glucose residues, are catalyzed in the ER by specific glycosidases and glycosyltransferases. During modification in the ER, there are specific proteins such as UDP-glucose:glycoprotein

glucosyltransferase, that monitor proper protein folding upon glucose cleavage prior to further modification steps (Gerlach *et al.*, 2012). Some proteins that are properly folded successfully leave the ER and move into the Golgi, and in the Golgi, a mannose subunit is removed to generate Man₈GlcNAc₂ to prevent further glucosylation (Avezov *et al.*, 2008).

1.5.2 *N*-glycosylation of EFSAM

Examination of the EFSAM primary amino acid sequence reveals two consensus *N*-linked glycosylation sites: Asn(residue 131)-Trp-Thr and Asn(residue 171)-Thr-Thr (Figure 1.2). Further, previous studies have indeed shown that the EFSAM domain can be *N*-glycosylated on Asn131 and Asn171 (Williams *et al.*, 2002; Csutora *et al.*, 2008; Kilch *et al.*, 2013). The first study by Williams and colleagues (Williams *et al.*, 2002) found that a fraction of STIM1 is localized to the PM, where the EFSAM domain is oriented in the extracellular space. Furthermore, they discovered that inhibition of *N*-glycosylation using tunicamycin prevented STIM1 localization to the PM. Williams and coworkers also showed that both *N*-linked glycosylation of Asn131 and Asn171 were endoglycosidase H (endoH)-sensitive (Williams *et al.*, 2002). EndoH is an enzyme that digests glycans and is commonly used to study *N*-glycosylated proteins. EndoH cleaves the chitobiose core dimer of β -1,4-linked GlcNAc in high mannose and some hybrid oligosaccharides that are modified in the Golgi, but is unable to cleave fully Golgi processed proteins with complex glycans. Therefore, the findings by Williams *et al.*, on the endoH sensitivity of STIM1 indicates the immature modification and the absence of full terminal processing in the Golgi is sufficient for cell surface expression of STIM1 (Williams *et al.*, 2002). Other STIM1 glycosylation studies by Csutora and Kilch and coworkers will be discussed below.

1.6 Rationale, hypothesis, and objectives

1.6.1 Rationale and hypothesis

While it is established that STIM1 has two *N*-glycosylation sites within the ER luminal region (i.e., the Asn131 site located in the short linker α -helix between the EF-hand and SAM domain and the second Asn171 site located within the SAM domain) the precise effect of *N*-glycosylation on the activation and function of STIM1 is unknown. Further, there are several ambiguous and inconsistent observations in the available literature on how *N*-glycosylation may affect SOCE (Mignen *et al.*, 2007; Csutora *et al.*, 2008; Czyz *et al.*, 2009; Kilch *et al.*, 2013). A study by Czyz and colleagues found SOCE activity is enhanced in tunicamycin treated Jurkat cells. Tunicamycin inhibits endogenous glycosylation of all proteins; moreover, measurement of cytosolic Ca^{2+} concentrations with fura2 showed enhanced SOCE in tunicamycin treated Jurkat cells (Czyz *et al.*, 2009). In a separate study, Kilch and colleagues, mutated the Asn131 and Asn171 of STIM1 to aspartic acid and glutamine (Gln), respectively, and found enhanced SOCE (Kilch *et al.*, 2013). However, when they mutated both residues to Gln, SOCE was abolished. Mignen *et al.*, also studied the effect of Asn to Gln double mutations in STIM1, but in contrast to the Kilch *et al.*, study they found that the Asn131Gln/Asn171Gln double mutant had no effect on CRAC channel function using electrophysiological measurements (Mignen *et al.*, 2007). On the other hand, work done by Csutora and coworkers showed that the Asn131Gln/Asn171Gln STIM1 double mutant inhibits SOCE (Csutora *et al.*, 2008). Csutora *et al.*, transfected the double mutant STIM1 into neuronal NG115 cells that endogenously express very low levels of STIM1 and found that SOCE was suppressed compared to the wild-type STIM1-mediated process (Csutora *et al.*, 2008).

The published inconsistencies on how STIM1 N-glycosylation affects STIM1 function reveal a pressing need to study the precise effect of glycosylation on EFSAM at the molecular and atomic levels. Since the initiation of the STIM activation process is entirely dependent on the EFSAM domain, a comparison of the structural, biophysical and biochemical changes caused by glycosylation of EFSAM should reveal how this modification affects STIM1 regulation of SOCE. Therefore, my thesis work focuses on how glycosylation affects the Ca^{2+} sensing properties of STIM1 EFSAM. I hypothesize that glucose conjugation to the STIM1 EFSAM domain at the Asn131 and/or Asn171 sites (i.e., neo-glycosylation) will alter the molecular properties of EFSAM as well as normal SOCE regulation.

1.6.2 Objectives

Aim 1: To express and purify recombinant wild type and mutant EFSAM proteins for site-specific neo-glycosylation.

I mutated Asn131 and Asn171 to cysteine (Cys) within an EFSAM recombinant expression vector to enable an enzyme-free *in vitro* approach for site-specifically controlling modifications at these sites. Cysteine residues have a thiol group that allows methanethiosulfonate-derivatized glucose to be covalently attached to the protein via disulfide bond formation. Glucose conjugation to the protein in this manner mimicked endogenous glycosylation with respect to the proximity of a glucose moiety close to the surface of the protein.

Aim 2: To study the effect of neo-glycosylation on the structure, stability, oligomerization, and Ca^{2+} binding properties of the EFSAM domain.

STIM1 structure is highly dynamic and its biophysical properties are intimately linked to its activation. Therefore, examining the neo-glycosylation-induced changes in structure, stability, oligomerization and Ca^{2+} binding affinity provides a better understanding of the mechanisms by which glycosylation regulates STIM1 activity and the SOCE pathway.

Aim 3: To examine the role of Asn131 and Asn171 glycosylation in STIM1 activated SOCE using HEK293 mammalian cell culture.

I overexpressed mCh-tagged STIM1 with Asn131Gln, Asn171Gln or Asn131Gln/Asn171Gln mutations in HEK293 cells that were stably expressing YFP-Orai1. The mutations to Gln were engineered to block endogenous glycosylation at these sites within STIM1 without dramatically altering the polypeptide properties due to the similar nature of the Asn and Gln side chains. HEK293 mammalian cells are a good model system because this cell line expresses little or no STIM1 and Orai1 (Williams *et al.*, 2001; Roos *et al.*, 2005; Dehaven *et al.*, 2007). The STIM1 activated cytosolic Ca^{2+} uptake in response to ER-luminal Ca^{2+} depletion by TG was studied using a fura2 ratiometric fluorescence approach.

Chapter 2

Methods

2.1 Constructs and Mutations

The human STIM1 Ca^{2+} sensing domain corresponding to residues 58-201 was expressed in *Escherichia coli* using the previously described pET-28 α -EFSAM vector (Stathopoulos *et al.*, 2006). The two asparagine residues (i.e., Asn131 and Asn171) were mutated to cysteines with High-Fidelity PCR polymerase (Thermo Scientific, Inc.), and mutagenic primers (Table 2.1). Two separate PCR mixtures, each with forward or reverse primers, were prepared and templates were amplified according to a 10-cycle mutagenesis program (Table 2.2). When 10 cycles were complete, the two separate PCR reactions were immediately mixed and amplified 25 additional cycles, using the same program (Table 2.2). After amplification was completed, the template vector was digested using DpnI (New England BioLabs, Inc.) for 2 h at 37 °C. The amplified DNA was subsequently transformed by heat shock into competent *E. coli* DH5 α to repair the nicks and propagate the plasmid. Colonies harboring the mutated pET-28 α -EFSAM plasmid were selected on kanamycin-containing agar plates. After two single mutations had been engineered (i.e., Asn131Cys and Asn171Cys), the pET-28 α -EFSAM-Asn131Cys was used as template to generate a cDNA containing the double mutation (i.e., Asn131Cys/Asn171Cys).

For mammalian cell protein expression, the previously described pCMV6 vector encoding full-length human STIM1 (i.e., residues 1-685) with mCh fused just after the ER signal peptide (i.e., residue 1-23) was used (Stathopoulos *et al.*, 2008). The Asn131 and Asn171 residues were mutated to glutamine in the pCMV6-mChSTIM1 vector using the same mutagenesis approach as described above and the mutagenic primers described in (Table 2.1). Colonies harboring the mutated pCMV6-mChSTIM1 plasmid were selected on ampicillin-containing agar plates. The double Asn131Gln/Asn171Gln mutation was also engineered using the pCMV6-mChSTIM1-Asn131Gln vector as a template.

Table 2.1. Primers used for mutagenesis and sequencing. All primers were synthesized by Sigma-Aldrich (St. Louis, MO).

Primer	Nucleotide Sequence
EFSAM Asn131Cys ^a	5'-GTCATCAGAAGTATACTGTTGGACCGTGGATGAGG-3' 3'-CAGTAGTCTTCATATGACAACCTGGCACCTACTCC-5'
EFSAM Asn171Cys ^a	5'-CCAAGGCTGGCTGTCACCTGCACCACCATGACAGGG-3' 3'-GGTTCCGACCGACAGTGGACGTGGTGGTACTGTCCC-5'
STIM1 Asn131Gln ^b	5'-GTCATCAGAAGTATAACCAGTGGACCGTGGATGAGG-3' 3'-CAGTAGTCTTCATATGGTCACCTGGCACCTACTCC-5'
STIM1 Asn171Gln ^b	5'-CCAAGGCTGGCTGTCACCCAAACCACCATGACAGGG-3' 3'-GGTTCCGACCGACAGTGGGTTTGGTGGTACTGTCCC-5'
T7 terminator ^c	5'-GCTAGTTATTGCTCAGCGG-3'
STIM1 ^c	5'-AGCTCGGGGGCCAACTCTGAGGAG-3'

^aMutagenesis primer for pET-28 α

^bMutagenesis primer for pCMV6-XL5-mCh-STIM1

^cSequencing primers

Table 2.2. PCR amplification template on LifeECO (Bioer)

			pET-28 α parameters		pCMV6 parameters		
	<i>10-Cycles</i>		<i>25-Cycles</i>		<i>25-Cycles</i>		
	Temp (°C)	Time	Temp (°C)	Time	Temp (°C)	Time	
Initial Denaturation	98.0	35 s	98.0	35 s	98.0	30 s	
<i>Denaturation</i>	98.0	10 s	98.0	10 s	98.0	10 s	
#-Cycles	<i>Annealing</i>	56.5	30 s	56.5	30 s	55.5	30 s
	<i>Extension</i>	72.0	5 min	72.0	5 min	72.0	3 min
Final Elongation			72.0	5 min 30 s	72.0	5 min	
Storage	4.0	Hold	4.0	Hold	4.0	Hold	

All mutant pET-28 α -EFSAM constructs (i.e., Asn131Cys, Asn171Cys, Asn131Cys/Asn171Cys) were verified by dideoxy sequencing using the T7 reverse terminator primer (Table 2.1) at the Robart's DNA Sequencing facility (<http://www.robarts.ca/london-regional-genomics-centre>). Successful mutagenesis of the pCMV6-mChSTIM1 constructs (i.e., Asn131Gln, Asn171Gln, Asn131Gln/Asn171Gln) was verified using an in-house designed primer (Table 2.1) and sequenced at the Robart's DNA Sequencing facility.

2.2 Protein expression and purification

2.2.1 Protein expression

pET-28 α -EFSAM (i.e., wild-type, Asn131Cys, Asn171Cys, Asn131Cys/Asn171Cys) were separately transformed into *E. coli* BL21 Δ E3 codon (+) competent cells and plated on kanamycin resistant Luria broth (LB) agar plates. A single colony was picked and subsequently cultured in 1 L of LB medium supplemented with 60 μ g/ml kanamycin at 37 $^{\circ}$ C and \sim 190 rpm, until the optical density at 600 nm (OD₆₀₀) reached 0.6-0.8. Subsequently, 200 μ M of isopropyl β -D-1-thiogalactopyranoside (IPTG) was added to induce protein expression. After IPTG addition, the cells were incubated at ambient temperature overnight with constant shaking. Bacteria were harvested by centrifugation in a J2-21M Induction drive centrifuge (Beckman, Inc.) with JA10 rotor at 7250 rpm, 4 $^{\circ}$ C for 25 min, and the cell pellet was collected and stored at -80 $^{\circ}$ C until purification.

For uniformly 15 N-labelled EFSAM proteins used in the solution NMR experiments (see below), bacterial cells were grown in M9 minimal media salts (i.e., 42.2 mM of

Na₂HPO₄ anhydrous, 22.0 mM of KH₂PO₄, 8.6 mM of NaCl, pH7.4 in 1 L) supplemented with a 0.2 µm filtered mixture of 0.2% w/v D-glucose, 100 µM CaCl₂, 50 µM thiamine, 1 mM MgSO₄, 1 mg/L biotin, 1 g/L ¹⁵N-NH₄Cl labeling, and 60 µg/ml kanamycin. Cell growth, IPTG induction, cell harvesting and purification (see below) were exactly as described for LB broth (see above).

2.2.2 Protein purification

Since EFSAM formed inclusions due to the low intracellular Ca²⁺ levels of *E. coli*, the frozen bacterial cell pellet was manually homogenized in 6 M guanidine-HCl and 20 mM Tris-HCl (pH 8), to resolubilize the aggregated protein. Approximately 30 mL of guanidine-HCl was added per 5 mL of wet cell pellet. Subsequently, the mixture was incubated for 90 min at ambient temperature with constant rotation in a hybridization oven. The homogenized mixture was subsequently centrifuged in J2-21M Induction drive centrifuge (Beckman, Inc.) with JA10 rotor at 7500 rpm, 8 °C for 40 min to separate the insoluble cell debris (pellet) from the soluble protein mixture (i.e., supernatant). 750 µL of a 50% (v/v) Ni-Nitrilotriacetic acid agarose bead slurry (Qiagen, Inc.) was added to the clarified lysate (~30 mL) and incubated for another 90 min at room temperature by inversion in a hybridization oven. Subsequently, the beads with captured 6×His-tagged proteins were collected in a gravity flow protein purification column and washed 3 times with 10 mL of 6 M urea with 20 mM Tris-HCl pH 8 and 5 mM β-mercaptoethanol for the mutant proteins. The proteins were eluted in 7 2-ml fractions using 6 M urea, 20 mM Tris-HCl pH 8, 300 mM imidazole, and 5 mM β-mercaptoethanol for the mutant proteins (Figure 2.1A). The eluted protein fractions were pooled into a dialysis membrane with a 3500 Da molecular weight cutoff (BioDesign Inc.) and incubated in 1 L refolding buffer (Table 2.3) at 4°C overnight.

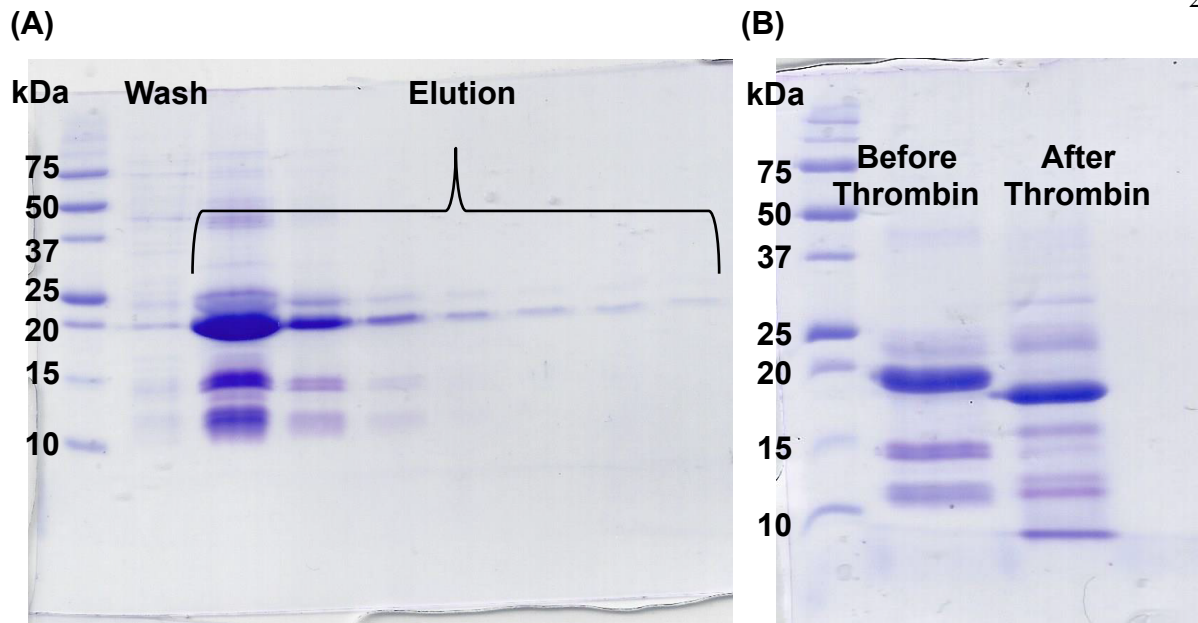


Figure 2.1. SDS-PAGE gel analyses of STIM1 EFSAM purification. (A) Wild-type 6×His-EFSAM (~19 kDa) protein elution fractions from Ni-NTA beads. (B) Migration of wild-type EFSAM before (~19 kDa) and after (~17 kDa) 6×His thrombin digestion. The gels in (A) and (B) were 15 % (v/v) stained with Coomassie blue, and the molecular weight marker migration is shown at the leftmost lane of each gel.

Table 2.3. Components of the experimental buffers used in the thesis research.

Refolding buffer	20 mM Tris-HCl pH 8.0, 150 mM NaCl, 5 mM CaCl ₂ , 1 mM dithiothreitol (DTT) for mutants
Ion Exchange Buffer A	20 mM Tris-HCl pH 8, 5 mM CaCl ₂ , 1 mM DTT for the mutants
Ion Exchange Buffer B	20 mM Tris-HCl pH 8, 1 M NaCl, 5 mM CaCl ₂ , 1 mM DTT for the mutants
Ca²⁺-loaded buffer	20 mM Tris-HCl pH 7.5, 150 mM NaCl, 5 mM CaCl ₂ , 1 mM tris(2-carboxyethyl)phosphine (TCEP) for non modified mutants
Ca²⁺-free buffer	20 mM Tris-HCl pH 7.5, 150 mM NaCl, 1 mM TCEP for non-modified mutants
Modification Buffer	20 mM 3-(N-morpholino)propanesulfonic acid (MOPS) pH 8.3, 150 mM NaCl, 5 mM CaCl ₂ , 0.1 mM TCEP
Modified Ca²⁺-loaded buffer	20 mM Tris-HCl pH 7.5, 150 mM NaCl, 5 mM CaCl ₂
Modified Ca²⁺-free buffer	20 mM Tris-HCl pH 7.5, 150 mM NaCl

After overnight refolding, approximately 1 U of thrombin (BioPharm Laboratories, Inc.) per mg of protein was added directly to the dialysis bag and incubated again at 4 °C overnight. Successful cleavage of 6×His tag was verified by a shift in the migration of the protein visualized by Coomassie-blue staining of denaturing polyacrylamide gels, after electrophoresis (Figure 2.1B). 100 μM of 4-(2-Aminoethyl) benzenesulfonyl fluoride hydrochloride (AEBSF) was added before further purification to inhibit thrombin and other proteases until further purification.

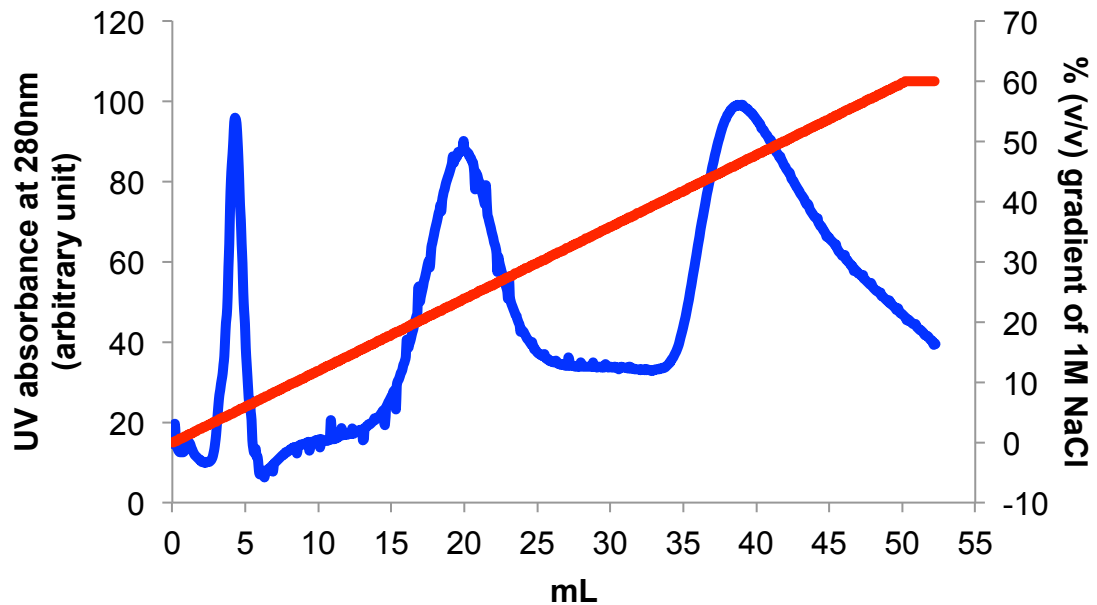
2.2.3 Anion Exchange chromatography

Anion exchange chromatography was used to further purify the EFSAM proteins, with an increasing NaCl gradient (Buffer B). Protein solutions were concentrated approximately 10-fold then re-diluted in a NaCl-free (Buffer A) (Table 2.3). Protein was manually loaded onto a HiTrap™ Q FF anion exchange column (GE Healthcare, Inc.) using a 10 mL syringe. Proteins were eluted in a gradient [i.e., 0 – 60 % (v/v)] of increasing Buffer B (Table 2.3) (Figure 2.2A). Ion exchange elution fractions were assessed for purity using Coomassie blue-stained SDS-PAGE gels (Figure 2.2B). Fractions with purity of > 95 % were pooled and exchanged to Ca²⁺-loaded buffer (Table 2.3) using a Vivaspin20 centrifugal concentrator (Sartorius, Inc.).

2.2.4 Preparation of Ca²⁺-free apo protein samples

To prepare Ca²⁺-free (i.e., apo) protein samples, 25 mM of ethylenediamine tetraacetic acid (EDTA) was added to the sample and incubated overnight at 4 °C. Samples were concentrated to ≤1 mL and diluted in the buffer of interest, Ca²⁺-free buffer (Table 2.3), to ~20 ml and re-concentrated to 1 mL using Vivaspin20 exchanger (Sartorius, Inc.). This process was repeated three times for a 20×20×20-fold exchange.

(A)



(B)

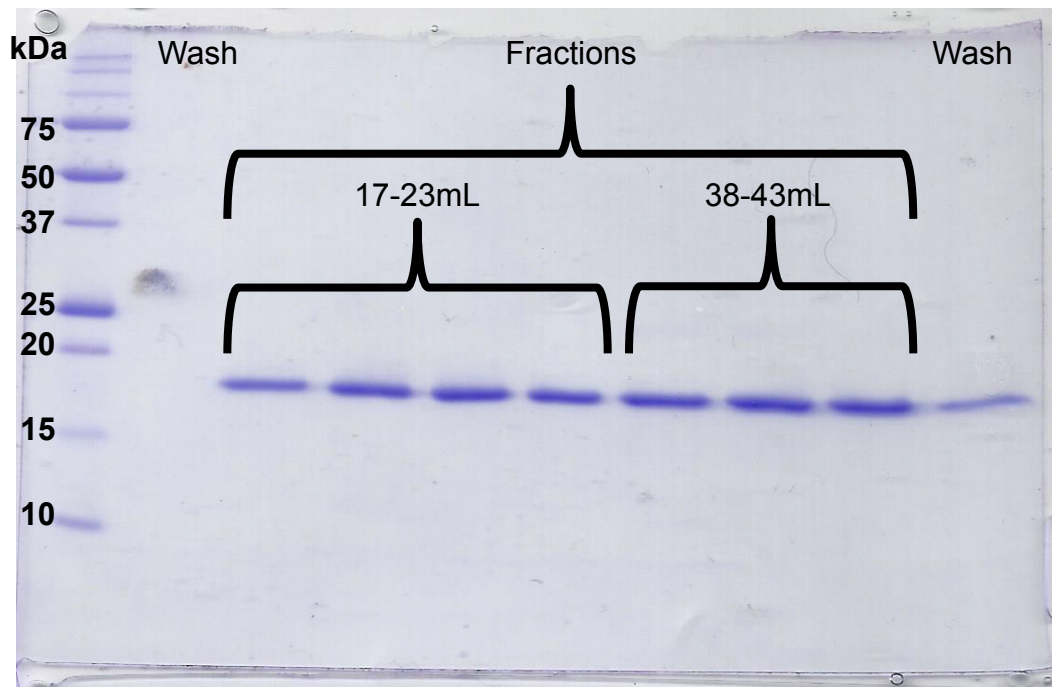


Figure 2.2. Anion exchange chromatographic separation of wild-type EFSAM protein. (A) Anion exchange chromatogram of wild-type EFSAM in an increasing NaCl gradient [i.e., 0 to 60 % (v/v)]. The blue line represents the UV absorbance at 280 nm and the red line represents the % (v/v) gradient of 1 M NaCl. (B) Coomassie blue stained SDS-PAGE gel [15 % (v/v)] of the wild-type EFSAM elution fractions shown in (A). The leftmost lane shows the molecular weight marker migration.

2.3 Neo-glycosylation of EFSAM

The protein sample was exchanged into the modification buffer (Table 2.3) using the same exchange approach mentioned above (2.2.4). A 55 mM stock solution of N-(β -D-glucopyranosyl)-N'-[2-methanethiosulfonyl]ethyl]urea (MTS-5-glucose) (Toronto Research Chemicals, Inc.) was prepared in dimethylsulfoxide (DMSO). A final concentration of 2 mM MTS-5-glucose was added to ~ 60 μ M protein samples and incubated in the dark for 1 h at ambient temperature with mixing by gentle tapping of the microfuge tube every 10 min. Subsequently, the protein was re-exchanged into the final modified Ca^{2+} -loaded buffer using a Vivaspin20 centrifugal concentrator (Sartorius, Inc.). Modified apo protein samples were prepared exactly as described for the Ca^{2+} loaded samples, using however, the modified Ca^{2+} -free buffer shown in Table 2.3. The glucose conjugation to the protein is termed neo-glycosylation in this thesis; therefore, modified EFSAM proteins are referred to as neo-glycosylated EFSAMs.

To validate the modification protocol, I performed electrospray ionization mass spectrometry on the Asn171Cys EFSAM protein sample which I was able to obtain at the highest yield, compared to all the mutant EFSAMs studied. The unmodified Asn171Cys mutant has a theoretical mass of 17,346.38 Da, and the MTS-5-glucose compound has a mass of 360.40 Da. Upon successful modification, the expected mass of gl-Asn171Cys protein (MTS-5-glucose modification represented as gl) is 17,626.67 Da [i.e., $17,346.38 - \text{H}^+ (1.01) + 360.40 - \text{CH}_3\text{SO}_2 (79.10)$]. The modified gl-Asn171Cys sample was exchanged into 20 mM ammonium bicarbonate and 2 mM CaCl_2 , pH 8 using the dialysis method. The prepared sample was sent to the Biological Mass Spectrometry Laboratory in London Regional Proteomic Centre (<http://www.uwo.ca/biochem/lrpc/LRPC.html>). The mass spectrum revealed the bulk of the protein had a mass of 17,628.05 Da, which was within 1.4 Da of the

expected theoretical mass for the glucose modified Asn171Cys protein (i.e., gl-Asn171Cys) (Figure 2.3). Importantly, no detectable unmodified Asn171Cys protein was observed in the spectrum above the baseline level, confirming a highly efficient modification procedure. The relatively large intensity peak observed at 17,380.78 Da corresponds to +34 Da or -247 Da compared to the unmodified and modified protein, respectively, and so the identity of this peak could not be reliably inferred. After validation of the modification protocol by this mass spectrometry experiment, a similar procedure was used to modify the Asn131Cys and Asn131Cys/Asn171Cys proteins; additional confirmation of the modification was obtained by solution NMR, which gave no indication of peak doubling associated with partial modification.

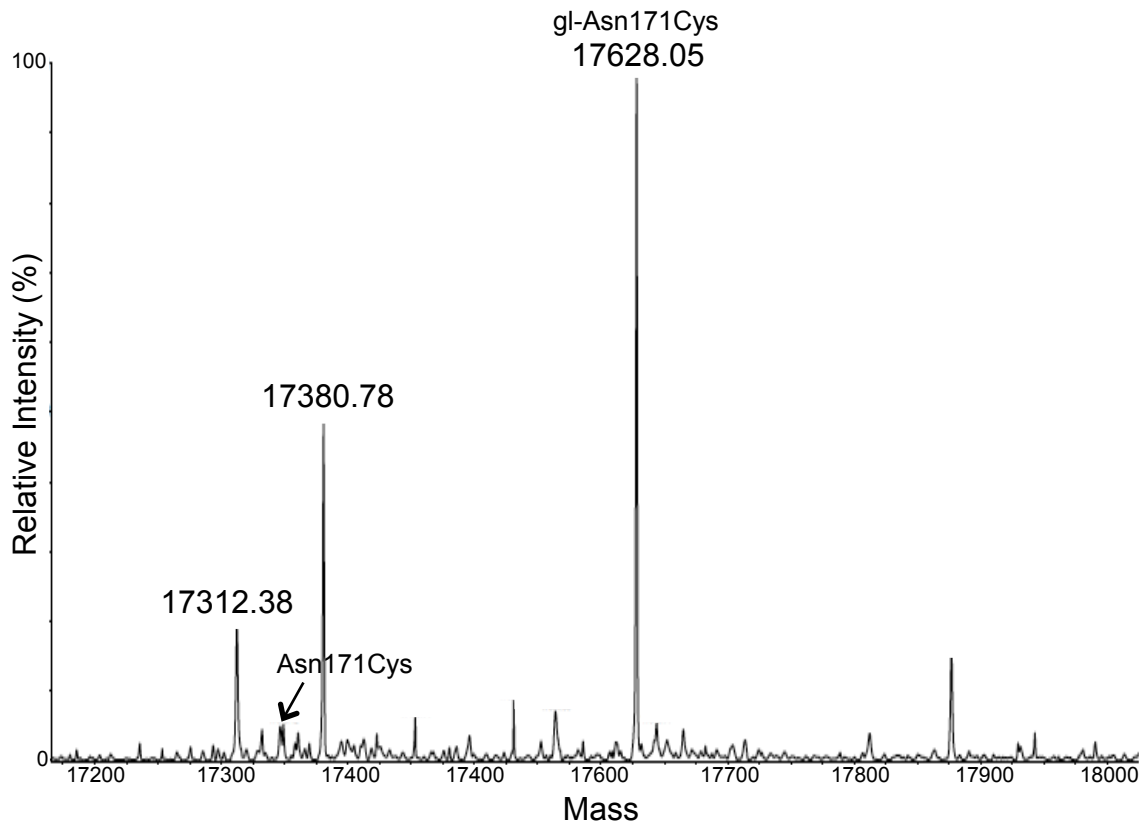


Figure 2.3. Positive ionization electrospray mass spectrum of glucose conjugated Asn171Cys EFSAM protein. Approximately 57 nM of protein was exchanged in 20 mM ammonium bicarbonate and 2 mM CaCl_2 , pH 8. The mass spectrometry measured mass of gl-Asn171Cys was within 1.4 Da of the expected theoretical mass; $\text{Asn171Cys} + \text{gl} = 17,346.38 + 280.40 = 17,626.78$.

2.4 Far-UV circular dichroism (CD) spectroscopy

A Jasco-J-810 Spectrometer equipped with a Jasco PTC-423S temperature controller was used to measure the far-UV CD spectra for samples prepared at 1 mg/mL in the presence and the absence of 5 mM CaCl₂. A 0.01 cm pathlength quartz cuvette was used to acquire the CD spectra. Spectra were collected at 4 °C between 250 nm to 190 nm, with a scanning speed of 20 nm/min, response time 8 s, an average of 3 accumulations and 1 nm data pitch. Protein spectra were corrected for buffer contributions.

2.4.1 Thermal stability using far-UV CD spectroscopy

Thermal stabilities were taken from the change in ellipticity at 225 nm as a function of temperature. For these thermal melts, a 0.1 cm pathlength quartz cuvette was used with protein concentrations of ~0.5 mg/mL. The temperature was increased from 4 °C to 75 °C at 1 °C/min and data were collected with an 8-s response time, and 1°C data pitch. From the spectrum, the apparent midpoint of temperature denaturation (T_m) was determined using the Boltzmann sigmoid equation:

$$Y = \frac{Min + (Max - Min)}{1 + 10^{\{(logT_m - X) \cdot slope\}}}$$

where Y is the change in CD signal, Min represents the bottom plateau, Max represents the top plateau, and X is the temperature.

2.4.2 Ca²⁺ binding affinity using far-UV CD spectroscopy

Ca²⁺ binding curves were constructed from the change in ellipticity at 225 nm as a function of changing CaCl₂ concentrations. For these binding curves, a 0.1 cm pathlength quartz cuvette was used with apo protein samples at 0.5 mg/mL. The far-UV CD spectra were acquired at 4 °C from 250 nm to 200 nm, with a scanning speed of 20 nm/min, response

time of 8 s, an average of 3 accumulations and 1 nm data pitch. A spectrum was acquired after the addition of fourteen CaCl₂ titration points between 0 and ~16 mM CaCl₂. The spectral intensities were corrected for the dilution associated with the volume change caused by the addition of each aliquot of CaCl₂. Ca²⁺ binding curves were fit and the fitted apparent equilibrium dissociation constant (K_d) was determined using a one site-binding model that takes into account protein concentration:

$$P + Ca \xrightleftharpoons{K_d} PCa, PCa = \frac{1}{2}[K_d + P_{tot} + Ca - \sqrt{(K_d + P_{tot} + Ca)^2 - 4P_{tot} \cdot Ca}]$$

where P is the free protein, Ca is the free Ca²⁺, PCa is the bound protein, and P_{tot} is the total protein concentration.

2.5 Solution NMR spectroscopy

Approximately 100-200 μM of protein solubilized in 20 mM Tris, 150 mM NaCl, pH 7.5 was supplemented with 60 μM of 4,4-dimethyl-4-silapentane-1-sulfonic acid (DSS) and 10 % D₂O (v/v) in a final volume of 600 μL. The samples were loaded into a 5 mm NMR tube. ¹H-¹⁵N HSQC spectra (Kay *et al.*, 1992; Farrow *et al.*, 1994) were obtained at 25 °C on a Varian Inova 600 MHz NMR spectrometer equipped with a triple resonance HCN cryogenic probe. The number of transients was set to 256, and the number of increments in the nitrogen dimension was set to 64 for all the samples. The ¹H and ¹⁵N sweep widths were 8,000 and 1,800 Hz, respectively. All NMR spectra shown were chosen based on the highest signal to noise given for each sample group: Wild-type (n=2), Asn131Cys and gl-Asn131Cys (n=3), Asn171Cys and gl-Asn171Cys (n=4), Asn131Cys/Asn171Cys and gl-Asn131Cys/gl-Asn171Cys (n=2). The neo-glycosylated spectra were compared to the unmodified spectra by supplementing the samples with 15 mM DTT to fully remove the glucose moiety by

reduction. Total chemical shift perturbations (CSP) were calculated from the chemical shift differences observed in the ^{15}N and ^1H dimensions of each peak and normalizing for the larger ^{15}N chemical shift range using the following equation:

$$CSP = \sqrt{[\Delta H^2 + (0.14 \cdot \Delta N^2)]}$$

where ΔH is the ppm change in proton dimension, and ΔN is the ppm change in the nitrogen dimension.

2.6 Static Light Scattering (SLS)

Stock protein samples were centrifuged at 8,500 g for 5 min at 4 °C to remove any pre-existing aggregates and precipitates. After measuring protein concentration using absorbance at wavelength 280nm and an extinction coefficient of 1.6062, samples were diluted to a concentration 0.2 mg/mL in the appropriate Ca^{2+} -loaded buffers (Table 2.3). 100 μL of 0.2 mg/mL protein samples were subsequently centrifuged in a Legend Micro 21R Centrifuge (Thermo Scientific, Inc.) at 15,000 g for 5 min at 4 °C. 25 μL of the supernatant was aliquoted into a clean quartz MicroCuvette and the SLS intensity at 90 ° was measured on a DynaPro Nanostar (Wyatt Technology) at 658 nm with the laser power attenuated to 10 %, for 6 consecutive measurements (10 s each) at 37 °C.

To assess the Ca^{2+} -depletion-dependent oligomerization propensity, 50 mM EDTA was added to the sample in the cuvette and mixed by pipetting. SLS intensity after the EDTA addition was measured with the laser power attenuated to 10 % for 360 consecutive measurements (i.e., 10 s each) at 37 °C. The 10 consecutive measurements that showed the highest intensity were taken for statistical analysis. To assess the Ca^{2+} -independent oligomerization propensity, 100 μL of 0.2 mg/mL protein samples were centrifuged in a Legend Micro 21R Centrifuge (Thermo Scientific, Inc.) at 15,000 x g for 5 min at 4°C.

Subsequently, 80 μL of the supernatant was removed. The pellet was re-suspended in the remaining 20 μL protein solution and 5 μL was used for the SLS measurements with the laser power attenuated to 10 % at 37°C for 9 consecutive measurements (10 s each).

2.7 Live cell experiments

2.7.1 Cell culture

HEK293 cells stably expressing YFP-Orai1 were generously gifted by Dr. Monica Vig from Washington University in St. Louis (St. Louis, MO) (Miao *et al.*, 2013). Cells were maintained at 37 °C in a 5% CO₂/95% air humidified incubator in Dulbecco's modified eagle medium (DMEM) supplemented with 10 % (v/v) fetal bovine serum (Wisent, Inc.), 100 $\mu\text{g}/\text{ml}$ penicillin-streptomycin, and 0.4 mg/ml G418 Disulfate (Fisher Scientific, Inc.). HEK293-YFP-Orai1 cells were passaged at ~80% confluency using the following procedure. First the cell culture medium was aspirated off the dish; subsequently, the adherent cells were gently washed with 10 mL of warm phosphate buffered saline (PBS). After PBS removal by aspiration, 1 mL trypsin/EDTA (Wisent, Inc.) was added per 10- cm plate, and the plate was incubated for ~3 min at 37°C. 9 mL of warm culture medium with serum was used to inhibit the trypsin and ~20-30% of the cell mixture was re-plated with fresh medium to 10 mL onto a new plate.

2.7.2 Transfection

The cells were transfected at ~70-80% confluency in a 10-cm dish with PolyJet™ In Vitro DNA transfection reagent (SignaGen Laboratories, Inc.) according to the manufacturer's instructions. 24 h before the experiment, the medium was replaced with 10 mL of fresh medium and the cells were cultured for 60 min at 37°C. 4 μg of DNA was mixed

with 10 μL of the Polyjet reagent in 500 μL of DMEM high serum free and incubated at room temperature for 15 min. The DNA/PolyJet mixture was then added to the cells dropwise, and the cultures were incubated at 37 $^{\circ}\text{C}$ for an additional 24 h.

Transfection efficiency was calculated as the percentage of cells showing mCherry Fluorescence, visualized on a Leica DMIRBE fluorescence microscope (Leica Microsystems, Inc.) equipped with an Orca-ER digital camera (Hamamatsu Photonics, Inc.) and Volocity 4.3.2 software.

2.7.3 Fura2- ratiometric Ca^{2+} imaging

After confirming an $\sim 80\%$ transfection efficiency level, the cell medium was aspirated and adherent cells were washed once with 5 mL per 10 cm dish of HBSS buffer (140 mM NaCl, 4.7 mM KCl, 1.13 mM MgCl, 10 mM glucose, 10 mM 4-(2-hydroxyethyl)-1-piperazineethanesulfonic acid (HEPES), pH 7.4) supplemented with 1.8 mM CaCl_2 . The cells were subsequently collected after lifting by gentle pipetting with 3 mL of HBSS buffer supplemented with 1.8 mM CaCl_2 , and 3 μM of fura2-AM (Alfa Aesar, Inc.), was added to the 3 mL of suspended cells and incubated for 45 min in the dark at 37 $^{\circ}\text{C}$. Subsequently, the cells were diluted to 15 mL with HBSS buffer supplemented with 1.8 mM CaCl_2 and incubated for another 15 min in the dark at 37 $^{\circ}\text{C}$. Next, the cells were washed 2 \times with HBSS buffer supplemented with 1.8 mM CaCl_2 by centrifuging at 1,000 \times g for 6 min at room temperature then aspirating the supernatant. The cells were finally washed with HBSS buffer nominally free of CaCl_2 and re-suspended in 1.2 mL of HBSS buffer. The final number of cells in 1.2 mL of HBSS was $\sim 5 \times 10^6$.

Fluorescence at 340 and 380 nm excitation and 510 nm emission was measured using a Cary Eclipse spectrofluorimeter (Varian/Agilent, Inc.) equilibrated at 20 $^{\circ}\text{C}$, with a

photomultiplier tube voltage of 700 V and slit widths at 5 and 10 nm. At 60 s, 0.5 μ M of TG and 0.1 mM EGTA were added. At 600 s, 0.5 mM of CaCl₂ and at 900 s, an additional 3.5 mM of CaCl₂ was added. The total experimental running time was 1500 s. Data were plotted as a normalized F/F₀ ratio to show relative changes in cytosolic Ca²⁺ levels, where F = emission intensity ratio calculated using 340 nm/380 nm excitation wavelengths and F₀ = average F prior to the addition of TG, as has been done previously (Glitsch *et al.*, 2002; Jaiswal *et al.*, 2009; Estrada *et al.*, 2012; Tamouza *et al.*, 2012; Chai *et al.*, 2013; Fuchs *et al.*, 2013; Muller *et al.*, 2015). Maximal changes in the fluorescence ratio after TG addition was taken as the difference between the average of 11 consecutive intensity responses (i.e. 5 before and 5 after the highest intensity) and the average baseline F before TG addition. Maximal changes after 0.5 mM CaCl₂ addition and 3.5 mM CaCl₂ were similarly calculated compared to the baseline F intensity.

Chapter 3
Results

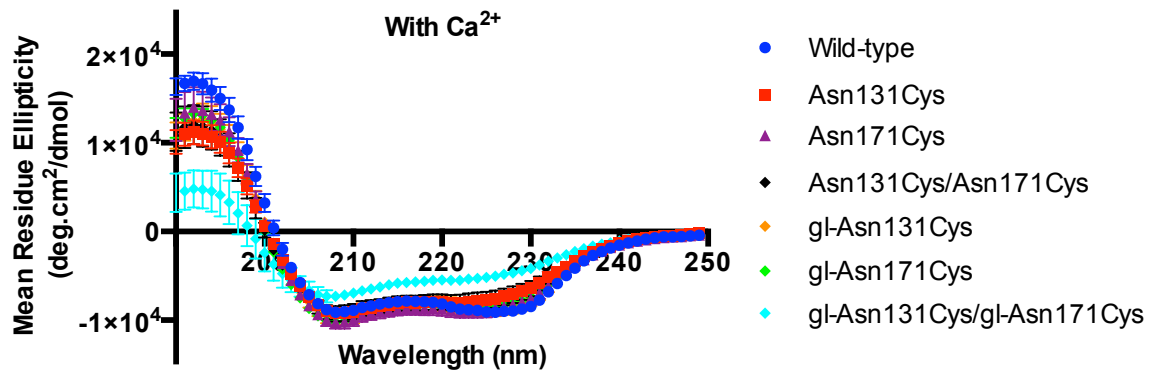
3.1 Double neo-glycosylated EFSAM constitutively loses α -helicity.

In the presence of Ca^{2+} , EFSAM proteins show strong α -helical secondary structure defined by negative ellipticity at ~ 208 and ~ 225 nm wavelengths in the far-UV circular dichroism (CD) spectra (Figure 3.1A). Wild type EFSAM as well as the three mutants (i.e., Asn131Cys, Asn171Cys, Asn131Cys/Asn171Cys) show similar α -helicity based on far-UV CD spectral shapes. Similarly, single modification of Asn131Cys or Asn171Cys minimally perturbs the level of α -helicity in the presence of Ca^{2+} . Remarkably, doubly modified gl-Asn131Cys/gl-Asn171Cys EFSAM displays less pronounced negative ellipticity at the 208 and 225 nm wavelengths, suggesting a loss of α -helical secondary structure.

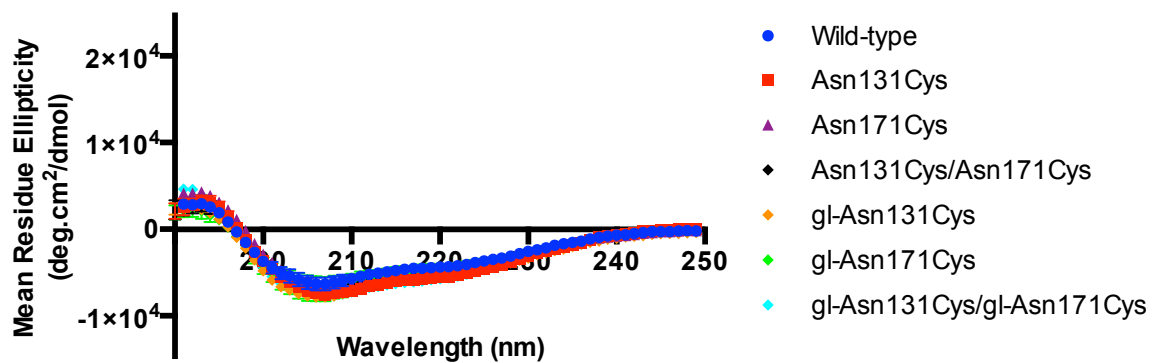
To estimate the fraction α -helicity of each of the EFSAM variants, we used the online web based tool DICHROWEB (Whitmore & Wallace, 2004). The CONTIN algorithm was used to deconvolute α -helicity levels. The wild-type protein showed $\sim 40\%$ α -helicity, and all the mutations and the single modified mutants showed comparable α -helicity levels (Figure 3.1C). However, the double glucose modified protein (i.e., gl-Asn131Cys/gl-Asn171Cys) showed a significant reduction in α -helicity levels compared to wild-type EFSAM.

In the absence of Ca^{2+} , modified and unmodified wild-type and mutant EFSAM proteins showed a marked loss in the α -helical secondary structure (Figure 3.1B and 3.1C). A qualitative assessment of the spectra shows less negative ellipticity at 208 nm and a major loss of the ellipticity at 225 nm. A deconvolution of the percentage secondary structure using the CONTIN algorithm in DICHROWEB revealed that all the modified and unmodified EFSAM proteins show $\sim 17\%$ α -helicity in the absence of Ca^{2+} , significantly less than the respective Ca^{2+} -loaded states (Figure 3.1C). Overall, double glucose modification of EFSAM results in a persistent partial loss of the α -helical secondary structure with or without Ca^{2+} .

(A)



(B)



(C)

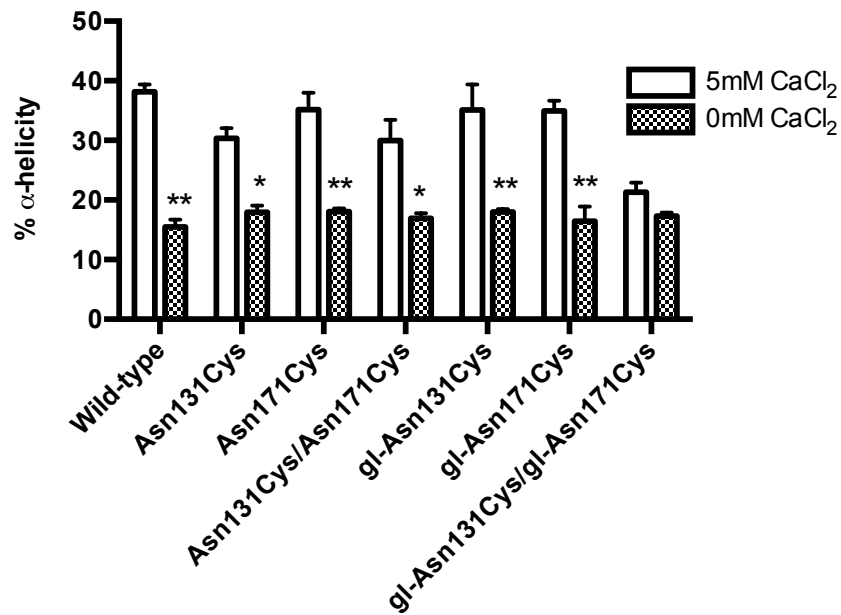


Figure 3.1. Far-UV CD spectra of wild-type, Asn131Cys, Asn171Cys, Asn131Cys/Asn171Cys, gl-Asn131Cys, gl-Asn171Cys, and gl-Asn131Cys/gl-Asn171Cys EF-SAM proteins. (A) Ca²⁺ loaded EFSAM far-UV CD spectra. Spectra were acquired in 5 mM CaCl₂, 20 mM Tris, 150 mM NaCl, pH 7.5, at 4°C. Unmodified and modified Ca²⁺ loaded proteins were assessed in the presence and absence of 1 mM TCEP, respectively. (B) Ca²⁺ depleted EFSAM far-UV CD spectra. Spectra were acquired in 0.5 mM EDTA, 20 mM Tris, 150 mM NaCl, pH 7.5, at 4°C. Unmodified and modified Ca²⁺ depleted proteins were assessed in the presence and absence of 1 mM TCEP, respectively. All the data in (A) and (B) are the means ± SEM of n=3-4 separate protein preparations. (C) Percent α-helicity of the proteins in the presence and absence of Ca²⁺. The percentages α-helicity were deconvoluted from the spectra shown in (A) and (B) using DICHROWEB. The statistical evaluation was two-way analysis of variance (ANOVA) with Bonferroni multiple comparisons test for data in the presence of 5 mM CaCl₂ and 0 mM CaCl₂; *p<0.005, **p<0.0001.

3.2 Neo-glycosylated EFSAM proteins are destabilized.

T_m was taken as a measure of protein stability and determined from the change in far-UV CD signal at 225 nm as a function of temperature. In the presence of Ca^{2+} , the T_m for the wild-type EFSAM protein was $\sim 48.5^\circ C$. All single and double mutants showed a significant thermal destabilization compared to the wild-type control with T_m values ranging from $\sim 42^\circ C$ to $44^\circ C$ (Figure 3.2A). Glucose conjugation of the single mutants marginally destabilized EFSAM further by ~ 0.3 - $2.0^\circ C$; on the other hand, double glucose modification at both the Asn131 and Asn171 sites (i.e., gl-Asn131Cys/gl-Asn171Cys) destabilized the protein by a more marked $\sim 3.7^\circ C$ (Table 3.1). Thus, EFSAM stability is sensitive to modifications at the Asn131 and Asn171 positions and glucose attachment close to the surface of the protein enhances the destabilization.

In the absence of Ca^{2+} , all protein samples were highly destabilized (Figure 3.2B). Such a loss in stability is coupled to the pronounced decrease in α -helicity shown in Figure 3.1B. Since the Ca^{2+} -depleted EFSAM proteins are in a persistently partially unfolded state, only a small additional change in ellipticity occurred during thermal unfolding resulting in considerable scatter in the data compared to the Ca^{2+} -loaded proteins. Thus, we were unable to reliably determine the T_m values in the absence of Ca^{2+} . Nevertheless, it is clear that glucose modified and unmodified Ca^{2+} -depleted EFSAM proteins have a strikingly reduced thermal stability compared to their Ca^{2+} -loaded counterparts (Fig. 3.1A and 3.1B).

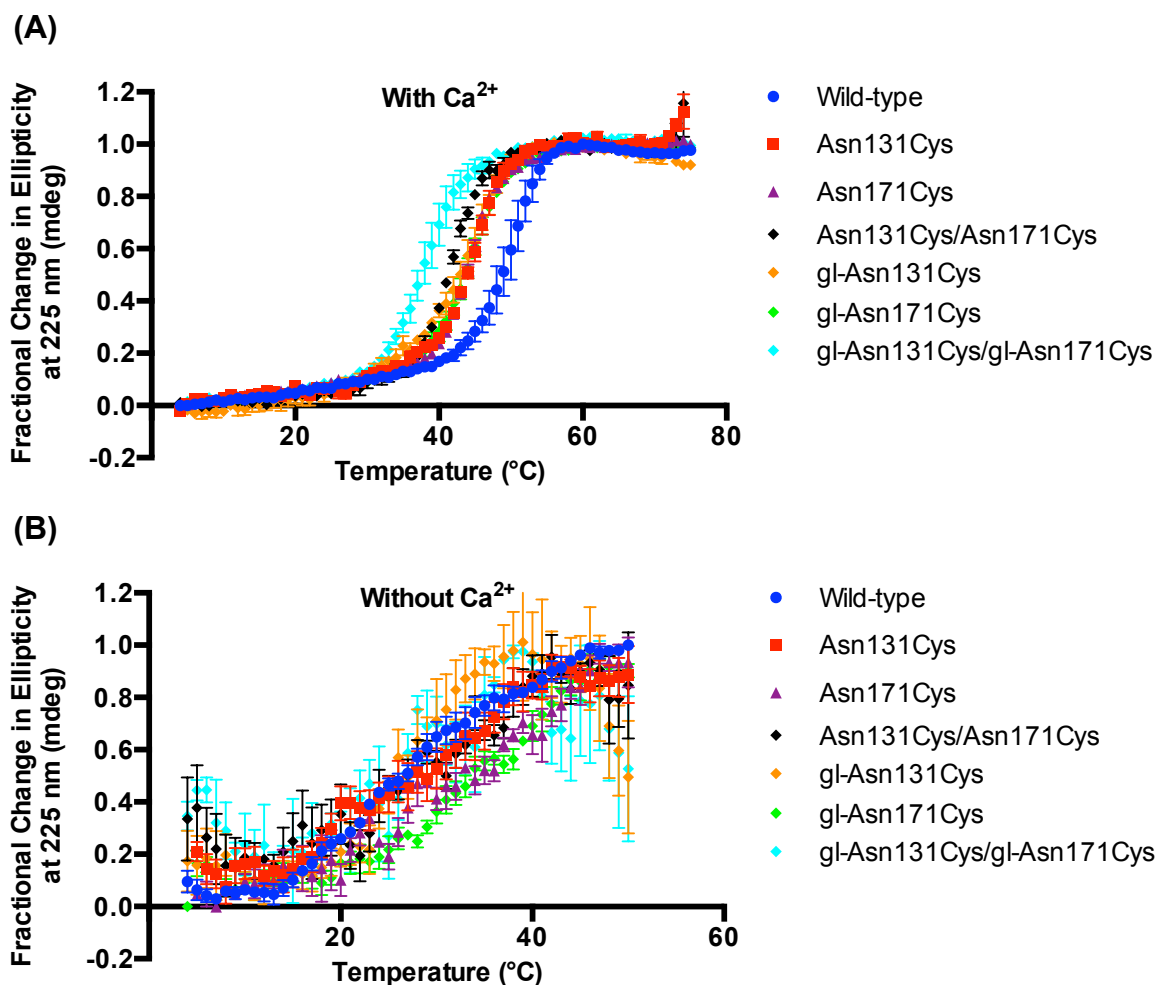


Figure 3.2. Thermal stability of wild-type, Asn131Cys, Asn171Cys, Asn131Cys/Asn171Cys, gl-Asn131Cys, gl-Asn171Cys, and gl-Asn131Cys/gl-Asn171Cys and EFSAM proteins. (A) Thermal melts were acquired in 5 mM CaCl_2 , 20 mM Tris, 150 mM NaCl, pH 7.5. Stability was estimated from the change in far-UV CD signal at 225 nm as function temperature. Unmodified and modified Ca^{2+} loaded proteins were assessed in the presence and absence of 1 mM TCEP, respectively. (B) Thermal melts were acquired in 0.5 mM EDTA, 20 mM Tris, 150 mM NaCl, pH 7.5. Unmodified and modified Ca^{2+} depleted proteins were assessed in the presence and absence of 1 mM TCEP, respectively. Data in (B) was partially smoothed using three point averaging. All data in (A) and (B) are the means \pm SEM of $n=3-4$ separate protein preparations.

Table 3.1. Summary of thermal stability changes for mutated and/or glucose modified EFSAM proteins.

Proteins with Ca ²⁺	T _m (°C) ^a	ΔT _{m mut} (°C) ^b	ΔT _{m mod} (°C) ^c
Wild-type	48.5 ± 0.18		
Asn131Cys	44.0 ± 0.16*	- 4.5 ± 0.24	
Asn171Cys	43.9 ± 0.09*	- 4.6 ± 0.20	
Asn131Cys/Asn171Cys	41.5 ± 0.18*	- 7.0 ± 0.25	
gl-Asn131Cys	42.0 ± 0.18*	- 6.5 ± 0.25	- 2.0 ± 0.24
gl-Asn171Cys	43.6 ± 0.09*	- 4.9 ± 0.20	- 0.3 ± 0.18
gl-Asn131Cys/gl-Asn171Cys	37.8 ± 0.14*	- 10.7 ± 0.23	- 3.7 ± 0.23

^aT_m using the Boltzmann's fit. One-way ANOVA with Bonferroni multiple comparisons test to the control group 'wild-type' was used for statistical analysis; *p<0.0001.

^bThe difference of all the other groups to T_{m(Wild-type)}; T_{m mut} = T_{m(mut/mod)} - T_{m(Wild-type)}

^cThe difference of T_{m(unmodified)} to that of T_{m(modified)}; T_{m mod} = T_{m(mod)} - T_{m(mut)}

3.3 Neo-glycosylation of EFSAM proteins causes local structural perturbations.

I used solution NMR to assess structural perturbations caused by the EFSAM modifications. Comparisons of the wild type with mutant and glucose-conjugated mutant EFSAM protein ^1H - ^{15}N -HSQC spectra reveal the changes in the backbone structures due to modifications at the Asn131 and Asn171 sites. The wild-type EFSAM spectrum closely matched the previously published spectrum for this protein which is ~80 % assigned (Stathopoulos *et al.*, 2008) (BMRB accession number 15851), allowing the assignments to be made by transference. Furthermore, reduced spectra with 15 mM DTT perfectly matched the mutant spectra before the glucose modification, indicating that DTT addition to the neo-glycosylated proteins fully reversed the modification process. I observed three CSP hotspots caused by the Asn131Cys mutation (i.e., ~between residues 65-73, 121-142 and residues 156-170) (Figure 3.4A). Glucose-attachment to the Asn131Cys caused further CSPs largely localized to these same areas relative to the primary sequence (Figure 3.4B). However, to evaluate the overall structural perturbations caused by all the changes at the Asn131 site (i.e., mutation + glucose attachment) I compared the gl-Asn131Cys to the wild-type spectrum (Figure 3.3) and calculated the CSPs (Figure 3.4C). I mapped the largest CSPs corresponding to those greater than 1 and 2 standard deviation (SD) higher than the mean CSPs of all residues on the wild-type EFSAM structure. While the three hotspots appear relatively distant in sequence space, the perturbation map on the 3D structure revealed that the largest CSPs were primarily localized to one face of the EFSAM domain within ~10 Å of the Asn131Cys residue (Figure 3.5).

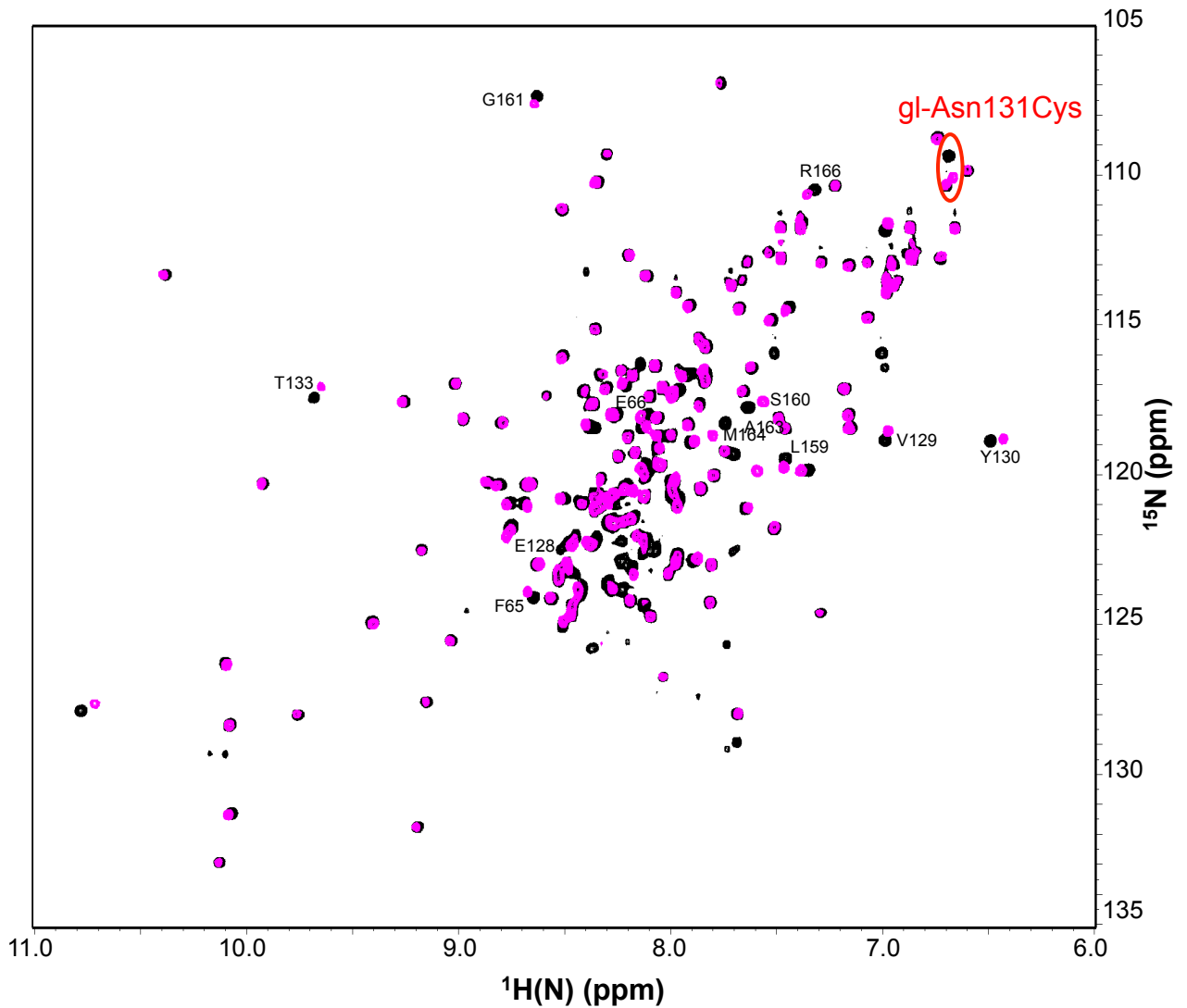
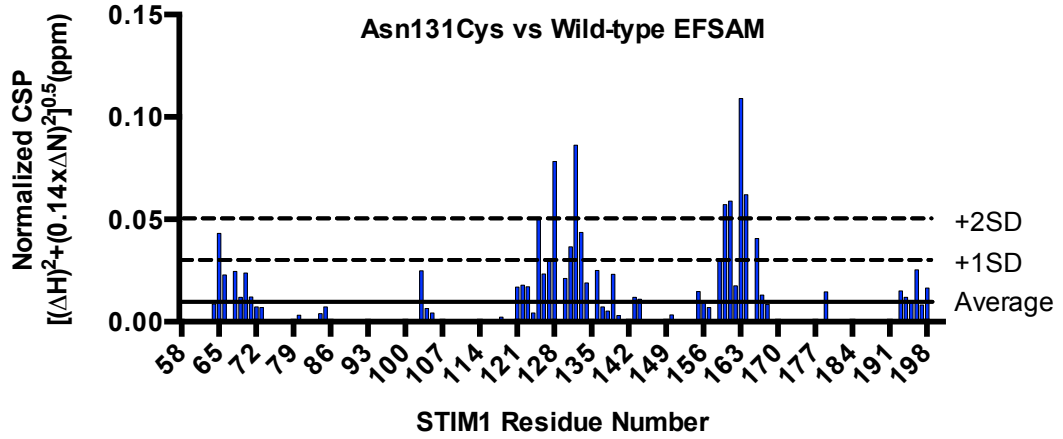
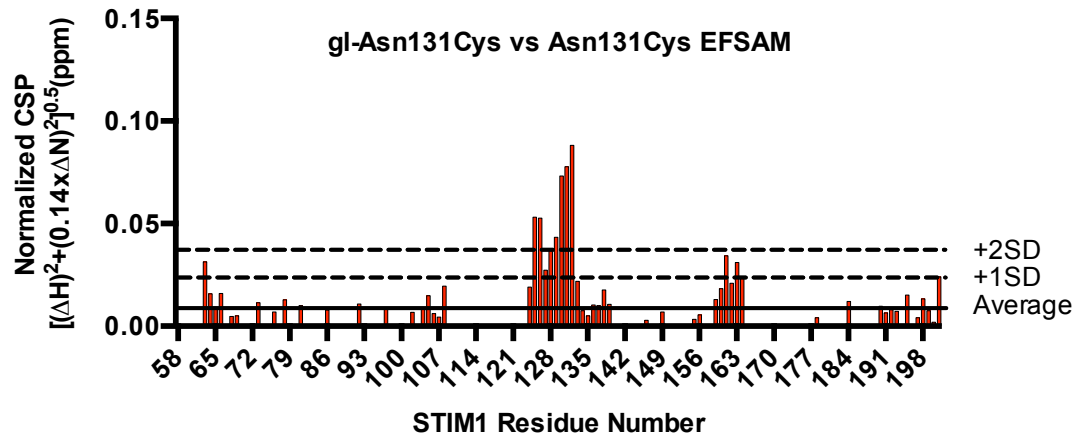


Figure 3.3. ^1H - ^{15}N HSQC spectrum of gl-Asn131Cys (magenta crosspeaks) overlaid with the wild-type (black crosspeaks) spectrum. The spectra were acquired in 5 mM CaCl_2 , 20 mM Tris, 150 mM NaCl, pH 7.5, 20 °C at 600 MHz. The amides of residues undergoing CSPs larger than the mean plus $1 \times \text{SD}$ due to the Cys mutation and the covalent addition of the glucose moiety are labeled. The location of gl-Asn171Cys amide is indicated with a red ellipse.

(A)



(B)



(C)

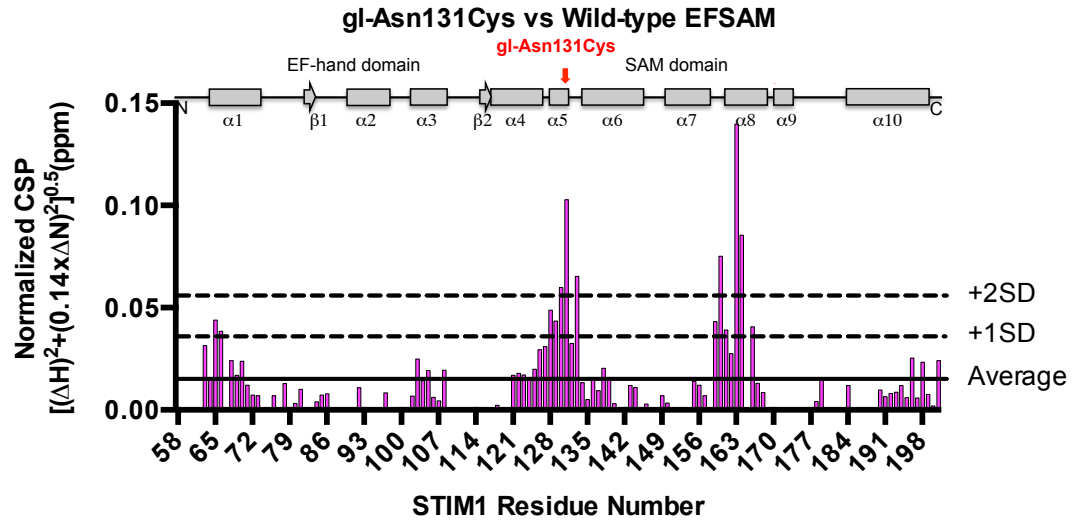


Figure 3.4. Normalized CSPs derived from the ^1H - ^{15}N HSQC spectra. (A) Normalized CSPs calculated from the Asn131Cys EFSAM spectrum compared to the wild-type EFSAM spectrum. (B) Normalized CSPs calculated from the gl-Asn131Cys EFSAM spectrum compared to the Asn131Cys EFSAM spectrum. (C) Normalized CSPs calculated from the gl-Asn131Cys EFSAM spectrum compared to the wild-type EFSAM spectrum. In (A) – (C), the CSPs are shown relative to the STIM1 EFSAM residue number, and the CSP levels of the mean (solid horizontal line) and the mean plus $1\times$ and $2\times$ the standard deviation (SD, broken horizontal lines) are shown. The relative location of the STIM1 EFSAM secondary structure elements are shown at the top of panel (C) with rectangles and arrows representing α -helical and β -strand elements, respectively.

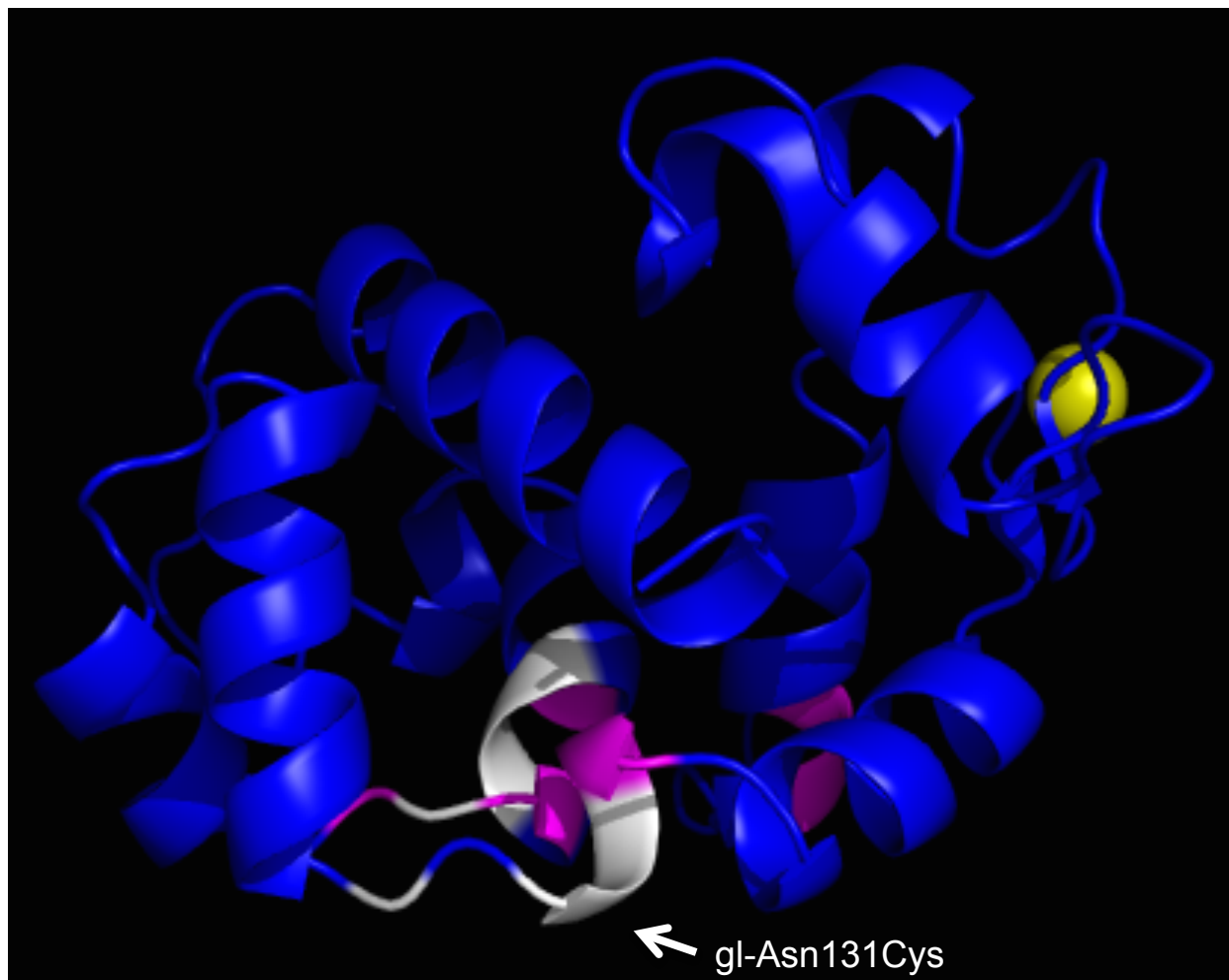


Figure 3.5. The largest magnitude CSPs of gl-Asn131Cys relative to wild-type EFSAM mapped on the 3D structure of wild-type EFSAM. The perturbations are shown as blue-magenta-white gradient on the backbone view of EFSAM where magenta indicates CSPs greater than the mean plus $1\times SD$, and white indicates CSPs greater than the mean plus $2\times SD$. The yellow sphere represents Ca^{2+} . The structure image was rendered in PyMOL using 2K60.pdb.

The Asn171Cys mutation resulted in two main CSP hotspots compared to wild-type (i.e., between residues ~64-73 and ~165-190) (Figure 3.7A). The gl-Asn171Cys spectrum showed further residue-specific CSPs in the same two regions, consistent with the attachment of the glucose moiety (Figure 3.7B). The gl-Asn171Cys spectral changes compared to wild-type (Figure 3.6) were used to determine the CSPs caused by all the modifications at the Asn171Cys site (Figure 3.7C). Similar to the gl-Asn131Cys protein, the two perturbation hotspots caused by the gl-Asn171Cys that were separated by hundreds of residues in sequence space localized to one face EFSAM within ~ 10 Å of the Asn171Cys site (Figure 3.8).

The spectrum obtained with the double mutant revealed three CSP hotspots between residues ~65-79, ~121-135 and ~156-198 (Figure 3.10A). My glucose modification procedure caused further residue-specific CSPs in these three hotspots, consistent with the attachment of the glucose moiety to both the Asn131Cys and Asn171Cys sites (Figure 3.10B). While the Asn131Cys modification also caused three CSP hotspots (Figure 3.4C), the double modification perturbed a broader range of residues in the SAM domain region, consistent with the modification of the Asn171Cys. I calculated the overall CSPs from the comparison of the gl-Asn131Cys/gl-Asn171Cys spectrum to wild-type spectrum (Figure 3.9). Again, while the three main CSP regions were separated in sequence space (Figure 3.10C), plotting the most perturbed residues on the 3D EFSAM structure revealed two distinct clusters of structural changes (Figure 3.11). The first cluster was around the Asn131Cys site and the second cluster surrounded to the Asn171Cys site.

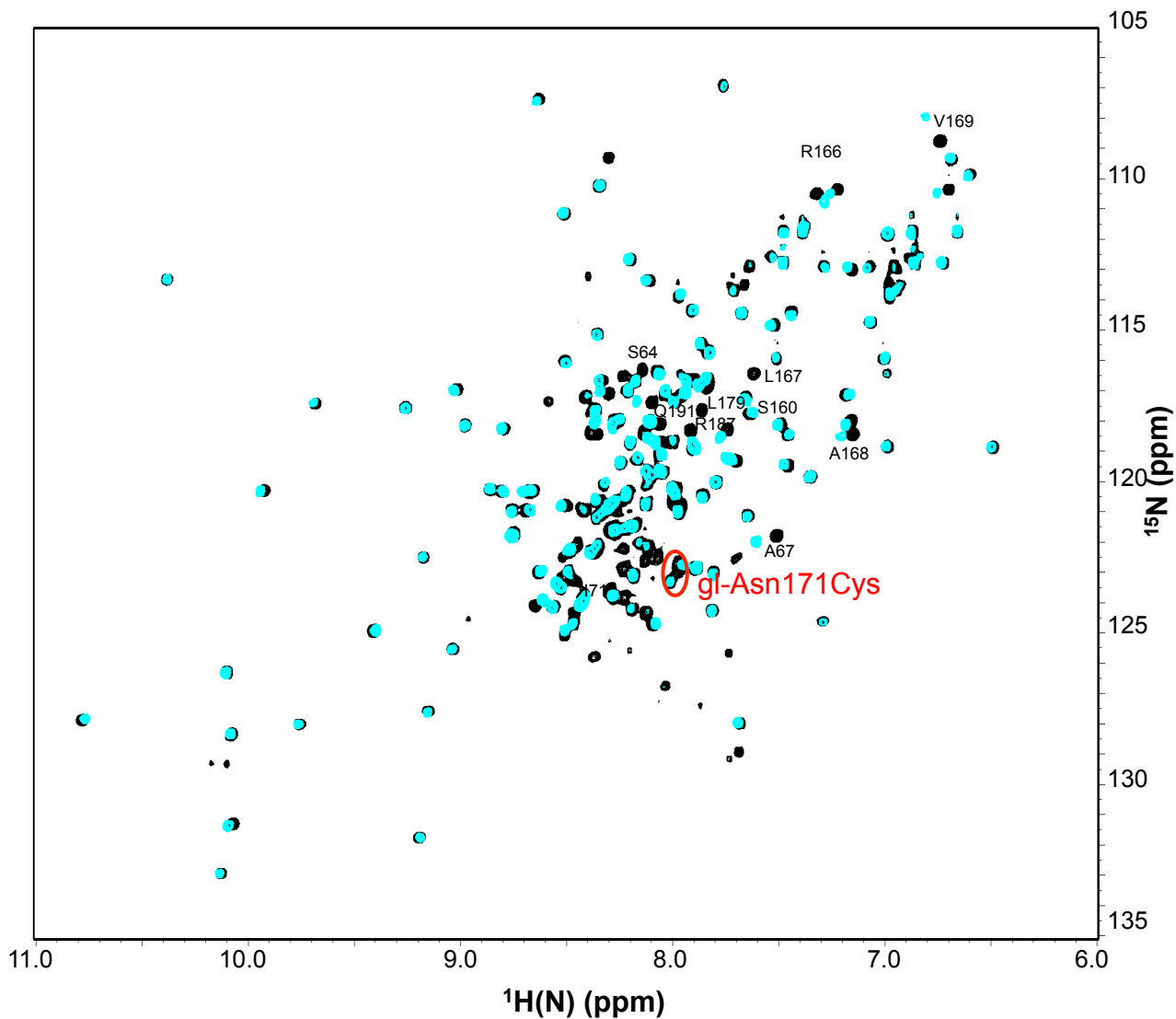
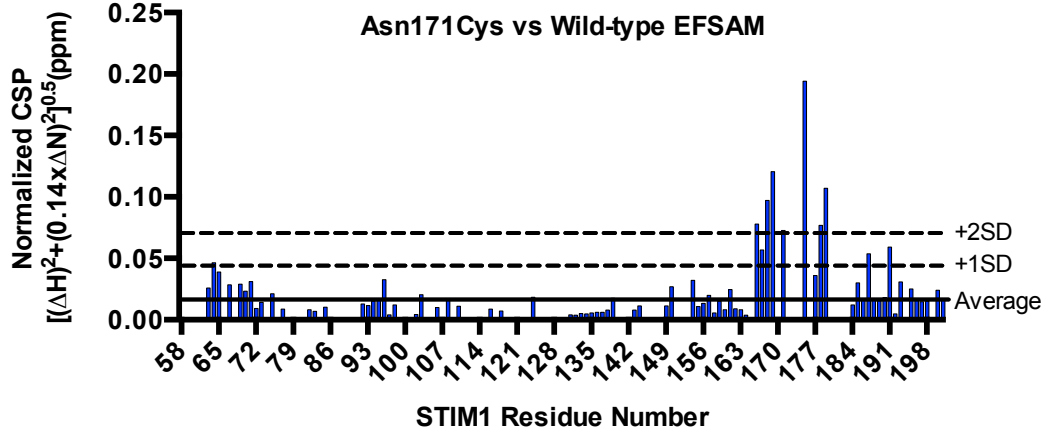
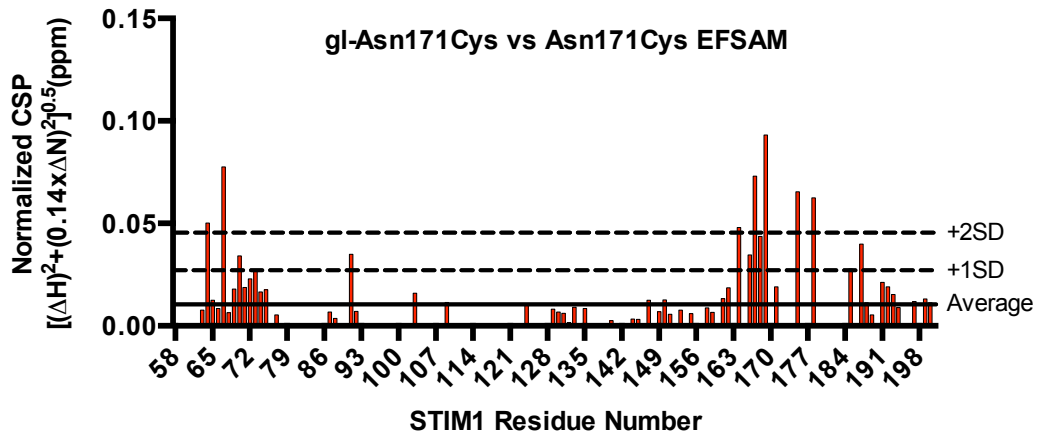


Figure 3.6. ^1H - ^{15}N HSQC spectrum of gl-Asn171Cys (cyan crosspeaks) overlaid with the wild-type (black crosspeaks) spectrum. The spectra were acquired in 5 mM CaCl_2 , 20 mM Tris, 150 mM NaCl, pH 7.5, 20 °C at 600 MHz. The amides of residues undergoing CSPs larger than the mean plus $1 \times \text{SD}$ due to the Cys mutation and the covalent addition of the glucose moiety are labeled. The location of gl-Asn171Cys amide is indicated with a red ellipse.

(A)



(B)



(C)

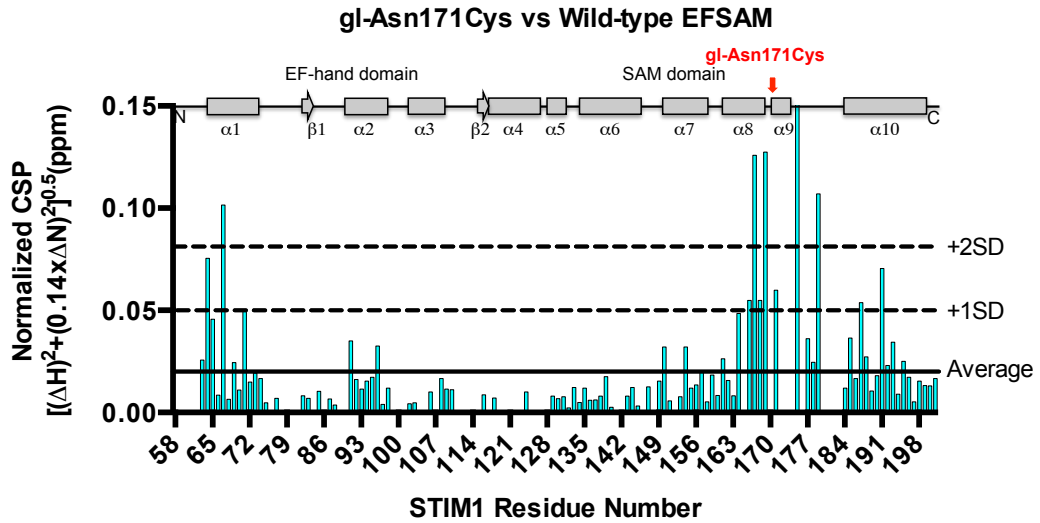


Figure 3.7. Normalized CSPs derived from the ^1H - ^{15}N HSQC spectra. (A) Normalized CSPs calculated from the Asn171Cys EFSAM spectrum compared to the wild-type EFSAM spectrum. (B) Normalized CSPs calculated from the gl-Asn171Cys EFSAM spectrum compared to the Asn171Cys EFSAM spectrum. (C) Normalized CSPs calculated from the gl-Asn171Cys EFSAM spectrum compared to the wild-type EFSAM spectrum. In (A) – (C), the CSPs are shown relative to the STIM1 EFSAM residue number, and the CSP levels of the mean (solid horizontal line) and the mean plus $1\times$ and $2\times$ the standard deviation (SD, broken horizontal lines) are shown. The relative location of the STIM1 EFSAM secondary structure elements are shown at the top of panel (C) with rectangles and arrows representing α -helical and β -strand elements, respectively.

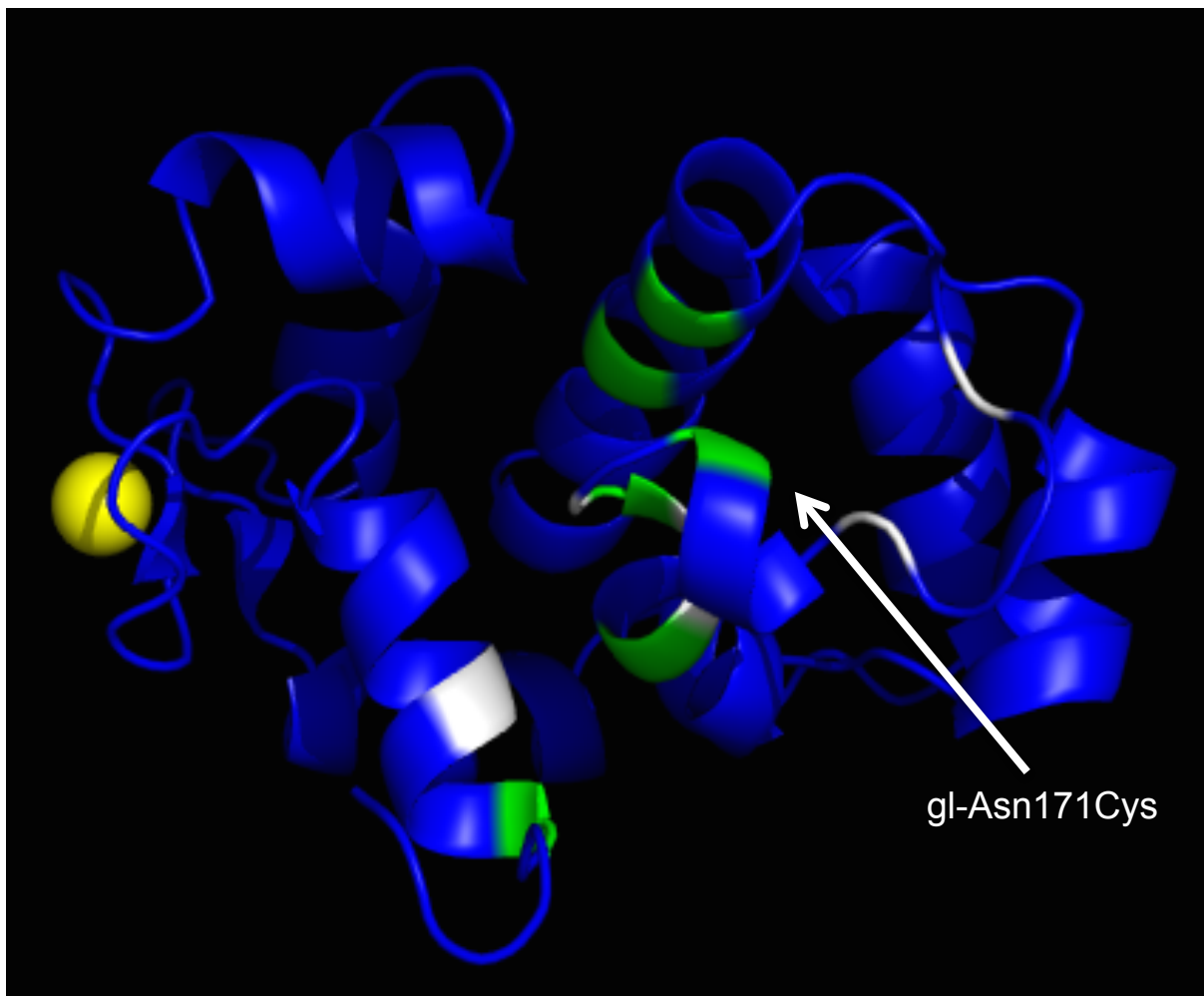


Figure 3.8. The largest magnitude CSPs of gl-Asn171Cys relative to wild-type EFSAM mapped on the 3D structure of wild-type EFSAM. The perturbations are shown as blue-green-white gradient on the backbone view of EFSAM where green indicates CSPs greater than the mean plus $1\times SD$, and white indicates CSPs greater than the mean plus $2\times SD$. The yellow sphere represents Ca^{2+} . The structure image was rendered in PyMOL using 2K60.pdb.

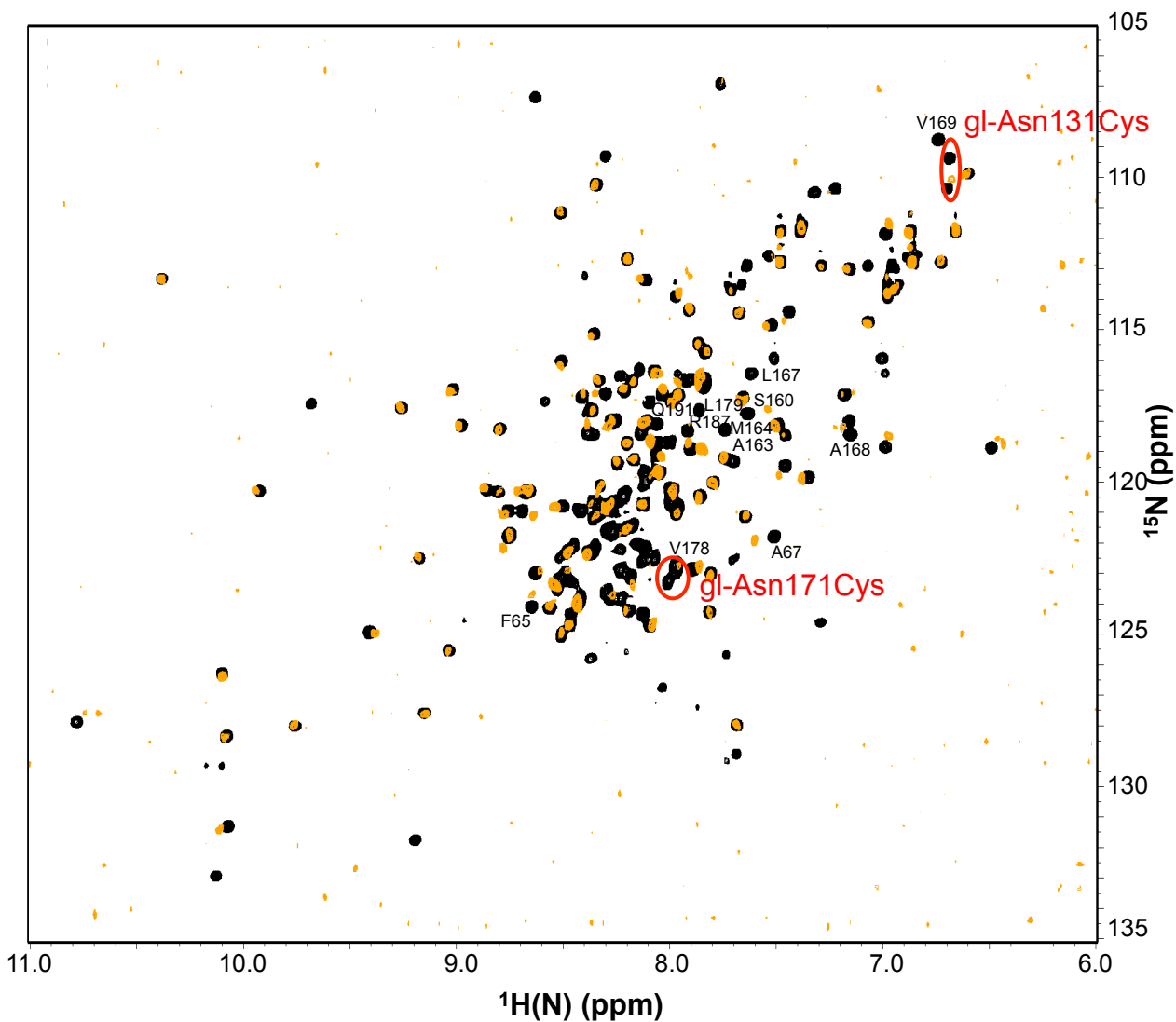
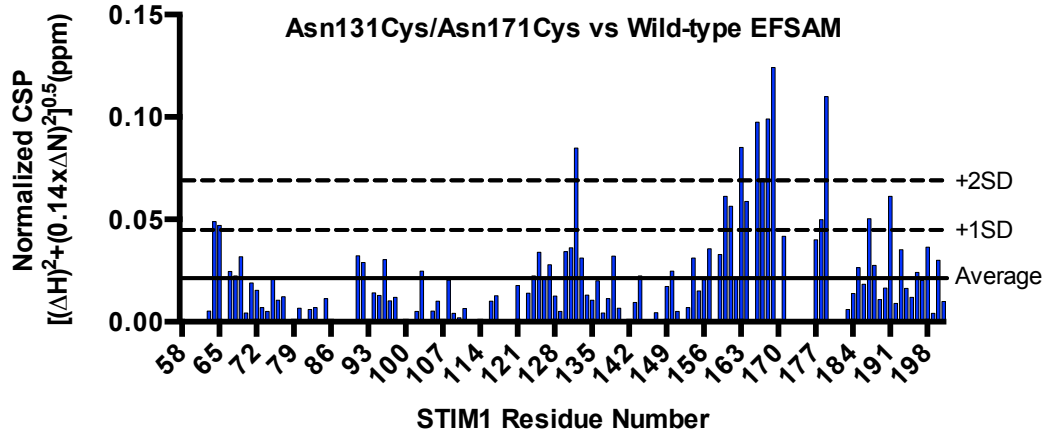
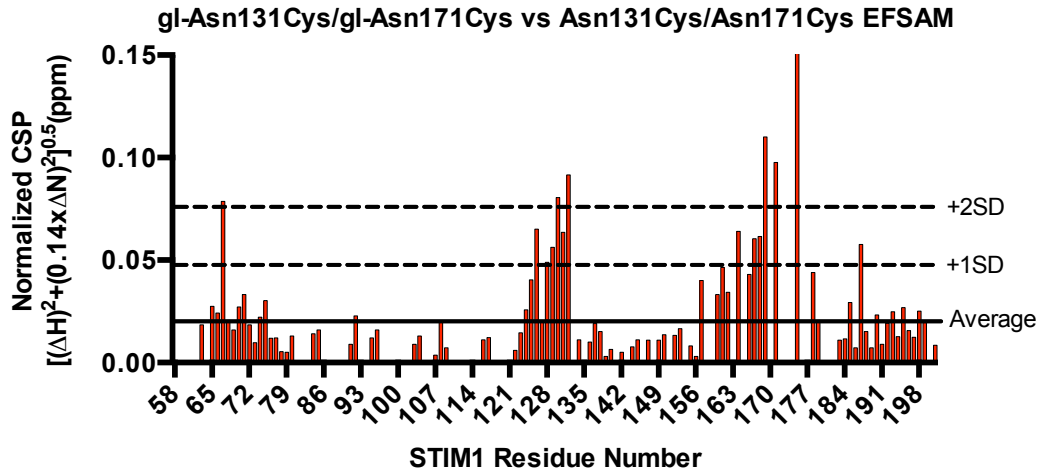


Figure 3.9. ^1H - ^{15}N HSQC spectrum of gl-Asn131Cys/gl-Asn171Cys (orange crosspeaks) overlaid with the wild-type (black crosspeaks) spectrum. The spectra were acquired in 5 mM CaCl_2 , 20 mM Tris, 150 mM NaCl, pH 7.5, 20 °C at 600 MHz. The amides of residues undergoing CSPs larger than the mean plus $1 \times \text{SD}$ due to the Cys mutations and the covalent addition of the glucose moieties are labeled. The location of gl-Asn131Cys and gl-Asn171Cys amides are indicated with red ellipses.

(A)



(B)



(C)

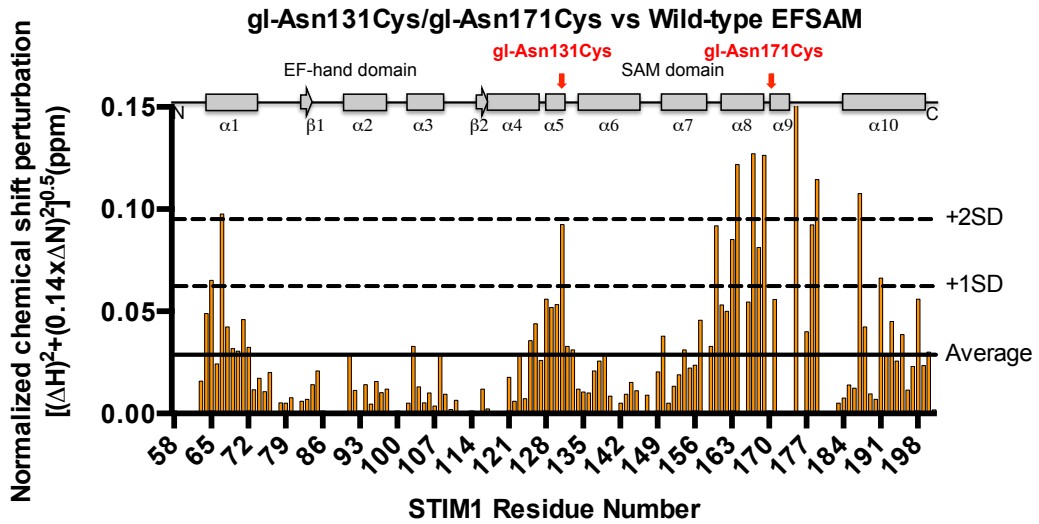


Figure 3.10. Normalized CSPs derived from the ^1H - ^{15}N HSQC spectra. (A) Normalized CSPs calculated from the Asn131Cys/Asn171Cys EFSAM spectrum compared to the wild-type EFSAM spectrum. **(B)** Normalized CSPs calculated from the gl-Asn131Cys/gl-Asn171Cys EFSAM spectrum compared to the Asn131Cys/Asn171Cys EFSAM spectrum. **(C)** Normalized CSPs calculated from the gl-Asn131Cys/gl-Asn171Cys EFSAM spectrum compared to the wild-type EFSAM spectrum. In (A) – (C), the CSPs are shown relative to the STIM1 EFSAM residue number, and the CSP levels of the mean (solid horizontal line) and mean plus $1\times$ and $2\times$ the standard deviation (SD, broken horizontal lines) are shown. The relative location of the STIM1 EFSAM secondary structure elements are shown at the top of panel (C) with rectangles and arrows representing α -helical and β -strand elements, respectively.

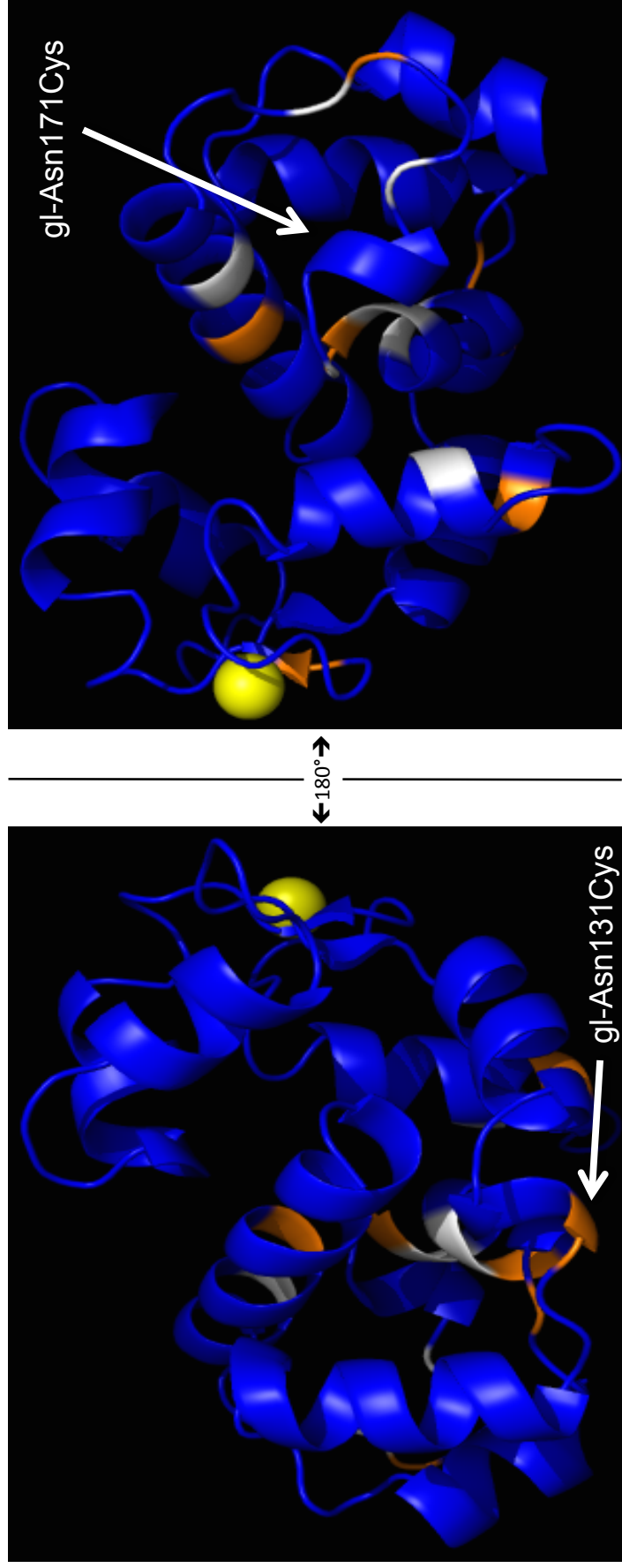


Figure 3.11. The largest magnitude CSPs of gl-Asn131Cys/gl-Asn171Cys relative to wild-type EFSAM mapped on the 3D structure of wild-type EFSAM. The perturbations are shown as blue-orange-white gradient on the backbone view of EFSAM where orange indicates CSPs greater than the mean plus $1 \times SD$, and white indicates CSPs greater than the mean plus $2 \times SD$. The yellow sphere represents Ca^{2+} . The structure image was rendered in PyMOL using 2K60.pdb.

Collectively, the structural analysis by solution NMR revealed successful site-specific glucose attachment to both the single and double mutant EFSAM proteins. Additionally, the CSPs revealed that the structural perturbations are localized to near the Asn131Cys or Asn171Cys sites for the single modifications and appear to be largely additive for the double mutant.

3.4 Neo-glycosylation lowers EFSAM Ca²⁺ binding affinity.

K_d values of Ca²⁺ binding were determined from the change in far-UV CD signal at 225 nm as a function of increasing Ca²⁺ concentrations (Figure 3.12A and 3.12B). Wild-type EFSAM had the lowest K_d value (~0.18 mM) compared to all other EFSAM proteins, indicating the highest Ca²⁺ affinity (Table 3.2). Mutation of Asn131 or Asn171 decreased the Ca²⁺ binding affinity by ~1 order of magnitude. Glucose modification did not appreciably alter these weakened affinities. Interestingly, the double mutation with or without the modifications showed the weakest affinities compared to wild-type EFSAM.

A comparison of the structural changes associated with Ca²⁺ binding shows that wild-type EFSAM regains considerable α -helicity as a function of increasing Ca²⁺ concentration (Figure 3.12C). On the other hand, the double modified mutant shows a resistance to refolding and remains in a persistent reduced α -helical state as a function increasing Ca²⁺ levels (Figure 3.12D). Together, these binding affinity data reveal a remarkable sensitivity of EFSAM to any modification associated with the Asn131 or Asn171 sites despite the peripheral localization of these residues far from the EF-hand Ca²⁺ coordinating residues; further, double mutation and/or modification of the Asn131 and Asn171 sites further potentiates weaker binding and leaves the EFSAM core in a persistently partially unfolded state.

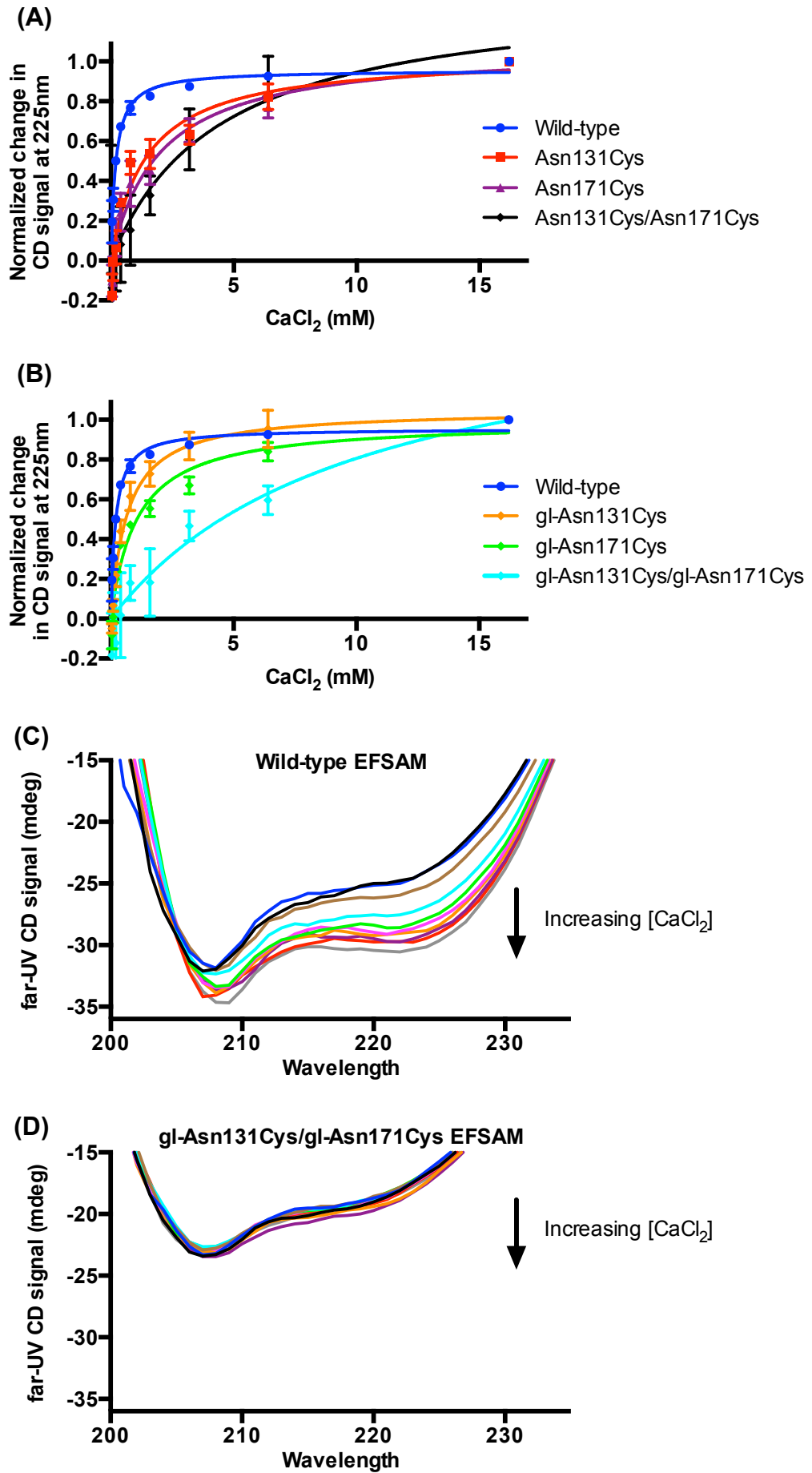


Figure 3.12. Ca²⁺ binding curves derived from changes in far-UV CD ellipticity as a function of Ca²⁺ concentration. (A) Unmodified wild-type and mutant EFSAM Ca²⁺ binding curves acquired in 20 mM Tris, 150 mM NaCl, 1 mM TCEP, pH 7.5. (B) Wild-type and gl-modified mutant EFSAM Ca²⁺ binding curves acquired in 20 mM Tris, 150 mM NaCl, pH 7.5. The binding experiments were performed at 4 °C with increasing CaCl₂ concentrations from 0 mM to 16.2 mM. All binding curves are constructed from n=3 separate experiments as mean responses ± SEM. (C) Representative far-UV CD spectral changes with increasing Ca²⁺ concentrations of wild-type EFSAM (from n=3 titrations). (D) Representative far-UV CD spectral changes with increasing Ca²⁺ concentrations of gl-Asn131Cys/gl-Asn171Cys EFSAM (from n=3 titrations).

Table 3.2. Summary of the equilibrium dissociation constants (K_d) extracted from the far-UV CD-derived Ca^{2+} binding curves.

	K_d (mM) ^a
Wild-type	0.18 ± 0.01
Asn131Cys	1.41 ± 0.48
Asn171Cys	1.95 ± 0.58
Asn131Cys/Asn171Cys	4.38 ± 2.33
gl-Asn131Cys	0.66 ± 0.11
gl-Asn171Cys	1.04 ± 0.18
gl-Asn131Cys/gl-Asn171Cys	9.94 ± 6.66

^a K_d was extracted using a one site-binding model that takes into account protein concentration.

3.5 Neo-glycosylation alters Ca^{2+} -dependent oligomerization propensity of EFSAM.

The Ca^{2+} sensitivity of EFSAM protein oligomerization was assessed using static light scattering (SLS) measurements. All samples were centrifuged for 15,000 g and 5 min (4 °C) to remove high scattering protein aggregates prior to the measurements. For each wild-type, mutant and modified-mutant sample a baseline SLS intensity in the presence of 5 mM Ca^{2+} was determined. Ca^{2+} -sensitive oligomerization was monitored as the increase in SLS intensity upon the addition of 10-fold excess EDTA. The time averaged SLS intensity is shown prior to and after the addition of the EDTA (Figure 3.13A). As expected, the wild-type EFSAM protein showed a dramatic increase in SLS intensity upon Ca^{2+} chelation indicative of Ca^{2+} -depletion-induced oligomerization. The single mutant EFSAMs maintained the ability to undergo Ca^{2+} -depletion-dependent oligomerization; however, the doubly mutated Asn131Cys/Asn171Cys EFSAM did not respond to Ca^{2+} -chelation. Similarly, the gl-Asn131Cys and the gl-Asn131Cys/gl-Asn171Cys protein solutions did not show increased SLS intensity upon EDTA addition indicative of a Ca^{2+} -insensitivity. Conversely, the gl-Asn171Cys protein showed an increased SLS after Ca^{2+} chelation as observed for wild-type EFSAM.

The Ca^{2+} insensitivity of Asn131Cys/Asn171Cys, gl-Asn131Cys and gl-Asn131Cys/gl-Asn131Cys may reflect the instability of these proteins which were the least thermally stable in the presence of Ca^{2+} (Table 3.1). The Asn131Cys, Asn171Cys and the gl-Asn171Cys all had a similar T_m and all were responsive to Ca^{2+} chelation (Table 3.1). Thus, I hypothesized that I did not observe persistently high SLS intensity for the Asn131Cys/Asn171Cys, gl-Asn131Cys and gl-Asn131Cys/gl-Asn131Cys proteins due to the centrifugation steps which removes protein aggregates. Therefore, to confirm that the

Asn131Cys/Asn171Cys, gl-Asn131Cys and gl-Asn131Cys/gl-Asn131Cys proteins were pre-aggregated, I re-suspended the pellets formed after centrifugation and measured the SLS intensity as an indicator of aggregation state. The samples with low SLS intensity before and after EDTA addition all exhibited significantly higher SLS intensity compared to wild-type EFSAM prior to EDTA addition, suggesting that significantly more protein aggregates formed even in the presence of Ca^{2+} compared to control (Figure 3.13B). Taken together, these light scattering data suggest that modifications of EFSAM at the Asn131 and Asn171 sites increase the propensity for EFSAM oligomerization.

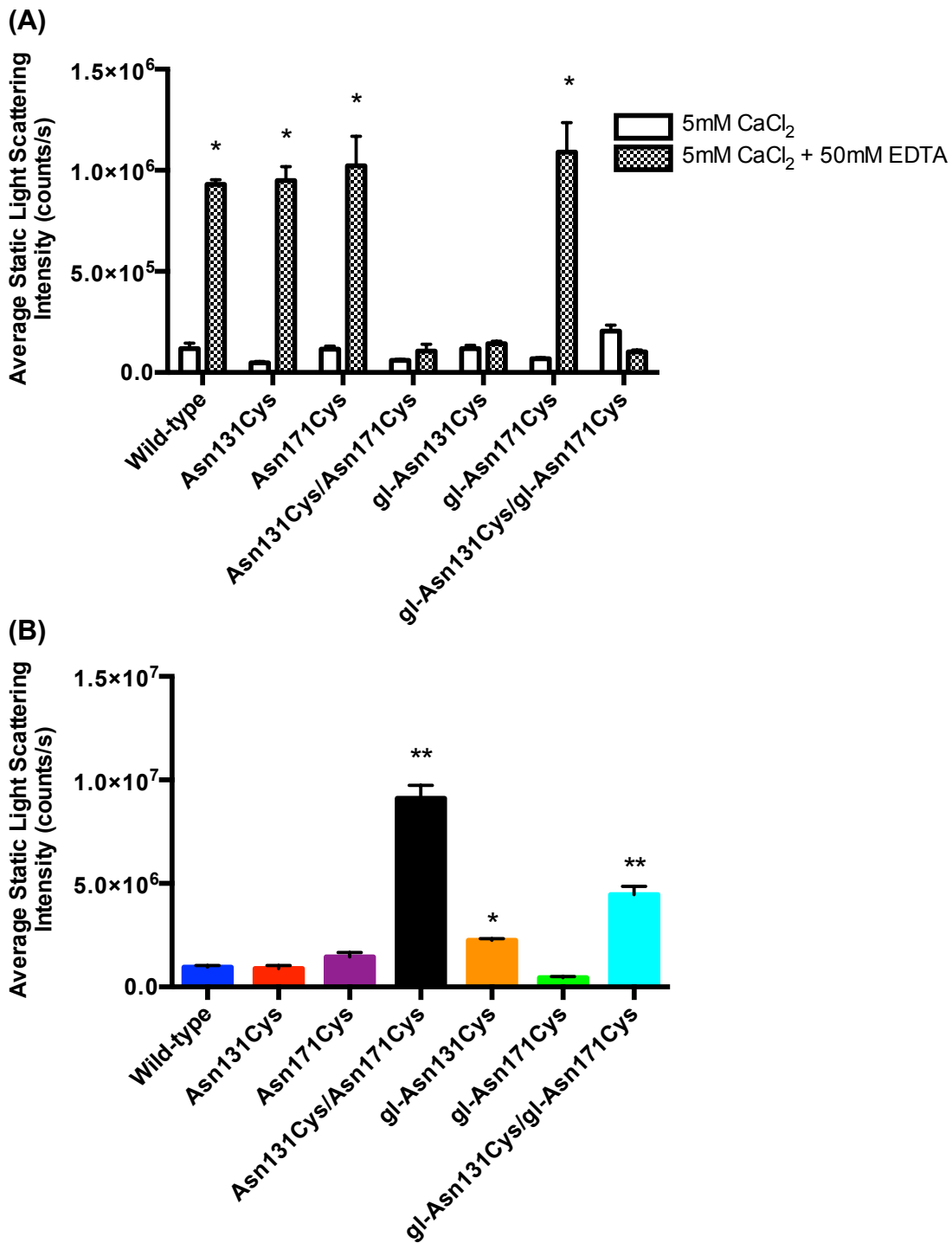


Figure 3.13. Oligomerization propensity of EFSAM proteins assessed by SLS intensity. (A) Ca²⁺-depletion dependent oligomerization assessed after chelation of Ca²⁺. SLS intensity is shown before and after Ca²⁺ chelation using EDTA for each protein sample. Statistical analysis is a two-way ANOVA with Bonferroni multiple comparisons test comparing SLS intensity before and after 50 mM EDTA addition within each group; *p<0.0001. (B) Ca²⁺-depletion independent oligomerization assessed in the absence of Ca²⁺ chelation. SLS intensity of the resuspended aggregates pelleted by centrifugation is shown for each protein sample. Statistical analysis was performed using one-way ANOVA with Dunnett multiple comparisons test to the wild-type control group; *p<0.05, **p<0.0001. All data in (A) and (B) are of n=3 separate experiments acquired in 5 mM CaCl₂ 20 mM Tris, 150 mM NaCl, 1 mM TCEP for unmodified mutants or no TCEP for modified mutants, pH 7.5.

3.6 Blocking EFSAM glycosylation within full-length STIM1 suppresses SOCE.

The ability of the wild-type and mutant STIMs to regulate Ca^{2+} uptake was tested using fura2 ratiometric fluorescence experiments using live HEK293 cells stably expressing YFP-Orai1. HEK293-Orai1 cells were transiently transfected with wild-type monomeric cherry tagged STIM1 (mChSTIM1) or the corresponding single Asn131Gln or Asn171Gln or double Asn131Gln/Asn171Gln glycosylation-incompetent mutants. Passive depletion of the ER Ca^{2+} store using TG caused a transient release of Ca^{2+} from the lumen that was not significantly different between the five groups (i.e., no transfection, mChSTIM1, mChSTIM1 Asn131Gln, mChSTIM1 Asn171Gln, mChSTIM1 Asn131Gln/Asn171Gln). However, upon the addition of 0.5 mM CaCl_2 to the external medium, the uptake of Ca^{2+} for cells transfected with doubly mutated STIM1 (i.e., mChSTIM1 Asn131Gln/Asn171Gln) displayed a significantly smaller rise in the fluorescence ratio, indicating there was lower Ca^{2+} uptake from the extracellular space compared to that of wild-type mChSTIM1 and single mutant expressing cells (Figure 3.14). Surprisingly, after supplementing the external medium with an additional 3.5 mM CaCl_2 both the mChSTIM1 and mChSTIM1 Asn131Gln/Asn171Gln proteins induced similar levels of uptake, whereas the single mutants maintained the trend observed at lower external CaCl_2 of inducing higher levels of Ca^{2+} entry compared to the double mutant. Taken together, these data show that blocking EFSAM glycosylation within full-length STIM1 decreases SOCE-mediated Ca^{2+} influx at relatively low levels of external Ca^{2+} consistent with a role for glycosylation in enhancing the oligomerization propensity of the domain and activation of Orai1 channels, and intriguingly, relatively high levels of external Ca^{2+} may differentially affect the function of glycosylated and nonglycosylated STIM proteins.

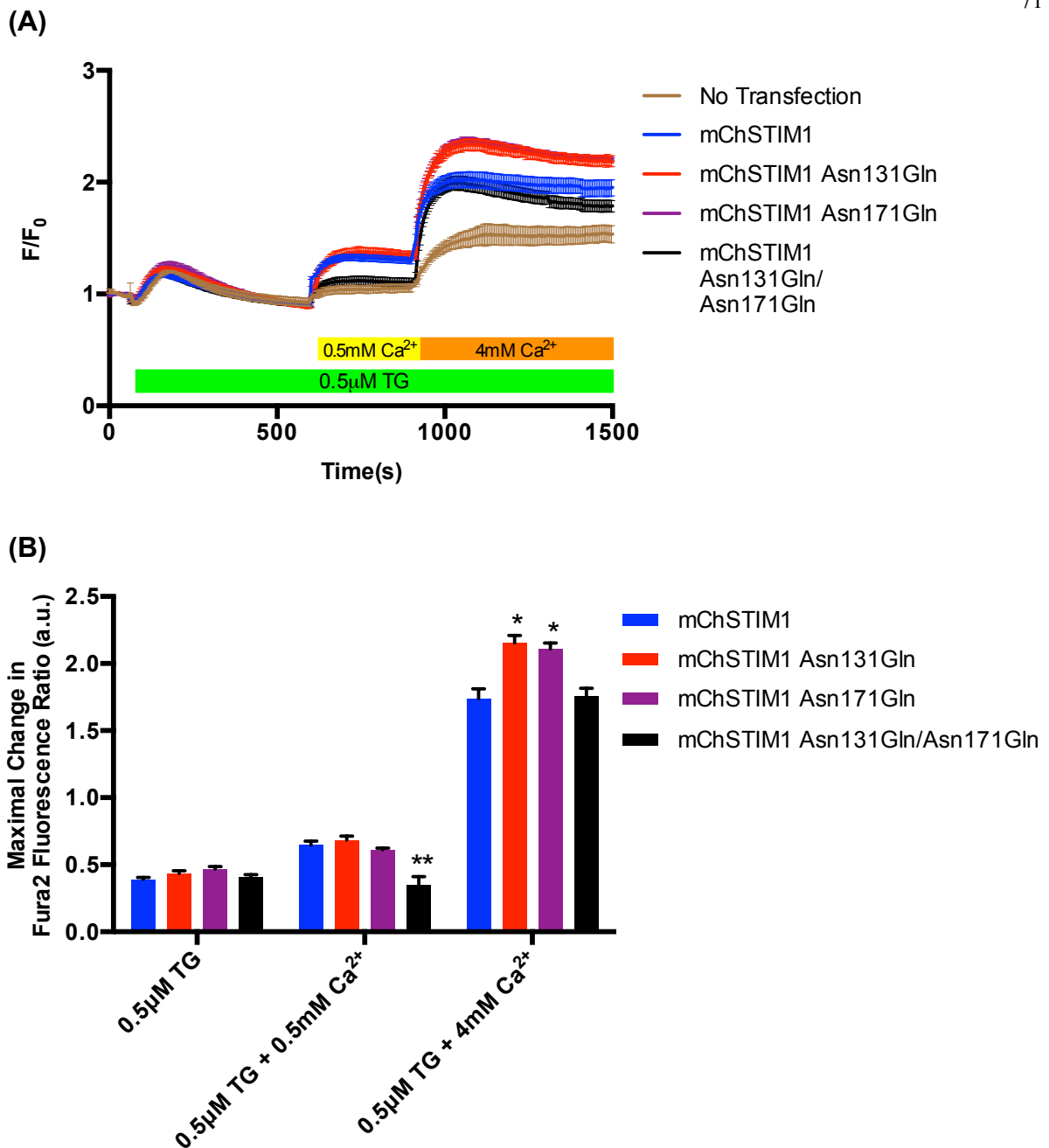


Figure 3.14. Assessment of SOCE mediated by wild-type and glycosylation-incompetent full length STIM1 proteins in HEK293 live cells. (A) Changes in the Fura-2 fluorescence ratio reporting the relative changes in the cytosolic Ca^{2+} levels upon depletion of ER Ca^{2+} stores by external addition of $0.5 \mu\text{M}$ TG and 0.1mM EGTA (horizontal green bar). SOCE was monitored after the addition of 0.5mM and 4.0mM excess CaCl_2 to the external medium at the time points indicated by the yellow and orange horizontal bars, respectively. **(B)** Maximal relative changes in the Fura-2 fluorescence ratio after 0.5mM TG, 0.5mM and 4.0mM external CaCl_2 additions. Statistical analysis was performed with two-way ANOVA with Bonferroni multiple comparisons test to the mChSTIM1 control group. * $p < 0.01$, ** $p < 0.001$. Data in (A) and (B) are from HEK293 cells stably expressing YFP-Orai1 and transiently co-expressing wild-type ($n=8$), Asn131Gln ($n=3$), Asn171Gln ($n=3$) or Asn131Gln/Asn171Gln ($n=14$) mChSTIM1.

Chapter 4

Discussion

4.1 Summary of key findings

Although the STIM1 glycosylation sites were identified over 15 years ago (Williams *et al.*, 2001, 2002), studies on how STIM1 *N*-glycosylation affects SOCE have been inconsistent and ambiguous (Mignen *et al.*, 2007; Csutora *et al.*, 2008; Czyz *et al.*, 2009; Kilch *et al.*, 2013). Therefore, this thesis investigated the effect of such glycosylation on the biophysical properties and structure of the Ca²⁺ sensing EFSAM domain, as well as the function of the modified domain within full-length STIM1. I hypothesized that neoglycosylation of the EFSAM domain alters the biophysical properties of the domain in a manner that is intimately tied to the ability of STIM1 to regulate SOCE. In summary, the double glucose-conjugated mutant EFSAM protein (i.e., gl-Asn131Cys/gl-Asn171Cys) exhibited a partial loss in α -helical secondary structure even in the presence of Ca²⁺. Consistent with this structural change, the double modified sample had the lowest thermal stability compared to all other groups. Moreover, variation of the Asn131 or Asn171 sites decreased the Ca²⁺ binding affinity, as well as revealed 3D structural perturbations localized near the modification site(s) when examined by NMR. From oligomerization studies, doubly mutated and doubly modified EFSAM samples showed increased oligomerization even in the presence of Ca²⁺, implying an increased ability to initiate and activate SOCE. Consistent with this notion, STIM1 functional studies showed a suppressed Ca²⁺ influx via the SOCE pathway when glycosylation was blocked by mutation at the Asn131 and Asn171 sites. Thus, my hypothesis was supported by my *in vitro* and mammalian cell culture results, demonstrating that glycosylation of the EFSAM domain endows STIM1 with another layer of regulation through modification of the Ca²⁺ sensing properties of the protein.

4.2 Neo-glycosylation alters the fundamental Ca²⁺ sensing properties EFSAM proteins.

4.2.1 Glycosylation structurally perturbs STIM1 EFSAM

STIM1 protein is activated when Ca²⁺ dissociates from its binding site, resulting in a partial unfolding coupled with destabilization of the domain; moreover, it has been suggested that the EF-hand domain of EFSAM adopts a “closed” conformation similar to CaM in the absence of Ca²⁺ (Stathopoulos *et al.*, 2008), but the precise atomic resolution structure of the apo state is unknown. Interestingly, I discovered that glucose-conjugated EFSAM proteins (i.e. gl-Asn131Cys/gl-Asn171Cys) displayed a significantly lower percentage α -helicity compared to wild-type EFSAM proteins, suggesting a constitutive partial loss in α -helicity in the presence of Ca²⁺ (Figure 3.1). This result is supported by my thermal stability studies (Figure 3.2) which showed that gl-Asn131Cys/gl-Asn171Cys had the lowest thermal stability ($T_m \sim 37.8$ °C), a value almost 11°C lower than that of the wild-type T_m (Table 3.1). These findings imply that even in the presence of Ca²⁺, fully glycosylated EFSAM within STIM1 would be partially unfolded and STIM1 would be activated. However, it is important to note that the non-conserved luminal region of STIM1 (i.e. residues 23-57) stabilizes the EFSAM core domain by ~ 15 °C (Stathopoulos *et al.*, 2009). Thus, the double glycosylation of EFSAM counteracts the stabilization caused by the non-conserved N-terminal residues by destabilizing the conserved EFSAM domain, thereby adapting the protein for a role in ER Ca²⁺ sensing associated with SOCE activation.

It has been previously shown that a balance between EF-hand Ca²⁺ binding affinity and SAM domain stability tunes the two human homologues of STIM1 and STIM2 to specific roles as a basal Ca²⁺ homeostasis regulator (i.e., STIM2) and a robust SOCE ON/OFF regulator (i.e., STIM1) (Zheng *et al.*, 2011). STIM1 has a higher Ca²⁺ binding

affinity and a lower SAM domain stability, and so it remains inactive after small reductions of ER luminal Ca^{2+} . STIM2 has a lower Ca^{2+} binding affinity, but a higher SAM domain stability, and so it is active even after small levels of ER luminal Ca^{2+} depletion. However, the lower SAM domain stability of STIM1 makes it robustly oligomerize after a larger magnitude ER Ca^{2+} depletion, while the higher SAM domain stability of STIM2 makes it less oligomerization prone after ER Ca^{2+} depletion (Zheng *et al.*, 2011). While the addition of the non-conserved luminal residues increases both Ca^{2+} binding affinity (Stathopoulos laboratory, unpublished data) and stability (Stathopoulos *et al.*, 2009), my data suggest that the double glycosylation, which is specific only to STIM1, contributes to this balance of Ca^{2+} binding affinity and stability by shifting STIM1 EFSAM to even lower binding affinity and stability, thus making STIM1 a robust ON/OFF regulator of SOCE.

From the differences observed in the secondary structural characteristics after glucose conjugation to the EFSAM domain, I expected the modification would also alter the 3D protein structure of this domain. Indeed, solution NMR spectroscopy demonstrated CSPs in the ^1H - ^{15}N HSQC spectra of EFSAM as a result of the modification(s). For the singly modified EFSAM samples (i.e. gl-Asn131Cys or gl-Asn171Cys), CSPs, and thus structural changes, were localized close to the modification sites in 3D space (i.e., ~ 10 Å maximum distance; Figures 3.5, 3.8). Interestingly, for the double-modified gl-Asn131Cys/gl-Asn171Cys protein, the CSPs appeared to be largely an additive function of the individual modifications (Figure 3.10). This result was somewhat unexpected because my far-UV CD analyses showed a significantly reduced α -helicity for the doubly modified protein (Figure 3.1), suggesting a potential synergistic perturbation. However, it is important to note that the double modified EFSAM protein tended to oligomerize (see below) even in the Ca^{2+} loaded state, and the fraction of oligomerized protein would not be observable in the standard HSQC

experiments due to size limitations of the standard NMR experiments. It is conceivable that the doubly modified protein exists in multiple conformations, with the oligomerized partially unfolded state not visible in the NMR spectrum. In addition to the CSPs, the doubly modified spectrum exhibited a considerable loss in peak intensity that could be caused by multiple conformations and/or increased homotypic protein-protein interactions.

4.2.2 Glycosylation lowers the Ca^{2+} affinity of STIM1 EFSAM

Because STIM1 protein activation is initiated by dissociation of Ca^{2+} from its binding site, I also examined the effect of neo-glycosylation on EFSAM Ca^{2+} binding affinity. All mutated or modified EFSAM proteins exhibited a decreased Ca^{2+} binding affinity compared to the wild-type unmodified EFSAM (Table 3.2). However, the apparent K_d was highest (i.e. weakest affinity) for the samples that were doubly mutated or doubly modified. Considering Ca^{2+} levels in the ER lumen vary from ~ 100 to $800 \mu\text{M}$, the K_d values estimated for the double mutated or double modified EFSAM proteins appear too high to respond to the range of changes in ER luminal Ca^{2+} levels. However, as mentioned above, the STIM1 non-conserved N-terminal region greatly stabilizes the core EFSAM domain (Stathopoulos *et al.*, 2009), and thus, I believe that the weakened Ca^{2+} binding affinity caused by glycosylation may compensate for the stabilization and increased affinity endowed by the variable N-terminal region.

4.2.3 Glycosylation enhances oligomerization of STIM1 EFSAM

Activated STIM1 forms oligomers which then translocate to ER-PM junctions where puncta form (Liou *et al.*, 2005, 2007; Zhang *et al.*, 2005). This process initiates Ca^{2+} influx through the SOCE pathway after coupling and activating Orai1 channels. It has been shown that artificial oligomerization of the luminal domain of STIM1 is sufficient to induce

translocation and activation of Orai1 channels (Luik *et al.*, 2008). Therefore, oligomerization of EFSAM is a fundamental initiation mechanism for STIM1 and SOCE activation. My data showed that neo-glycosylation results in EFSAM partial unfolding, decreased stability and lower Ca^{2+} binding affinity that could play a role in increased protein activation. Thus, EFSAM oligomerization was studied in response to glucose modification. As predicted, gl-Asn131Cys/gl-Asn171Cys protein demonstrated persistent oligomerization even in the presence of Ca^{2+} (Figure 3.13). Interestingly, the double mutant EFSAM (i.e. Asn131Cy/Asn171Cys) as well as gl-Asn131Cys EFSAM also exhibited oligomers in the presence of Ca^{2+} . At the same time, the thermal stability data indicated that Asn131Cys/Asn171Cys, gl-Asn131Cys, and gl-Asn131Cys/gl-Asn171Cys proteins had the lowest T_m values of 41.5 °C, 42.0 °C, and 37.8 °C respectively, reinforcing the intimate link between oligomerization propensity and stability.

4.3 SOCE is suppressed after blocking of STIM1 glycosylation in mammalian cells.

While my biophysical studies indicated double glucose modification lowers Ca^{2+} binding affinity, destabilizes, partially unfolds and increases protein oligomerization of EFSAM, the link between glycosylation of EFSAM and full-length STIM1 function in the cell was unclear based on contradictory findings from multiple groups (see Chapter 1.6.1). Therefore, I conducted fura2 cytosolic Ca^{2+} imaging to examine the effect of glycosylation on STIM1 function and SOCE. Remarkably, I discovered that at relatively low levels of extracellular CaCl_2 (i.e. ~0.5 mM) cells expressing the mChSTIM1 Asn131Gln/Asn171Gln double mutant which blocks glycosylation at those mutated sites displayed significantly less Ca^{2+} influx compared to wild-type (Figure 3.14). This data at relatively low extracellular

CaCl₂ is fully consistent with my biophysical studies where glucose-modification enhances EFSAM oligomerization via decreased Ca²⁺ binding affinity, partial unfolding and destabilization. Thus, in the full-length STIM1 context, glycosylation of the EFSAM region enhances the activation of the molecule in response to ER Ca²⁺ depletion. These differences observed at ~0.5 mM external CaCl₂ levels are consistent with a previous study using a similar concentration of external CaCl₂ with cells expressing Asn to Gln double mutant STIM1 (Kilch *et al.*, 2013).

Interestingly, after the initial uptake at ~0.5 mM CaCl₂, supplementing the external medium with an additional 3.5 mM CaCl₂ (i.e., ~4.0 mM total external bath CaCl₂) decreased Ca²⁺ influx for the wild-type mChSTIM1 compared to the single Asn131Gln or Asn171Gln mutant mChSTIM1. It has been known that SOCE can be regulated by extracellular Ca²⁺ for over 20 years (Petersen & Berridge, 1994), and it is well established that a fraction of STIM1 is located on the PM with the N-terminus facing the extracellular medium (Manji *et al.*, 2000; Zhang *et al.*, 2005; Lopez *et al.*, 2006; Spassova *et al.*, 2006). More recently, a study using human platelets demonstrated an extracellular Ca²⁺ dependent decrease in the rate of Mn²⁺ uptake through Orai1 channels at extracellular Ca²⁺ levels between 0 – 3 mM (Jardín *et al.*, 2009). Further, this inhibition was attributed to PM localized STIM1 since external incubation of the cells with an antibody that recognizes STIM1 eliminated the inhibitory effect without cell permeabilization (Jardín *et al.*, 2009). Thus, I speculate that the differences in SOCE observed at 0.5 mM and 4.0 mM extracellular Ca²⁺ could be driven by the inhibitory effects of extracellular Ca²⁺. The blocked glycosylation of mChSTIM1 Asn131Gln or mChSTIM1 Asn171Gln would prevent targeting to the PM (Williams *et al.*, 2002) and any inhibitory effects exerted by extracellular Ca²⁺ on these proteins. Thus, SOCE mediated by the wild-type mCh-STIM1 would be inhibited by the high extracellular Ca²⁺,

while the ER-resident single and double glycosylation mutants would be unaffected, resulting in the significantly lower uptake of the wild-type compared to the single mutants. This intriguing inhibitory effect of extracellular Ca^{2+} may also help explain some of the ambiguities observed in the past glycosylation studies with single as well as double mutant STIM1s (Mignen *et al.*, 2007; Csutora *et al.*, 2008; Czyz *et al.*, 2009; Kilch *et al.*, 2013). However, we cannot rule out the possibility that suppressed SOCE was due to the mutation rather than blocked *N*-glycosylation. Thus, further investigation on the biophysical effects of the Gln mutation with respect to STIM1 function is needed for a more complete study. Nevertheless, my experiments using HEK293 cells showed that fully preventing STIM1 luminal domain glycosylation suppresses the SOCE activity at relatively low external Ca^{2+} levels, consistent with my *in vitro* biophysical and structural assessments.

4.4 Future studies

My work demonstrated that glycosylation of the EFSAM domain results in increased protein activation and function by altering the structure such that the protein partially loses α -helicity in the presence of Ca^{2+} , causes destabilization and lowers Ca^{2+} binding affinity. Further, I found that blocking glycosylation in the full-length STIM1 molecules suppresses SOCE activation at relatively low external Ca^{2+} levels. While the NMR data identified regions of EFSAM that are structurally perturbed upon glucose attachment, solving the 3D structure of EFSAM in the modified state(s) would reveal precisely how the tertiary structure and fold of EFSAM changes in response to the modifications. This proposed structural work could provide new high-resolution insights into the oligomerization-prone EFSAM conformation, data that are currently lacking in the field. Additionally, it is important to assess the effects of mature glycans on the EFSAM biophysical properties and structure in

the singly or doubly attached scenarios. Experiments with mature glycans may reveal additional reasons behind the Ca^{2+} -dependent effect on SOCE I observed in the cell culture experiments.

Previous studies have found that the Asn131 and Asn171 residues on STIM1 proteins are glycosylated endogenously (Williams *et al.*, 2001, 2002). However, the exact fraction of STIM1 proteins that is modified in this regard is unclear; moreover, the glycosylation levels in different tissues and cell types are unknown. Therefore, determining how partial protein modification affects the overall function of SOCE is another intriguing study to be performed to further understand the role of this cellular protein modification on SOCE. An experiment where incompletely modified EFSAM proteins are mixed with different percentages of modified EFSAMs to mimic the various scenarios in the cells would assess if modified EFSAM proteins can trigger unmodified EFSAM activation, and thus, an increase in SOCE function.

Lastly, the SOCE pathway is heavily involved and studied in conjunction with many physiological diseases such as SCID, heart diseases and cancer (Roos *et al.*, 2005; Yang *et al.*, 2009; Vashisht *et al.*, 2015; Pla *et al.*, 2016). Since this thesis shows a role of glycosylation in protein activation and function, additional research on how glycosylation levels change in various diseases could provide important clues into the changes in SOCE that are involved in the manifestation of disease. For example, in certain cancers such as the breast cancer, it is already known that Ca^{2+} uptake through SOCE is increased; furthermore, there is increased protein glycosylation indicated by increased glycan levels in metastasizing breast cancer cells (Yang *et al.*, 2009; Kölbl *et al.*, 2015; Vashisht *et al.*, 2015). Therefore, comparing the amount of endogenously glycosylated STIM1 proteins in normal and cancer cells would provide a mechanistic basis for the increased SOCE apart from changes in

protein expression patterns. Importantly, my work on the mechanisms of glycosylation-induced enhanced STIM1 activation may lead to a new rationale for the development of therapeutics by modulating STIM1 function and SOCE.

4.5 Overall Conclusion

Protein modifications, such as glycosylation, are important not only for proper trafficking of molecules within the cell, but also for fine-tuning protein functions. Therefore, studying how these modifications alter the biophysical properties of proteins is crucial for understanding the mechanisms of function. The ER Ca^{2+} sensor for the SOCE pathway STIM1 is glycosylated at residues Asn131 and Asn171. This thesis investigated the effect of glucose conjugation on the biophysical properties of the Ca^{2+} sensing STIM1 EFSAM domain that mediates protein activation. Through my analysis of α -helicity, thermal stability, 3D structure, Ca^{2+} binding affinity, and oligomerization, I found that glycosylation of the two Asn residues at the 131 and 171 residue sites of the EFSAM domain increases protein activation through changes in structure, Ca^{2+} binding affinity, oligomerization and ability to signal Ca^{2+} influx in cells (Table 4.1). Remarkably, the Asn131Cys and Asn171Cys mutations without any glucose conjugation promoted changes to critical Ca^{2+} sensing properties of EFSAM that were further enhanced after glucose attachment. This discovery indicates that even though Asn131 and Asn171 sites are at the structural periphery of EFSAM, these locations play important roles in the folding, structure and Ca^{2+} sensing mechanism of EFSAM.

There are several novel aspects to this thesis research. First, I established a site-specific chemical approach to conjugating sugars to EFSAM and studying the structural and biophysical consequences of this attachment. I show that neo-glycosylation of the Asn131

and Asn171 sites within the vital EFSAM Ca^{2+} sensing domain results in structural perturbations that lead to modified folding, stability, Ca^{2+} binding affinity and oligomerization, properties that ultimately favor STIM1 activation. My work provides the first structural and mechanistic insights into how *N*-glycosylation effects the Ca^{2+} sensing properties of STIM1 with respect to the regulation of SOCE, and importantly, a framework for future studies investigating how different glycans at various stages of processing effect STIM1 Ca^{2+} sensing and SOCE activity. Collectively, my data suggests that glycosylation of STIM1 makes this protein more responsive to ER Ca^{2+} store depletion by decreasing foldedness, stability and Ca^{2+} binding affinity. Such a mechanism counteracts the stabilization caused by the non-conserved far N-terminal residues, making STIM1 very well suited as an ON/OFF activator of SOCE. Thus, modified STIM1 would be more sensitive to fluctuating Ca^{2+} levels in the ER, resulting in more fine responses to maintain ER Ca^{2+} levels at a certain concentration, while meeting the cytosolic Ca^{2+} demand (Figure 4.1).

Table 4.1. Summary of the changes in EFSAM Ca²⁺ sensing function and SOCE activation due to *N*-glycosylation.

	<i>x</i> Glycosylation	✓ Glycosylation
α-helicity ^a	↑	↓
Thermal stability ^a	↑	↓
Ca ²⁺ affinity ^a	↑	↓
Oligomerization ^a	↓	↑
Ca ²⁺ influx ^b	↓	↑

^aRecombinant EFSAM *in vitro* work.

^bFull-length mChSTIM1 live cell work.

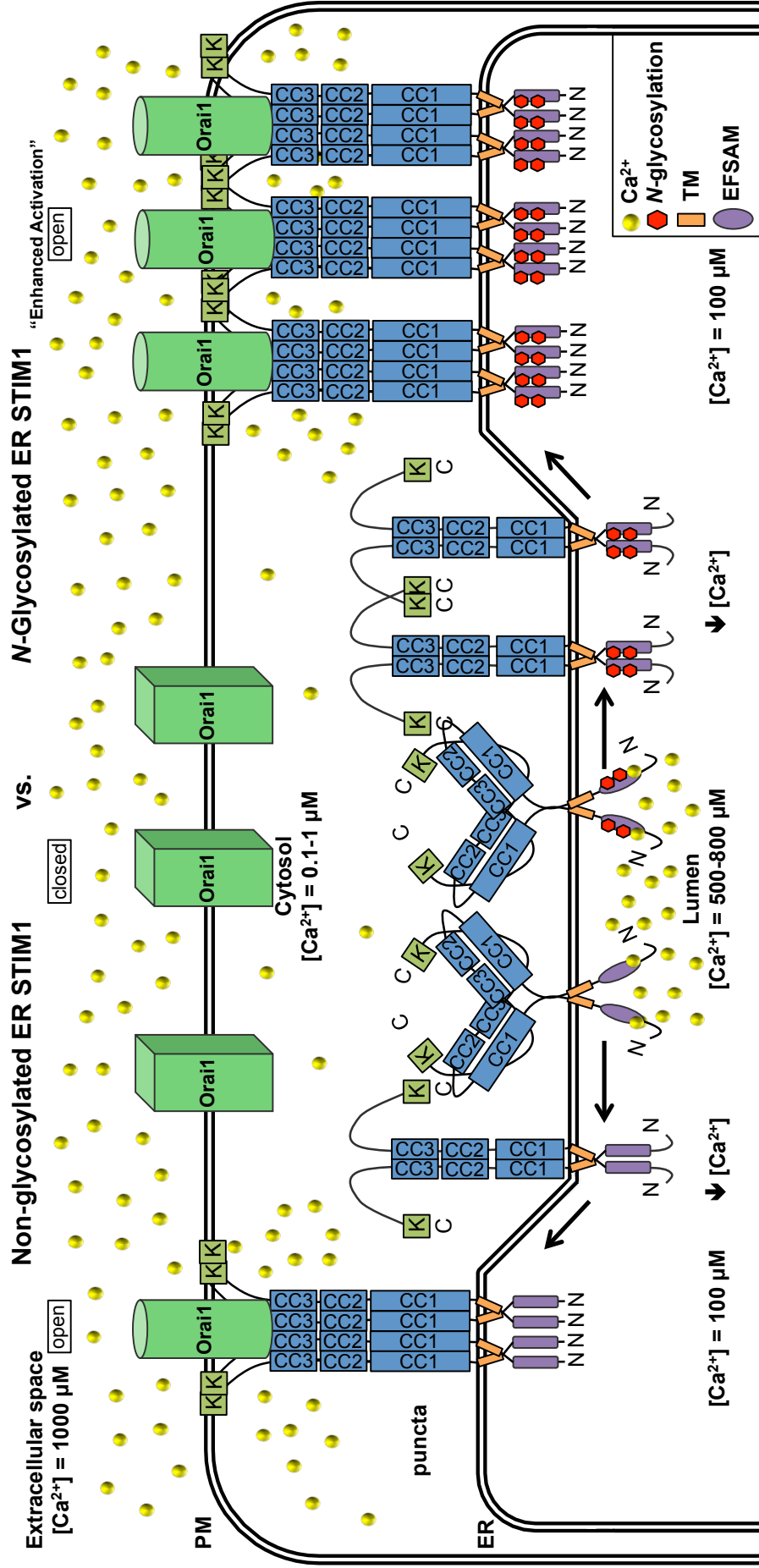


Figure 4.1. Proposed model of non-glycosylated and N-glycosylated STIM1-mediated SOCE activation. Decreases in ER stored Ca^{2+} levels results in EFSAM destabilization coupled dimerization/oligomerization of the luminal domain which induces a cytosolic CC1-CC2-CC3 extension and conformational rearrangement. The present thesis work suggests that N-glycosylation promotes EFSAM domain activation via enhanced destabilization resulting in increased activation of Orai1 channels compared to non-glycosylated STIM1 proteins, depicted here as a greater number of active channels at ER-PM junctions.

References

- Avezov E, Frenkel Z, Ehrlich M, Herscovics A & Lederkremer GZ (2008). Endoplasmic reticulum (ER) mannosidase I is compartmentalized and required for N-Glycan trimming to Man₅₋₆GlcNAc₂ in glycoprotein ER-associated degradation. *Mol Biol Cell* **19**, 216–225.
- Baba Y, Hayashi K, Fujii Y, Mizushima A, Watarai H, Wakamori M, Numaga T, Mori Y, Iino M, Hikida M & Kurosaki T (2006). Coupling of STIM1 to store-operated Ca²⁺ entry through its constitutive and inducible movement in the endoplasmic reticulum. *PNAS* **103**, 16704–16709.
- Berridge MJ (1993). Inositol trisphosphate and calcium signalling. *Nature* **361**, 315–325.
- Berridge MJ (2002). The endoplasmic reticulum: a multifunctional signaling organelle. *Cell Calcium* **32**, 235–249.
- Berridge MJ, Bootman MD & Roderick HL (2003). Calcium signalling: dynamics, homeostasis and remodelling. *Nat Rev Mol Cell Biol* **4**, 517–529.
- Bogeski I, Al-Ansary D, Qu B, Niemeyer BA, Hoth M, Bogeski I, Al-ansary D, Qu B, Niemeyer BA, Hoth M, Al-ansary D, Qu B & Barbara A (2010). Pharmacology of ORAI channels as a tool to understand their physiological functions. *Expert Rev Clin Pharmacol* **3**, 291–303.
- Bootman MD, Collins TJ, Peppiatt CM, Prothero LS, MacKenzie L, De Smet P, Travers M, Tovey SC, Seo JT, Berridge MJ, Ciccolini F & Lipp P (2001). Calcium signalling—an overview. *Semin Cell Dev Biol* **12**, 3–10.
- Boscher C, Dennis JW & Nabi IR (2011). Glycosylation, galectins and cellular signaling. *Curr Opin Cell Biol* **23**, 383–392.
- Cai X (2007a). Molecular evolution and functional divergence of the Ca²⁺ sensor protein in store-operated Ca²⁺ entry: stromal interaction molecule. *PLoS One* **2**, e609.
- Cai X (2007b). Molecular evolution and structural analysis of the Ca²⁺ release-activated Ca²⁺ channel subunit, Orai. *J Mol Biol* **368**, 1284–1291.
- Chai Q, Wang X, Zeldin DC & Lee H (2013). Role of caveolae in shear stress-mediated endothelium-dependent dilation in coronary arteries. *Cardiovasc Res* **100**, 151–159.
- Chin D & Means AR (2000). Calmodulin: a prototypical calcium sensor. *Trends Cell Biol* **10**, 322–328.
- Clapham DE (1995). Calcium signaling. *Cell* **80**, 259–268.
- Csutora P, Peter K, Kilic H, Park KM, Zarayskiy V, Gwozdz T & Bolotina VM (2008). Novel role for STIM1 as a trigger for calcium influx factor production. *J Biol Chem* **283**, 14524–14531.

- Czyz A, Brutkowski W, Fronk J, Duszyński J & Zabłocki K (2009). Tunicamycin desensitizes store-operated Ca^{2+} entry to ATP and mitochondrial potential. *Biochem Biophys Res Commun* **381**, 176–180.
- Darbellay B, Arnaudeau S, Bader CR, König S & Bernheim L (2011). STIM1L is a new actin-binding splice variant involved in fast repetitive Ca^{2+} release. *J Cell Biol* **194**, 335–346.
- Dehaven WI, Smyth JT, Boyles RR, Putney JW & Carolina N (2007). Calcium inhibition and calcium potentiation of Orai1, Orai2, and Orai3 calcium release-activated calcium channels. *J Biol Chem* **282**, 17548–17556.
- Dennis JW, Lau KS & Nabi IR (2009). Adaptive regulation at the cell surface by *N*-glycosylation. *Traffic* **10**, 1569–1578.
- Estrada IA, Donthamsetty R, Debski P, Zhou M-H, Zhang SL, Yuan JX-J, Han W & Makino A (2012). STIM1 restores coronary endothelial function in Type 1 diabetic mice. *Circ Res* **111**, 1166–1175.
- Farrow NA, Muhandham JR, Singer AU, Pascal SM, Kay CM, Gish G, Shoelson SE, Pawson T, Forman-kay JD & Kay LE (1994). Backbone dynamics of a free and a phosphopeptide-complexed src homology 2 domain studied by ^{15}N NMR relaxation. *Biochemistry* **33**, 5984–6003.
- Feske S (2007). Calcium signalling in lymphocyte activation and disease. *Nat Rev Immunol* **7**, 690–702.
- Frischauf I, Muik M, Derler I, Bergsmann J, Fahrner M, Schindl R, Groschner K & Romanin C (2009). Molecular determinants of the coupling between STIM1 and Orai Channels. *J Biol Chem* **284**, 21696–21706.
- Fuchs A, Kutterer S, Tobias M, Duda J, Sch B, Liss B, Keller BU & Roeper J (2013). Selective mitochondrial Ca^{2+} uptake deficit in disease endstage vulnerable motoneurons of the SOD1 G93A mouse model of amyotrophic lateral sclerosis. *J Physiol* **591**, 2723–2745.
- Gerlach JQ, Sharma S & Leister KJ (2012). *A tight-knit group: protein glycosylation, endoplasmic reticulum stress and the unfolded protein reponse*. Springer, Dordrecht.
- Glitsch MD, Bakowski D & Parekh AB (2002). Store-operated Ca^{2+} entry depends on mitochondrial Ca^{2+} uptake. *EMBO J* **21**, 6744–6754.
- Graham SJL, Dziadek MA & Johnstone LS (2011). A cytosolic STIM2 preprotein created by signal peptide inefficiency activates ORAI1 in a store-independent manner. *J Biol Chem* **286**, 16174–16185.

- Gudlur A, Quintana A, Zhou Y, Hirve N, Mahapatra S & Hogan PG (2014). STIM1 triggers a gating rearrangement at the extracellular mouth of the Orai1 channel. *Nat Commun* **5**, 1–11.
- Gwack Y, Srikanth S, Feske S, Cruz-guilloty F, Oh-hora M, Neems DS, Hogan PG & Rao A (2007). Biochemical and functional characterization of Orai proteins. *J Biol Chem* **282**, 16232–16243.
- Hill SJ (1990). Distribution, properties, and functional characteristics of three classes of histamine receptor. *Am Soc Pharmacol Exp Ther* **42**, 46–73.
- Hogan PG, Hogan PG, Chen L & Chen L (2003). Transcriptional regulation by calcium, calcineurin. *Genes Dev* **17**, 2205–2232.
- Horinouchi T, Higashi T, Higa T, Terada K, Mai Y, Aoyagi H, Hatate C, Horiguchi M, Harada T & Miwa S (2012). Different binding property of STIM1 and its novel splice variant STIM1L to Orai1, TRPC3, and TRPC6 channels. *Biochem Biophys Res Commun* **428**, 252–258.
- Hou X, Pedi L, Diver MM & Long SB (2012). Crystal structure of the calcium release-activated calcium channel Orai. *Science (80-)* **338**, 1308–1313.
- Huang Y, Zhou Y, Wong H, Chen Y, Chen Y, Wang S, Liu A & Yang JJ (2009). A single ER-hand isolated from STIM1 forms dimer in the absence and presence of Ca²⁺. *FEBS J* **276**, 5589–5597.
- Ikura M, Minowa O & Hikichi K (1985). Hydrogen bonding in the carboxyl-terminal half-fragment 78-148 of calmodulin as studied by two-dimensional nuclear magnetic resonance. *Biochemistry* **24**, 4264–4269.
- Jackson TR, Patterson SI, Thastrup O & Hanley MR (1988). A novel tumour promoter, thapsigargin, transiently increases cytoplasmic free Ca²⁺ without generation of inositol phosphates in NG115-401L neuronal cells. *Biochem J* **253**, 81–86.
- Jaiswal MK, Zech W, Goos M, Leutbecher C, Ferri A, Zippelius A, Carri MT, Nau R & Keller BU (2009). Impairment of mitochondrial calcium handling in a mtSOD1 cell culture model of motoneuron disease. *BMC Neurosci*; DOI: 10.1186/1471-2202-10-64.
- Janis R & Triggle D (1983). New developments in Ca²⁺ channel antagonists. *J Med Chem* **26**, 775–785.
- Jardín I, López JJ, Redondo PC, Salido GM & Rosado JA (2009). Store-operated Ca²⁺ entry is sensitive to the extracellular Ca²⁺ concentration through plasma membrane STIM1. *BBA - Mol Cell Res* **1793**, 1614–1622.

- Kay LE, Keifer P & Saarinen T (1992). Pure absorption gradient enhanced heteronuclear single quantum correlation spectroscopy with improved sensitivity. *J Am Chem Soc* **114**, 10663–10665.
- Kilch T, Alansary D, Peglow M, Dorr K, Rychkov G, Rieger H, Peinelt C & Niemeyer BA. (2013). Mutations of the Ca²⁺-sensing stromal interaction molecule stim1 regulate Ca²⁺ influx by altered oligomerization of stim1 and by destabilization of the Ca²⁺ channel orai1. *J Biol Chem* **288**, 1653–1664.
- Kölbl AC, Andergassen U & Jeschke U (2015). The role of glycosylation in breast cancer metastasis and cancer control. *Front Oncol* **5**, 1–5.
- Kretsinger RH & Nockolds CE (1973). Carp muscle calcium-binding protein. *J Biol Chem* **248**, 3313–3326.
- van Leeuwen JE & Samelson LE (1999). T cell antigen-receptor signal transduction. *Curr Opin Immunol* **11**, 242–248.
- Leurs R, Smit MJ & Timmerman H (1995). Molecular aspects of histamine receptors. *Pharmacol Ther* **66**, 413–463.
- Liou J, Fivaz M, Inoue T & Meyer T (2007). Live-cell imaging reveals sequential oligomerization and local plasma membrane targeting of stromal interaction molecule 1 after Ca²⁺ store depletion. *Cell Biol* **104**, 9301–9306.
- Liou J, Kim ML, Heo W Do, Jones JT, Myers JW, Ferrell JE & Meyer T (2005). STIM is a Ca²⁺ sensor essential for Ca²⁺-store-depletion-triggered Ca²⁺ influx. *Curr Biol* **15**, 1235–1241.
- Lis A, Peinelt C, Beck A, Parvez S, Monteilh-zoller M, Fleig A & Penner R (2007). CRACM1, CRACM2, and CRACM3 are store-operated Ca²⁺ channels with distinct functional properties. *Curr Biol* **17**, 794–800.
- Lopez JJ, Salido M, Pariente A & Rosado JA (2006). Interaction of STIM1 with Endogenously Expressed Human Canonical TRP1 upon Depletion of Intracellular Ca²⁺ Stores. *J Biol Chem* **281**, 28254–28264.
- Lucas JA, Miller AT, Berg LJ & Berg LJ (2003). The role of Tec family kinases in T cell development and function. *Immunol Rev* **191**, 119–138.
- Luik RM, Wang B, Prakriya M, Wu MM, Lewis RS & Physiology C (2008). Oligomerization of STIM1 couples ER calcium depletion to CRAC channel activation. *Nature* **454**, 538–542.
- Lytton J, Weslin M & Hanley MR (1991). Thapsigargin inhibits the sarcoplasmic or endoplasmic reticulum Ca-ATPase family of calcium pumps. *J Biol Chem* **26**, 17067–17071.

- Manji SS, Parker NJ, Williams RT, van Stekelenburg L, Pearson RB, Dziadek M & Smith PJ (2000). STIM1: a novel phosphoprotein located at the cell surface. *Biochim Biophys Acta* **1481**, 147–155.
- Mercer JC, Dehaven WI, Smyth JT, Wedel B, Boyles RR, Bird GS, Putney JW & Carolina N (2006). Large store-operated calcium selective currents due to co-expression of Orai1 or Orai2 with the intracellular calcium sensor, Stim1. *J Biol Chem* **281**, 24979–24990.
- Miao Y, Miner C, Zhang L, Hanson PI, Dani A & Vig M (2013). An essential and NSF independent role for α -SNAP in store-operated calcium entry. *Elife* **2**, e00802.
- Mignen O, Thompson JL & Shuttleworth TJ (2007). STIM1 regulates Ca^{2+} entry via arachidonate-regulated Ca^{2+} -selective (ARC) channels without store depletion or translocation to the plasma membrane. *J Physiol* **579**, 703–715.
- Mignen O, Thompson JL & Shuttleworth TJ (2008). Orai1 subunit stoichiometry of the mammalian CRAC channel pore. *J Physiol* **586**, 419–425.
- Muller MS, Pedersen SE, Walls AB, Waagepetersen HS & Bak LK (2015). Isoform-selective regulation of glycogen phosphorylase by energy deprivation and phosphorylation in astrocytes. *Glia* **63**, 154–162.
- Nilsson T, Au CE & Bergeron JJM (2009). Sorting out glycosylation enzymes in the golgi apparatus. *FEBS Lett* **583**, 3764–3769.
- Parod RJ & Putney JW (1978). The role of calcium in the receptor mediated control of potassium permeability in the rat lacrimal gland. *J Physiol* **281**, 371–381.
- Pearse BR & Hebert DN (2010). Lectin chaperones help direct the maturation of glycoproteins in the endoplasmic reticulum. *Biochim Biophys Acta* **1803**, 684–693.
- Petersen CCH & Berridge MJ (1994). The regulation of capacitative calcium entry by calcium and protein kinase C in *Xenopus* oocytes. *J Biol Chem* **269**, 32246–32253.
- Pla AF, Kondratska K & Prevarskaya N (2016). STIMs and ORAIs proteins: crucial roles in hallmarks of cancer. *Am J Physiol - Cell Physiol* **10**, c509–c519.
- Prakriya M, Feske S, Gwack Y, Srikanth S, Rao A & Hogan PG (2006). Orai1 is an essential pore subunit of the CRAC channel. *Nature* **443**, 230–233.
- Putney JW (1976). Biphasic modulation of potassium release in rat parotid gland by carbachol and phenylephrine. *J Pharmacol Exp Ther* **198**, 375–384.
- Putney JW (1986). A model for receptor-regulated calcium entry. *Cell Calcium* **7**, 1–12.
- Rasmussen H (1970). Cell communication, calcium ion, and cyclic adenosine monophosphate. *Am Assoc Adv Sci* **170**, 404–412.

- Ringer S (1883). A further contribution regarding the influence of the different constituents of the blood on the contraction of the heart. *J Physiol* **4**, 29–42.3.
- Roos J, DiGregorio PJ, Yeromin A V, Ohlsen K, Lioudyno M, Zhang S, Safrina O, Kozak JA, Wagner SL, Cahalan MD, Velicelebi G & Stauderman KA (2005). STIM1, an essential and conserved component of store-operated Ca^{2+} channel function. *J Cell Biol* **169**, 435–445.
- Schindl R, Frischauf I, Bergsmann J, Muik M, Derler I, Lackner B, Groschner K & Romanin C (2009). Plasticity in Ca^{2+} selectivity of Orai1/Orai3 heteromeric channel. *PNAS* **106**, 19623–19628.
- Schlessinger J (2000). Cell signaling by receptor tyrosine kinases. *Cell* **103**, 211–225.
- Shaw P & Feske S (2013). Physiological and pathological functions of SOCE in the immune system. *Front Biosci (Elite Ed)* **4**, 2253–2268.
- Sievers F, Wilm A, Dineen D, Gibson TJ, Karplus K, Li W, Lopez R, Thompson JD, Higgins DG, McWilliam H, Remmert M & So J (2011). Fast, scalable generation of high-quality protein multiple sequence alignments using Clustal Omega. *Mol Syst Biol* **7**, 1–6.
- Spassova MA, Soboloff J, He L, Xu W, Dziadek MA & Gill DL (2006). STIM1 has a plasma membrane role in the activation of store-operated Ca^{2+} channels. *PNAS* **103**, 4040–4045.
- Stanley P (2011). Golgi glycosylation. *Cold Spring Harb Perspect Biol* **3**, a005199.
- Stanley P, Schachter H & Taniguchi N (2014). *N-Glycans*. Cold Spring Harbor, New York.
- Stathopoulos PB & Ikura M (2013a). *Structure and function of endoplasmic reticulum STIM calcium sensors*. Elsevier Inc., Amsterdam.
- Stathopoulos PB & Ikura M (2013b). Structural aspects of calcium-release activated calcium channel function. *Channels* **7**, 1–10.
- Stathopoulos PB, Li G, Plevin MJ, Ames JB & Ikura M (2006). Stored Ca^{2+} depletion-induced oligomerization of stromal interaction molecule 1 (STIM1) via the EF-SAM region. *J Biol Chem* **281**, 35855–35862.
- Stathopoulos PB, Schindl R, Fahrner M, Zheng L, Gasmi-Seabrook GM, Muik M, Romanin C & Ikura M (2013). STIM1/Orai1 coiled-coil interplay in the regulation of store-operated calcium entry. *Nat Commun* **4**, 2963.
- Stathopoulos PB, Zheng L & Ikura M (2009). Stromal interaction molecule (STIM) 1 and STIM2 calcium sensing regions exhibit distinct unfolding and oligomerization kinetics. *J Biol Chem* **284**, 728–732.

- Stathopoulos PB, Zheng L, Li G-Y, Plevin MJ & Ikura M (2008). Structural and mechanistic insights into STIM1-mediated initiation of store-operated calcium entry. *Cell* **135**, 110–122.
- Tamouza H, Chemouny JM, Kafkova LR, Berthelot L, Flamant M, Demion M, Mesnard L, Paubelle E, Walker F, Tiwari MK, Camara NOS, Vrtovsnik F, Julian BA, Tissandie E, Benhamou M, Novak J, Monteiro RC & Moura IC (2012). The IgA1 immune complex-mediated activation of the MAPK/ERK kinase pathway in mesangial cells is associated with glomerular damage in IgA nephropathy. *Kidney Int* **82**, 1284–1296.
- Thompson JL & Shuttleworth TJ (2013). How many Orai's does it take to make a CRAC channel? *Sci Rep* **3**, 1961.
- Treiman M, Caspersen C, Treiman M, Caspersen C & Brøgger S (1998). A tool coming of age: thapsigargin as an inhibitor of sarco-endoplasmic reticulum Ca²⁺-ATPases. *Trends Pharmacol Sci* **19**, 131–135.
- Varga-Szabo D, Braun A & Nieswandt B (2011). STIM and Orai in platelet function. *Cell Calcium* **50**, 270–278.
- Vashisht A, Trebak M & Motiani RK (2015). STIM and Orai proteins as novel targets for cancer therapy. *Am J Physiol - Cell Physiol* **309**, C457–C469.
- Walsh CT, Garneau-Tsodikova S & Gatto Jr. GJ (2005). Protein posttranslational modifications: the chemistry of proteome diversifications. *Angew Chemie Int Ed* **44**, 7342–7372.
- Whitmore L & Wallace BA (2004). DICHROWEB, an online server for protein secondary structure analyses from circular dichroism spectroscopic data. *Nucleic Acids Res* **32**, 668–673.
- Williams RT, Manji SS, Parker NJ, Hancock MS, Van Stekelenburg L, Eid JP, Senior P V, Kazenwadel JS, Shandala T, Saint R, Smith PJ & Dziadek M a (2001). Identification and characterization of the STIM (stromal interaction molecule) gene family: coding for a novel class of transmembrane proteins. *Biochem J* **357**, 673–685.
- Williams RT, Senior P V., Van Stekelenburg L, Layton JE, Smith PJ & Dziadek M a. (2002). Stromal interaction molecule 1 (STIM1), a transmembrane protein with growth suppressor activity, contains an extracellular SAM domain modified by N-linked glycosylation. *Biochim Biophys Acta* **1596**, 131–137.
- Yang S, Zhang JJ & Huang XY (2009). Orai1 and STIM1 are critical for breast tumor cell migration and metastasis. *Cancer Cell* **15**, 124–134.
- Yeromin AV, Zhang SL, Jiang W, Yu Y, Safrina O & Cahalan MD (2006). Molecular identification of the CRAC channel by altered ion selectivity in a mutant of Orai. *Nature* **443**, 226–229.

- Zhang SL, Yeromin A V, Zhang XH, Yu Y, Safrina O, Penna A, Roos J, Stauderman KA & Cahalan MD (2006a). Genome-wide RNAi screen of Ca^{2+} influx identifies genes that regulate Ca^{2+} release-activated Ca^{2+} channel activity. *PNAS* **103**, 9357–9362.
- Zhang SL, Yu Y, Roos J, Kozak JA, Deerinck TJ, Ellisman MH, Stauderman KA & Cahalan MD (2005). STIM1 is a Ca^{2+} sensor that activates CRAC channels and migrates from the Ca^{2+} store to the plasma membrane. *Nature* **437**, 902–905.
- Zheng L, Stathopoulos PB, Schindl R, Li G, Romanin C & Ikura M (2011). Auto-inhibitory role of the EF-SAM domain of STIM proteins in store-operated calcium entry. *PNAS* **108**, 1337–1342.

Curriculum Vitae

Name: Yoo Jung Choi

Post-secondary Education and Degrees: Western University
London, Ontario, Canada
Honors Specialization BMSc
2010-2014

Western University
London, Ontario, Canada
MSc in Physiology and Pharmacology
2014-2016

Honours and Awards: Dean's Honor List
2011-2014

Western Graduate Research Scholarship
2014-2016

Ontario Graduate Scholarship
2014-2016

Physiology & Pharmacology Research Day
Graduate student poster presentation
2nd place in the Cell Biology category
2015

Related Work Experience Research Assistant
Western University
2012-2014

Teaching Assistant
Physiology 3120
Western University
2014-2016

Publications:

Stathopoulos PB & Choi YJ (2016). Conformational changes mediating stromal interaction molecule-1 function. *Min Rev Med Chem. (In progress)*

Choi YJ, Zhao Y, Bhattacharya M & Stathopoulos PB (2016). Structural perturbations induced by Asn131 and Asn171 glycosylation converge within the EFSAM core and enhance stromal interaction molecule-1 mediated store operated calcium entry. *BBA – Mol Cell Res. (In review)*

Presentations:

Physiology and Pharmacology Research Day

Title: The effect of neo-glycosylation on the structure and function of stromal interaction molecule-1 luminal domain

Western University

London, ON

2015

London Health Research Day

Title: The effect of neo-glycosylation on the structure and function of stromal interaction molecule-1 luminal domain

London, ON

2015

London Health Research Day

Title: The effect of neo-glycosylation on the structure and function of stromal interaction molecule-1 luminal domain

London, ON

2016